

GALLIUM SUBSTITUTION IN ALUMOSILICATE SODALITES

**Vom Fachbereich Geowissenschaften und Geographie
der Universität Hannover**

zur Erlangung des Grades

**Doktor der Naturwissenschaften
Dr. rer. nat.**

genehmigte Dissertation

von

**MOHAMMAD MANGIR MURSHED
geboren am 31 Dezember 1975 in Chandpur, Bangladesch**

**Institut für Mineralogie
Februar 2005**

Referent : PD Dr. habil. Thorsten Michael Gesing

Koreferent : Professor Dr. Josef-Christian Buhl

Professor Dr. Wulf Depmeier

Dr. Andrew John Baer

Tag der Promotion: 14 Februar 2005

Dedicated to my wife Lipi

Acknowledgement

I am extremely thankful to PD Dr. habil. Thorsten Michael Gesing who introduced me to the exciting field of zeolite chemistry, X-ray diffractometry and Rietveld refinement. His continuous supervision at each and every part has made this study as a full fledged thesis. He was exceptionally enthusiastic in providing new ideas in structure refining as well as supportive in implementation of novel suggestions. My sincere gratitude is also due for his tireless effort in designing, editing and discussions which have brought this thesis to its present form.

I am proud to have him as my direct supervisor.

I am indebt to Professor Dr. Josef-Christian Buhl for his sincere support and help in learning basic crystallography, scanning electron microscopy and EDX. His valuable suggestions and discussion on hydrothermal syntheses have helped me tremendously in many successful experiments throughout my research.

I gratefully remember PD Dr. habil. Claus H. Rüscher whose constructive criticism on infrared spectra has been invaluable. I am thankful to him for his efforts.

I am humbly indebted to the Ministry of Science and Culture, Land Niedersachsen, Germany for providing the 'Georg –Christoph-Lichtenberg-Stipendium'.

My heartfelt remembrances are for Dr. Hiltrud Grondey (University of Toronto) who recently passed away. She had earnestly taken care of my well being while I had a chance to work with her on Solid State MAS NMR in Toronto. In addition from the University of Toronto, I am especially grateful to Dr. Andrew J. Baer for his continuous help in measuring MAS NMR.

My grateful appreciations are due for Dr. habil. Michael Fechtelkord (Ruhr University, Bochum) and Dr. Sylvio Indris (Institute of Physical Chemistry and Electrochemistry, University of Hannover) for their sincere support in measuring MAS NMR and constructive discussion.

Above and beyond, I thank all my colleagues in the institute of mineralogy for providing a cordial atmosphere and support in the lab.

1 General Introduction	6
2 Experimental Methods	15
2.1 Synthesis	15
2.2 X-ray Powder Diffraction	15
2.3 X-ray Powder Data Rietveld Refinement	16
2.4 FTIR Spectroscopy	16
2.5 MAS NMR Spectroscopy	16
2.6 Chemicals	17
3 Gallium Substituted Alumosilicate Nitrite Sodalites	18
3.1 Introduction	18
3.2 Results and Discussion	19
3.2.1 Synthesis	19
3.2.2 XRD Investigations and Rietveld Refinements	21
3.2.3 MAS NMR Investigations	28
3.2.4 FTIR Investigations	30
3.3 Conclusion	32
4 Gallium Substituted Alumosilicate Chloride and Bromide Sodalites	33
4.1 Introduction	33
4.2 Results and Discussion	34
4.2.1 Synthesis	34
4.2.2 XRD Investigations and Rietveld Refinements	36
4.2.3 MAS NMR Investigations	43
4.2.4 FTIR Investigations	45
4.3 Conclusion	49
5 Gallium Substituted Alumosilicate Hydro-hydroxy and Hydro Sodalites	50
5.1 Introduction	50
5.2 Results and Discussion	51
5.2.1 Synthesis	51
5.2.2 XRD Investigations and Rietveld Refinements	54
5.2.3 MAS NMR Investigations	62
5.2.4 FTIR Investigations	65
5.3 Conclusion	67
6 Summary	68
6.1 English	68
6.2 Deutsch	71
7 Literature	74
8 Attachment	82

1 GENERAL INTRODUCTION

Sodalite, most commonly considered as a feldspathoid [1-5], occurs most extensively in unsaturated rocks. It often forms along with, or in place of, nepheline in phonolites, and with leucite in leucite tephrites and leucite phonolites [5, 6]. Occasionally, sodalite occurs in metasomatized limestone blocks and other metamorphic environments [5]. Feldspathoids are poorly defined group of minerals contain no volatile anions (Cl^- , SO_4^{2-} , CO_3^{2-} , OH^- and H_2O) though sodalite does. Sodalite has chemistry and structure that are quite different from that of the feldspars or the feldspathoids. However, its structure is closely related to the zeolites, but it is not zeolite either, proper. Therefore *zeoloids* [7] may be appropriate for sodalite, cancrinite and scapolite.

The chemical composition of many common sodalites can be written as $\text{M}_{6+x}[\text{T}^1\text{T}^2\text{O}_4]_6\text{Y}_x(\text{H}_2\text{O})_{8-4x}$ where M is typically an alkali metal and particularly Li, Na, K or Rb, $0 \leq x \leq 2$, $\text{T}^1 = \text{Al, Ga}$, $\text{T}^2 = \text{Si, Ge}$ etc. and Y represents the encapsulated guest species, i.e., halogen, NO_2^- , NO_3^- , OH^- , CO_3^{2-} , SO_4^{2-} etc.. The diversity of guest species can easily be grasped as sodalites intercalated with ClO_4^- [8, 10], ClO_3^- and BrO_3^- [8], SCN^- [8, 9, 67], MnO_4^{2-} [8, 10], MoO_4^- [11], WO_4^{2-} and CrO_4^{2-} [12, 20] and $(\text{B}(\text{OH})_4)^-$ [13] are well known. Besides, $(\text{S}_2/\text{S}_3)^-$, Se^{2-} and $\{(\text{OH})_{2-x}(\text{SeCN})_x\}^{2-}$ [8] synthetic sodalites are also claimed. Wiebcke et al. [14] reported H_3O_2^- containing sodalite. Very recently tetrahydroborate alumosilicate sodalite $\text{Na}_8[\text{AlSiO}_4]_6(\text{BH}_4)_2$ [15] was reported. Organic guest species enclathrated silica sodalites $\text{Si}_{12}\text{O}_{24} \cdot 2\text{C}_2\text{H}_4(\text{OH})_2$ [16] and $[\text{Si}_{12}\text{O}_{24}] \cdot 2\text{C}_3\text{H}_6\text{O}_3$ [17] opened another versatile window in this research arena. Therefore a diverse family of materials is possible with the main constraint being the cage dimension [18]. The mixed cation sodalites, i.e. $\text{Li}_{3.85}\text{Na}_{4.15}[\text{AlSiO}_4]_6\text{Cl}_2$ [19], $\text{K}_{7.7}\text{Na}_{0.3}[\text{AlSiO}_4]_6(\text{ClO}_4)_2$ [10], $(\text{Ca}_{1-x}\text{Sr}_x)_8[\text{Al}_{12}\text{O}_{24}](\text{WO}_4)_2$ [20] etc. and mixed anion sodalites like $\text{Na}_8[\text{AlSiO}_4]_6(\text{Cl, Br})_2$ and $\text{Na}_8[\text{AlSiO}_4]_6(\text{Cl, I})_2$ [21], $\text{Na}_8[\text{AlSiO}_4]_6(\text{NO}_2, \text{NO}_3)_2$ [22] etc. further prove the compositional varieties within the framework matrix. In this connection heavy metal sodalites $\text{Tl}_6[(\text{AlSiO}_4)_6]$ [23], $(\text{Pb}_2(\text{OH})(\text{H}_2\text{O})_3)_2[\text{Al}_3\text{Si}_3\text{O}_{12}]_2$ [24] and $(\text{Ag}_3(\text{H}_2\text{O})_4)_2[\text{Al}_3\text{Si}_3\text{O}_{12}]_2$ [25] are noteworthy.

The crystal structure of sodalite $\text{Na}_8[\text{AlSiO}_4]_6\text{Cl}_2$ was first solved by Pauling [26]. Löns and Schulz [27] refined the structural parameters on the basis of intensity data obtained from Weissenberg photograph. A structure refinement including anisotropic thermal displacement parameters was carried out by Hassan and Grundy on data obtained from a four circle diffractometer [28]. The crystal structure is built up from TO_4 tetrahedral building blocks, alternating linked together to form a truncated octahedral β -cage containing eight sixring windows and six fourring windows parallel to $\{111\}$ and $\{100\}$ planes, respectively (Figure 1.1).

The six-membered rings are stacked in a cubic ABCABC...sequence and the unit cell contains two β -cages at $(0, 0, 0)$ and $(\frac{1}{2}, \frac{1}{2}, \frac{1}{2})$. The T atoms need not to be all of the same

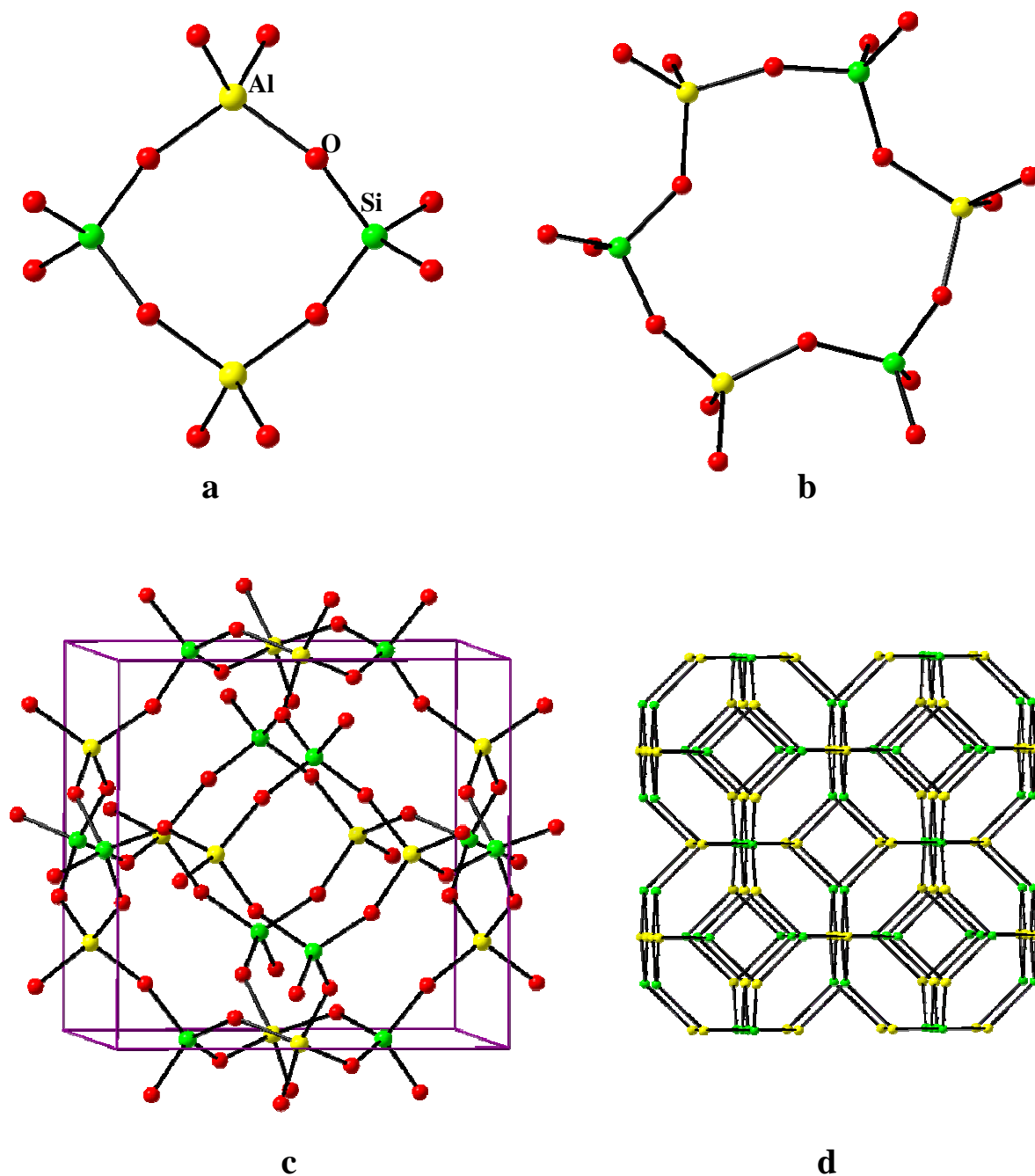


Figure 1.1: (a) Four-membered ring made of AlO_4 and SiO_4 tetrahedra (b) six-membered ring (c) sodalite β -cage within the unit cell edge (d) stacking sequence of the β -cages and the three dimensional network

kind in a given structure. The most common $[\text{Al}_6\text{Si}_6\text{O}_{24}]^{6-}$ framework matrix obviously needs charge compensation to maintain electroneutrality. This is achieved by balancing the negative charges of the framework by a combination of cations and anions being situated in the β -cage. Each cage therefore contains one $[\text{Na}_4\text{Cl}]^{3+}$ cluster in $\text{Na}_8[\text{AlSiO}_4]_6\text{Cl}_2$ sodalite. Chlorine occupies the centre of the cage, and is tetrahedrally coordinated by four sodium cations that are on the cube diagonals. Of course, the shape, and therefore the inner β -cage geometry, of the cluster could be more complex depends on number, proportion and types of the constituent's atoms [8-25]. In addition to charge compensation, these cage clusters serve another important function as they prevent the open framework from collapsing [26, 29].

The space group of the mineral sodalite $\text{Na}_8[\text{AlSiO}_4]_6\text{Cl}_2$ is P-43n [27]. The highest possible symmetry of sodalite isotype is Im-3m. This symmetry is only rarely realised [30]. However it was observed with few high temperature phases of $\text{Sr}_8[\text{Al}_{12}\text{O}_{24}](\text{MoO}_4)_2$ [31], $\text{Sr}_8[\text{Al}_{12}\text{O}_{24}](\text{WO}_4)_2$ [31] and, with some reservation, $\text{Sr}_8[\text{Al}_{12}\text{O}_{24}](\text{CrO}_4)_2$ [32] having one T-atom type in the framework. Pm-3n space group is also known from the high temperature $\text{Na}_8[\text{AlSiO}_4]_6(\text{NO}_3)_2$ sodalite [33]. Usually, one observes lower symmetry and most frequently P-43n (Figure 1.2). As also stated earlier, the cage clusters serve as a form of spacer and when they are smaller than the size corresponding to the maximum expansion (Im-3m), the framework adapts itself to the size of the cage ions [29]. Pauling [26] called this volume reduction a 'partial collapse'. The mechanism by which the framework reduces its cage volume is called tilt mechanism. It consists of cooperative rotations of the corner connected TO_4 tetrahedra about local -4 axis which runs parallel to the unit cell edges of the fully expanded framework (Figure 1.2) [26, 28-34]. Taylor [34] explained that this tilt process also reduces the volume of the unit cell. The tilt mechanism allows the framework to adapt itself the size corresponding to the cage cluster. From the symmetry point of view it destroys the inversion centre but preserves the cubic symmetry (Figure 1.3) as well as the body centring. Therefore the highest possible symmetry for a sodalite having a tilt angle higher than zero is thus I-43m. Some minerals with sodalite-type structure (Bicchulite [35], $\text{Na}_8[\text{AlGeO}_4]_6(\text{OH})_2$ [36] etc.) possess this space group. Most of the common sodalites have two kinds of T-atoms (for example, $\text{Na}_8[\text{Al}_6\text{Si}_6\text{O}_{24}]\text{Cl}_2$). The T-site ordering results in alternate occupation of the TO_4 tetrahedra by Si^{4+} and Al^{3+} . In this way the body centring is destroyed but cubic symmetry is still preserved and the inversion centre, if present. Consequently, the corresponding higher symmetry reduces from I-43m to P-43n [29, 30, 34]. As a matter of fact, all the partially collapsed sodalites consist of T-site ordering or in other words possesses P-43n space group. Notably, the Si-Al ordering played a certain role in the development of Loewenstein's ideas concerning aluminium avoidance rule [37].

Since Pauling [26] sodalite has been a research topic to chemists, mineralogists, crystallographers, solid state physicists and especially to zeolite scientists. Sodalites have

attracted much attention as a model compound to study the discrete β -cage effects on intra-zeolite chemistry for larger and complicated zeolitic systems as β -cages are the building blocks of many zeolites, i.e., A-, X-, and Y-type zeolites. Typical zeolitic reactions are possible in sodalites as they undergo ion exchange reactions, subject to the typical size restrictions imposed by the sixring inter-cavity windows [38]. The facile exchange of silver for sodium has been rationalised in terms of hard /soft acid /base interactions [25, 39]. Reversible dehydration /hydration and its dramatic effect on framework geometry have revealed interesting zeolitic behaviours [40-43].

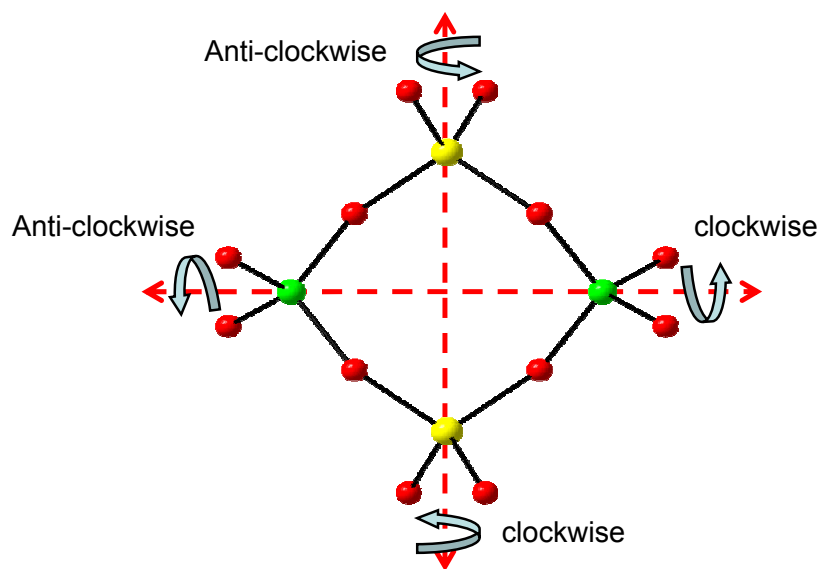


Figure 1.2: Tilt mechanism via the cooperative rotation of the TO₄ tetrahedra about the -4 axis.

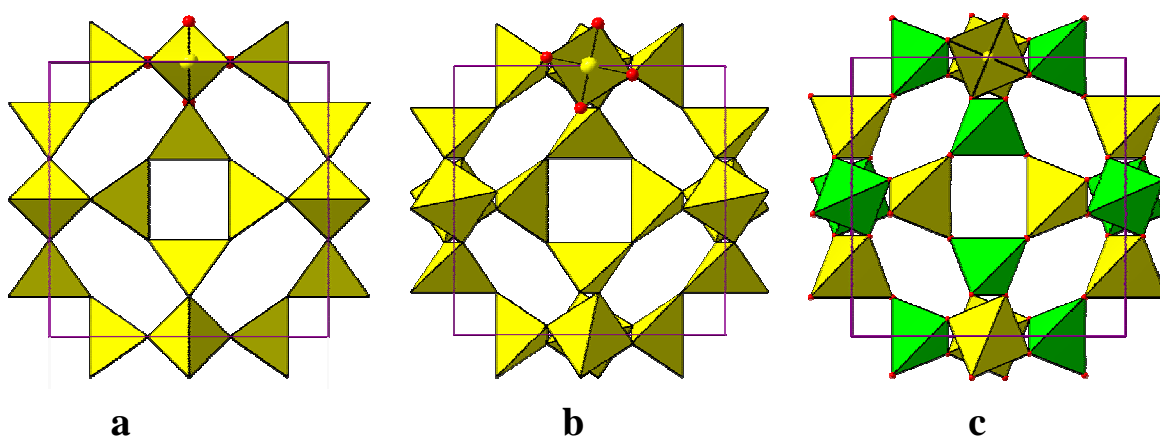


Figure 1.3: Symmetries adapted by the tilt mechanism and types of T-atoms. (a) fully expanded β -cage with one type T-atom (Im-3m), (b) twisted β -cage with single T-atom (I-43m) and (c) twisted β -cage with two types T-atoms (P-43n).

Discrete cubic $(\text{CdS})_8$ was incorporated inside the sodalite cages of zeolite A-, X- and Y- [44]. At low Cd^{2+} loading these clusters were isolated but formed an interconnecting extended supercluster structure as the cluster concentration increased. Moller et al. [45] introduced the CdSe clusters in zeolite Y which are of interest in the study of photosensitised electron transfer reactions utilized for solar energy conversion and photocatalysis. In short, the importance of the β -cage modelling could be realised for the subtle architecture of the advanced zeolitic framework as well as the guest cluster. Sodalites have not been used in the applications involving catalysis or gas separation. However, closer inspection leads to the realisation that the sodalite lattice forms a convenient matrix for encapsulation of a variety of guests, as also cited above, it is possible to form cluster and extended supercluster structures in the quantum sized regime, similar to those semiconductor superclusters [46]. Sodalite entirely comprised of close-packed β -cages rather than the coexisting supercages of other zeolite hosts, thereby permitting direct or through-bond interaction between guests in all cages. By judicious selection of the guest species (anion /cation) one could form packaged insulators and semiconductors as well as metals within the sodalite framework. The composition-dependent optical and electronic tunability of the sodalite analogue $\text{Zn}_8\text{X}_2[\text{BO}_2]_{12}$ (X = O, S, Se) and $\text{Cd}_y\text{Zn}_{1-y}[\text{BeSi}_x\text{Ge}_{1-x}\text{O}_4]_6(\text{X})_2$ (X = S, Se and Te) [47] are some of those advanced materials. Sodalites are dielectric materials with a band gap of approximately 6.1 eV, 5.9 eV and 5.2 eV for chloride, bromide and iodide sodalite, respectively [48]. They can be viewed as a heavily ‘doped’ SiO_2 (1:1) with both p-type (Al) and n-type (alkali metal) ‘impurities’ [49]. Therefore a high probability for trapping charged particles is expected by vapour phase deposition with electron donor and /or acceptors. $\text{Na}_3^{3+} : \text{Na}_4^{3+}$ cluster ratio larger than 1:10 in the β -cage indicates the onset of insulator-metal transition [50].

Sodalites are very interesting for their pro-chromic behaviours: barochromic, hydrochromic, photochromic and cathodochromic [46, 48, 51-65]. Among those, the photochromic and cathodochromic phenomena were thoroughly studied since Medved [51]. Although naturally occurring sodalite exists in various colours (blue, green, pink, magenta, colourless), it is known to be typically blue. Kirk [52] and Bershov et al. [53] had attributed the permanent blue colour due to the presence of sulphur impurities. Photochromism results from the light induced charge transfer from an electron donor to an already existing halogen vacancy [48, 51-65]. Sodalite has been doped with sulphur [48, 54], iron [58], selenium and tellurium [59] to supply the necessary donors. Williams et al. [54] argued that 5 to 10% of the chlorine of normal sodalite ($\text{Na}_8[\text{AlSiO}_4]_6(\text{Cl}\cdot\text{S})_2$) with sulphur gives a product with optimum photochromic response. The colour centre, i.e., an unpaired electron trapped in a chlorine vacancy between four sodium atoms inside the β -cage, was believed to derive its electron from a sulphur species thought to be S_2^{2-} . Williams et al. [54] also concluded that an increasing sulphur will slow down the bleaching rate and further excess will produce a

pigment. A partial substitution of bromine, iodine or fluorine for chlorine appeared either to speed up or slow down the rate of colouration or bleaching, depending on the electronegativity of the halogen concerned. For instance, when bromine is substituted for the chlorine in sodalite the resultant photochromic material develops a purple colour rather than magenta [58]. Additionally, one could note that the absorption peaks of Cl^- , Br^- , and I^- sodalite shift progressively towards longer wavelengths, which correspond to the increasing trend of their lattice parameters [62, 63]. In contrast to photochromism, sodalite cathodochromic behaviour can be explained in two ways: optically reversible cathodochromism and thermally reversible cathodochromism. The first one results from the trapping of an electron in a halogen vacancy site [60, 61]. In this case, many electron hole pairs are created by the primary electron beam. Doping with donor impurities is not necessary. Therefore it implies that $\text{Na}_8[\text{AlSiO}_4]_6\text{Cl}_2$ sodalite can exhibit optically reversible cathodochromism without being photochromic [57-60]. Out of few, Faughnan et al. [60, 61] model is chosen here to explain the thermally reversible cathodochromism of sodalite which suggests that the thermal mode colouration is the result of the presence of double-defect cages caused by the annealing process. A double-defect cage is created by the removal of halogen (Cl^- , Br^- , I^-) and an alkali ion (Na^+) from the ClNa_4 tetrahedra. They propose that when the exciting electron beam strikes the material sodium ions are ejected from their respective positions in the lattice. These ions diffuse throughout the materials to double-defect cages where they take the position of missing alkali ions. The F-centres are formed by the subsequent trapping of electrons at the halogen ion vacancy sites in these cages. In order to erase this type of colouration the temperature must be high enough to cause the sodium ions to diffuse throughout the material back to its original states. The trapped ions are then freed, thus recreating the original uncoloured states. In addition to elaborately studied photochromism and cathodochromism of sodalite, barochromic (white Ag, OH-SOD or Ag, HCO_2 -SOD samples darken upon application of pressure) and hydrochromic (Ag, OH-SOD undergoes a reversible colour change upon dehydration) properties [46] are noteworthy.

The thermal behaviour of sodalites occupies an important position in zeolite research. The uptake of CO_2 at elevated temperature offers a versatile tool for waste management [66]. Heating upon SCN^- , NO_3^- , H_2O , ($\text{OH}\cdot\text{H}_2\text{O}$) etc. enclathrated sodalite have shown interesting intracage redox reactions and phase transitions [22, 67-70]. The sodalite structure has been shown to undergo cation exchange rapidly at high temperature by direct reaction between solids [18]. High temperature ion-exchange reaction has been used to prepare lithium halide sodalites [67]. The rate of these reactions indicates that sodalites are reasonably good ion conductors at these temperatures. Ion conductivity of nitrite sodalite was studied by Weller et al. [71] by a.c. methods. He tuned the conductivity by sodium substitution with silver as well as by temperature variation. Several authors [56, 66, 68-70, 72] reported the phase transitions in sodalite upon progressive heating and their results are in good agreement. Most of them

observed that transition of sodalite to carnegieite occurred at 1173 K to 1273 K and then carnegieite to nepheline at 1423 K to 1473 K. To some extent, the inconsistency of the reported data within a reasonable deviation is mainly due to the specimen composition. For instance, the synthetic (not always in controllable form) and natural chloride sodalite does not contain Cl^- and Na^+ strictly but isomorphic impurities with OH^- , H_2O , S^{2-} are commonly available even along with or /without unoccupied β -cages. By losing all eight water molecules upon dehydration the $\text{Na}_6[\text{ZnPO}_4]_6(\text{H}_2\text{O})_8$ and $\text{Na}_6[\text{ZnAsO}_4]_6(\text{H}_2\text{O})_8$ sodalites transformed their P-43n symmetry into hexagonal phases at 415 K and 448 K, respectively [69]. Gesing [70] reported the hexagonal NaGaSiO_4 phase in the P6_3 space group upon dehydration of the $\text{Na}_6[\text{GaSiO}_4]_6(\text{H}_2\text{O})_8$ composition at 1173 K. Notably, he could not identify two reflections in the mentioned space group and stated that the compound plausibly crystallised in a pseudo-hexagonal orthorhombic space group. Aluminate sodalites [12, 73-75] possessing only AlO_4 tetrahedra in the framework, to some extent, violate the Loewenstein rule [37]. In these materials, with non-spherical anions WO_4^{2-} and CrO_4^{2-} [73-75], the occurrence of superstructure, availability of lower symmetry sodalite than usual, and existence of phase transition are very interesting. $\text{Ca}_8[\text{Al}_{12}\text{O}_{24}](\text{WO}_4)_2$ phase is cubic (I-43m) between 656 K and 783 K only [12]. This cubic phase was characterised by dynamical disorder of the tetrahedral cage anions WO_4 about six equivalent tetragonal orientation states. The resulting structure is, actually, cubic only on the space /time average. The orientational disorder of the relative bulk WO_4 is transmitted as positional disorder of the framework as well as the Ca^{2+} cation inside the β -cage. At a given temperature (studied also at room temperature) this thermally activated process breaks down, the anion disorder condenses, and the cubic symmetry gets lost. This is accompanied by the formation of superstructures and the appearance of spontaneous strain. The above observation was thoroughly studied by Depmeier [12] and further added elsewhere [30]. Very recently Rüscher et al. [33] reported the P-43n \leftrightarrow Pm-3n phase transition in $\text{Na}_8[\text{AlSiO}_4]_6(\text{NO}_3)_2$ sodalite system at an elevated temperature (935 K). At this temperature the sodium ion (8e (x, x, x) in P-43n) becomes statistically distributed on 16i (x, x, x) followed by shift of framework oxygen position (general position in P-43n) to special position ($z = 0.5$) in the Pm-3n space group. The detailed could easily be grasped from the thermal expansion behaviour of several sodalites reported elsewhere [12, 33, 76-81].

The mechanism for thermal expansion of sodalite group minerals is implicit the Pauling [26] description of the structure. Increasing temperature accelerates the movement of the guest atoms (also cited above) occluded in the β -cage thereby increases the volume of the guest cluster, for instance, $[\text{Na}_4\text{Cl}]^{3+}$ in the $\text{Na}_8[\text{AlSiO}_4]_6\text{Cl}_2$ sodalite system (Figure 1.4). As a result: sodium displaces towards the mean plane of the six-membered ring in the $\langle 111 \rangle$ direction, the Na-O distance increases, Na-O' distance decreases, followed by the untwisting of the AlO_4 and SiO_4 tetrahedra and augmentation of Al-O-Si angle. The AlO_4 and SiO_4 groups execute independent rigid body motion without changing their Al-O and Si-O

distances, respectively [69, 71, 74]. The non-linear expansion of cell constant was thus explained mainly from the decreasing of the tilt angles (Figure 1.2). $\text{Na}_8[\text{AlSiO}_4]_6\text{Cl}_2$ sodalite melts at about 1352 K and begins to lose NaCl [74] before going to its fully expanded state though earlier Bhalla [64] stated that the sample with the same composition emitted chlorine at 923 K.

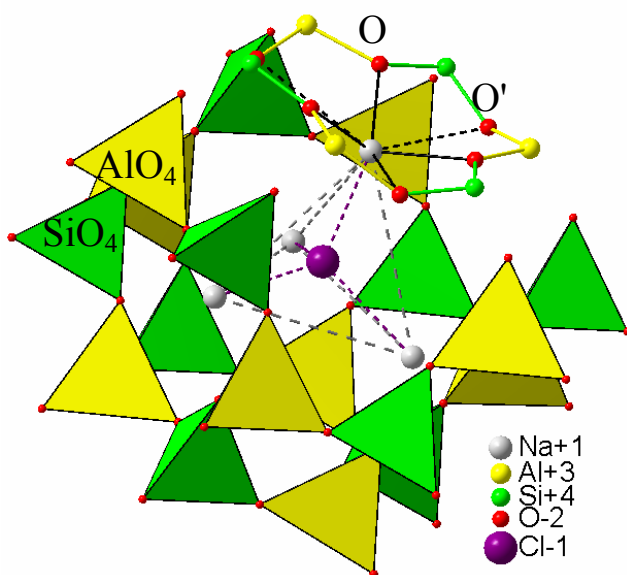


Figure 1.4: Sodalite β -cage occluded with $(\text{Na}_4\text{Cl})^{3+}$ cluster. O and O' are viewed as the nearest and the farthest framework oxygen from sodium, respectively, in the sixring.

On the other hand, exerting pressure on sodalite plays just the opposite role as played by temperature [82-84]. Hazen and Sharp [82] first investigated sodalite under high pressure. They observed that the specimen deteriorated on increasing the pressure above 3.0 GPa while Werner et al. [84] observed the onset of pressure induced amorphisation within the narrow range between 7.3 GPa and 7.4 GPa. One could only argue on the composition of the samples as Hazen and Sharp used the natural $\text{Na}_{7.99}\text{K}_{0.01}[\text{Al}_{5.98}\text{Si}_{5.98}\text{Fe}^{3+}_{0.04}\text{O}_{23.99}]\text{Cl}_{1.98}(\text{SO}_4)_{0.02}$ sodalite while synthetic and natural $\text{Na}_8[\text{AlSiO}_4]_6\text{Cl}_2$ sodalites were used by Werner et al.. Fütterer et al. [17] studied compression mechanism in trioxane silica sodalite employing up to 1.3 GPa. They explained the higher compressibility of this material may due to the differences in the lattice energies or to differences in the steric requirements of the template molecule trioxane in comparison with the $[\text{Na}_4\text{Cl}]^{3+}$ clusters. $\text{Sr}_8[\text{Al}_{12}\text{O}_{24}](\text{CrO}_4)_2$ was found topologically stable up to a pressure of 7.2 GPa, studied by Mezler et al. [83]. They explained the appearance of superstructure reflections were related to two new phase transitions: the first one occurred between 0.37 GPa and 0.5 GPa and the second one at about 2.0 GPa, although the structure of the new phases were not detected due to the experimental limitation. In this connection it is

also noteworthy that phase transitions in sodalites generally lead to problems of pseudosymmetry [83] and are characterised by very small deviations from the cubic high temperature-ambient pressure phase because of the fact that the weak reflections or some peak splittings are often observed below the resolution limit of conventional X-ray technique.

Isomorphous substitution both in the host and guest species offers the availabilities of a large variety of natural and synthetic sodalites [1-25]. Complete isomorphous substitution in the framework T-sites of sodalites has long been a study of much interest in zeolite chemistry. Some specific properties of the sodalites depend on the structural composition of the framework and thereby substituting the T-atoms lead to a variation of the physical-chemical properties. Sodalites with silicon and aluminium sites fully substituted by germanium and gallium, respectively, with several guest species were reported [8, 70, 85-88]. Partial substitution of silicon with germanium in the $\text{Na}_8[\text{AlSi}_x\text{Ge}_{1-x}\text{O}_4]_6\text{Br}_2$ was reported by Perlmutter et al. [90]. Tranjan et al. [63] described the F-centre properties as a function of germanium substitution within the same composition. Catalytic implications of T-atom substitution was reviewed by Tielen et. al. [89]. Gallium substitution in the tectosilicate framework could play a vital role in catalytic point of views [91]. Gallium containing zeolite catalyst was reported by Thomas and Liu [85] for the conversion of short chain paraffin into aromatics. Partial isomorphous substitution for aluminium with gallium revealed an extensive isomorphous miscibility in the $\text{Na}_{6+x}[\text{Al}_{1-y}\text{Ga}_y\text{SiO}_4]_6\text{Y}_x(\text{H}_2\text{O})_{8-4x}$ sodalite system for various 'x', 'y' and 'Y' magnitudes. The tuning of sixring window of β -cage is inevitably important almost all in the above studies: ion exchange, F-centre concentration, metal guest cluster ratio ($\text{Na}_3^{3+}:\text{Na}_4^{3+}$), ionic conductivity, extended supercluster structure, band gap engineering etc., which could be done by successive partial T-site substitution.

From these important point of views the author has been highly motivated and therefore chose the $\text{Na}_{6+x}[\text{Al}_{1-y}\text{Ga}_y\text{SiO}_4]_6\text{Y}_x(\text{H}_2\text{O})_{8-4x}$ sodalite system. The present study will mainly be involved with synthesis and characterisation of sodium alumosilicate, gallosilicate and alumogallosilicate nitrite, chloride, bromide, hydro-hydroxy and hydro sodalites. The Al/Ga ratio in the trivalent T-site of the respective sodalite frameworks was systematically controlled, which leads to carry much interest in zeolites, mineralogy and crystallography as well advanced material sciences.

2 EXPERIMENTAL METHODS

2.1 SYNTHESIS

Samples were synthesised by means of hydrothermal synthesis. All the syntheses were carried out in the alkaline medium using NaOH solution. The concentration was varied batch to batch according to the appropriate requirement. Na_2SiO_3 was used as silicon source in all the experiments. In some cases binary oxide sources (Ga_2O_3 and $\gamma\text{-Al}_2\text{O}_3$) were used. However, in most of the syntheses NaAlO_2 and NaGaO_2 were chosen appropriate for aluminium and gallium sources, respectively. NaGaO_2 was prepared from 1.8g of Na_2CO_3 and 3.2g of Ga_2O_3 at 1073 K for 48 hours in a platinum crucible. NaCl, NaBr and NaNO_2 salts were used for the purpose of occlusion in the sodalite β -cages as guest species. Hydro sodalites were obtained via exchange washing procedure in a 100 ml beaker within a controlled pH value of about 5.5 to 6.5 using acetic acid. Gallosilicate hydro sodalites was produced from gallosilicate iodide sodalite via autoclave exchange experiment. Hydro-hydroxy sodalites were used as source materials for corresponding hydro sodalite compositions. Deionised water was used in all purposes concerning synthesis and washing. The amounts of starting materials for a particular sodalite composition and the corresponding reaction conditions are summarised in the respective sections. The appropriate amounts of powdered reactants were put into a 50 ml Teflon-coated steel autoclaves. All the reactions were carried out at autogenous pressure. The products were washed through some subsequent centrifugal processes by decanting the mother liquor and finally dried at 373 K for ~ 24 hours.

2.2 X-RAY POWDER DIFFRACTION

Philips PW 1800 diffractometer, with Bragg-Brentano geometry using graphite monochromised CuK_α radiation, was frequently used to check the quality and phase of the products only. Brucker D4 was also used in this purpose. Notably, these XRD data were not used for structure refinements in any case. Almost all the structures were refined from x-ray powder data collected with a STOE STADI P diffractometer in transmission mode fitted with Debye-Scherrer geometry using a focusing germanium (111) monochromised $\text{CuK}_{\alpha 1}$ radiation with positional sensitive detector (PSD). The intensity data were carried out from 10 to 90 two theta (2θ) with a step width of 0.02 2θ and a collection time of 20 to 90 sec /step at room temperature. In some cases Brucker D8 coupled with Göbel mirror was also used to collect the XRD data for structure refinements. The powder samples were ground with an agate mortar and put into a glass capillary of 0.3 mm diameter and finally sealed.

2.3 XRD POWDER DATA RIETVELD REFINEMENT

Structure refinement of each sodalite composition was performed using the Rietveld refinement software RIETAN 97 [92]. During the refinements, general parameters as the scale factor, maximum twelve background parameters, the zero point of the counter and six profile parameters (U, V, W, X, Y, asymmetry) were optimised. Additionally, the cell parameters, the atomic positional parameters, displacement parameters were refined. In some cases linear constraints were used for occupancy and displacement parameters. Linear restraints were rarely used only for framework T-O interatomic distances. The diversities and types of the Rietveld refinements were elaborately explained for different sodalite types in different sections.

2.4 FTIR SPECTROSCOPY

Fourier transform infrared (FTIR) spectra were performed on a Bruker IFS 66v/S spectrometer in a range of 370 cm^{-1} to 4000 cm^{-1} using the KBr method. 1-2 mg sample was mixed with about 200 mg dried KBr and the pellets were made at a pressure of about 1 Kbar. In fact, the FTIR data have served three important purposes throughout the investigations: (1) the bending /stretching modes of the occluded guest species, (2) the asymmetric stretching (ν_{As} T-O-T), symmetric stretching (ν_s T-O-T) and bending (δ O-T-O) modes and their respective role to the corresponding structure and (3) one of the δ O-T-O modes was used to calculate the Al/Ga ratio in the alumogallosilicate sodalite systems.

2.5 MAS NMR SPECTROSCOPY

Magic angle spinning nuclear magnetic resonance for the ^{29}Si isotopes (^{29}Si MAS NMR) measurements were recorded on Bruker Avance DSX 400 and Bruker Avance DSX 200 spectrometers (Solid State NMR Lab., University of Toronto), Bruker ASX 400 (Institut für Geologie, Mineralogie und Geophysik der Ruhr-Universität Bochum) spectrometer using standard 4 mm and 7 mm MAS probes at 79.49 MHz with a spinning rate of 4-10 KHz. 3 μs single pulse duration and 10 s recycle delay were used for ^{29}Si NMR. On the other hand, ^1H MAS NMR was performed on Bruker ASX 400 using a standard 4 mm MAS probes at a spinning rate of 14 KHz. 2 μs second single pulse and 5 second recycle delay were used. Chemical shifts were determined using tetrakis-(trimethylsilyl)-silan ($\text{Si}(\text{Si}(\text{CH}_3)_3)_4$, -9.885 ppm from TMS) and TMS as external standard. The peaks of different spectra were fitted with 'dmfit2003' software [93]. The Ga/Al ratios for several compositions were accounted

from the analytical integration of the different NMR peaks fitted with Gaussian /Lorentzian profiles (Figure 2.1).

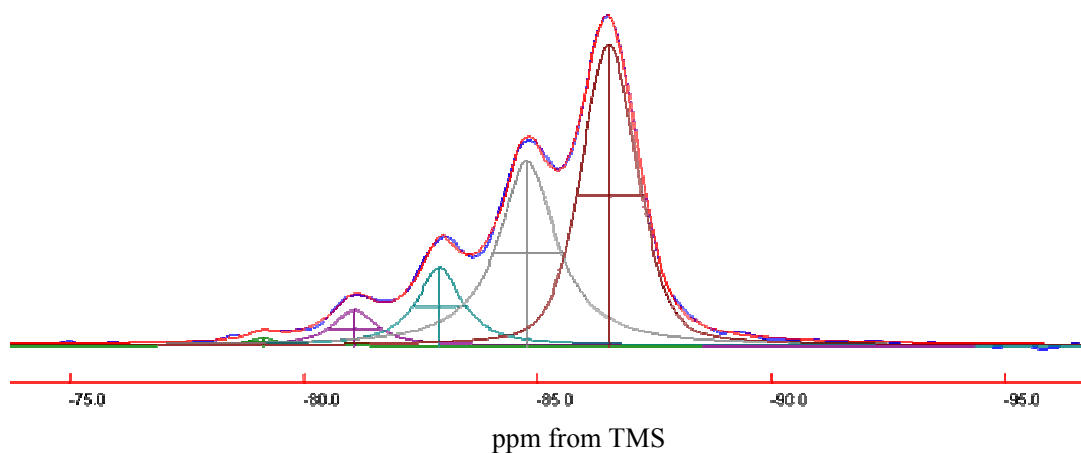


Figure 2.1: ^{29}Si MAS NMR fit spectra.

2.6 CHEMICALS

The chemical substances used in the present study are summarised in the Table 2.1.

Table 2.1: Different chemicals used in syntheses

Substance	Company	Code Number
Na_2SiO_3	Aldrich	30.781-5
$\gamma\text{-Al}_2\text{O}_3$	Merck	413595
Ga_2O_3	Aldrich	21.506-6
NaAlO_2	Riedel-de Haen	13404
NaOH	Fluka	71691
Na_2CO_3	Merck	9658662
NaCl	Merck	1.06404.1000
NaBr	Fluka	71330
NaNO_2	Fluka	71759
CH_3COOH	Riedel-de Haen	27221

3 GALLIUM SUBSTITUTED ALUMOSILICATE NITRITE SODALITES

3.1 INTRODUCTION

NO_2^- containing sodalites were studied as gas sensors [98], ion conductors [71] and intracage redox materials [67]. Theoretical studies of the dynamics of discrete NO_2^- inside the β -cage [99] added a new and interesting dimension to establish the real position of this particular oxoanion. Recently in a conference contribution a series of partial trivalent T-site substituted sodalites [96] were reported, from which this present study follows up with this series of partial gallium substituted aluminosilicate nitrite sodalites. These synthesised alumogallosilicate nitrite sodalites provide relevant information concerning the framework order-disorder for the simultaneous presence of three T-atoms in the framework when the six-ring window is tuned with the Al/Ga ratios in the trivalent T¹-sites. The present study also includes detailed structural features along with possible dynamical behaviour of NO_2^- inside the sodalite β -cage (Figure 3.1).

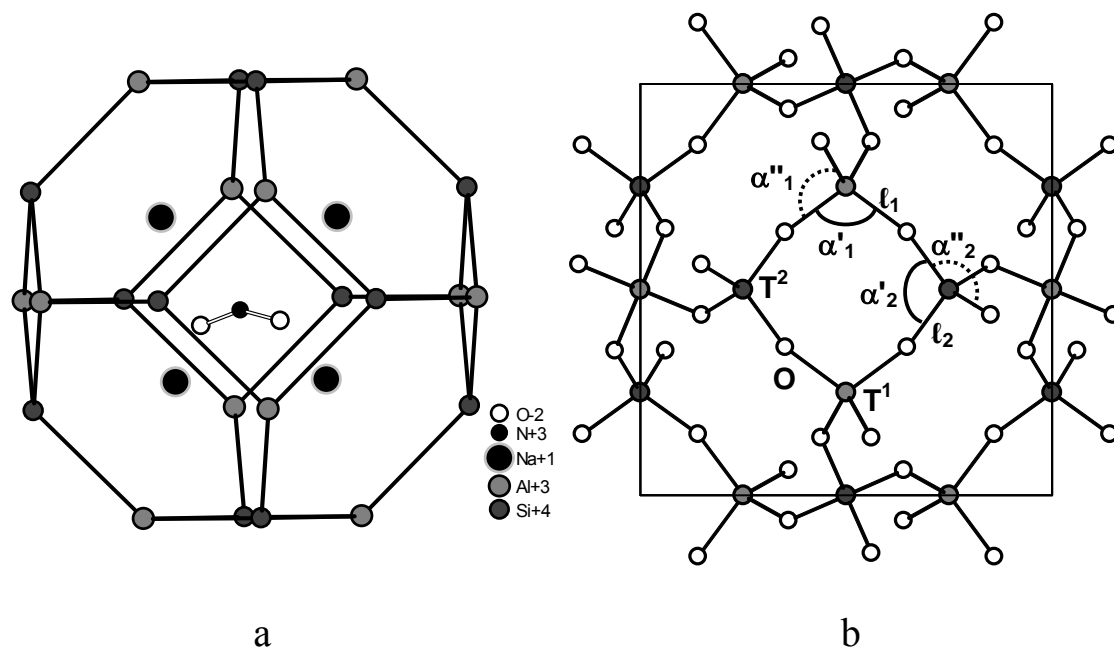


Figure 3.1: (a) Sodalite β -cage occluded with NO_2^- in one possible orientation. (b) Upper half of sodalite β -cage in $\langle 100 \rangle$ direction along with the T^1O_4 (Al/GaO₄) and T^2O_4 (SiO₄) tetrahedra. α' and α'' are the O-T-O angle of TO_4 tetrahedron linked with four-membered and six-membered ring, respectively. l_1 is the corresponding T¹-O distance. For the T² coordination the parameters are subscripted 2.

3.2 RESULTS AND DISCUSSION

3.2.1 SYNTHESIS

The results of the hydrothermal syntheses are summarised in Table 3.1. Whereas the Ga concentration in the refined sodalites was controlled by the initial amount of NaAlO₂ and NaGaO₂, a high amount [8] of NaNO₂ (15 g) was used to avoid the formation of basic nitrite sodalite [100]. Due to the mild reaction conditions (473 K, autogenous pressure) the products were obtained as white polycrystalline powders. Corresponding single crystal formation requires stronger conditions, i.e., 570 K and 0.1 GPa [101]. In the reaction liquid, an alkalinity of 2M NaOH was chosen because of good solubility of NaAlO₂, NaGaO₂ and Na₂SiO₃ and the observed higher yields of product in contrast to other syntheses done using higher NaOH concentrations.

Experiments using these starting materials with 8M or higher NaOH concentrations produced a few milligrams of the pure alumosilicate nitrite sodalites or clear solution, respectively, and gallium was rarely observed in the resultant powder. Using binary oxide sources of aluminium and gallium (γ -Al₂O₃ and Ga₂O₃) required more alkaline reaction solutions (6-8M NaOH) due to the poor solubility of aluminium oxide in 2M NaOH. These experimental conditions also resulted in a poor gallium concentration in the framework compared to the theoretical stoichiometry [90, 95].

Table 3.1 provides a comparison of the initial gallium concentration of the starting materials with the amount present in the final product. The use of a high initial concentration of aluminium results in the incorporation of the majority of gallium present in the starting materials (Figure 3.2). By increasing the gallium concentration the relative incorporation shifts towards aluminium. At high initial concentrations of gallium (~ 70%), this behaviour begins to change and at very high gallium concentrations the ratio of aluminium to gallium in the framework is again close to the initial concentrations in the starting materials. This might indicate that the alumosilicate sodalite is more stable than the corresponding gallosilicate sodalite. Therefore the uptake of aluminium is higher during the synthesis with a low initial gallium concentration. However, if the amount of gallium is too high in the reaction solution, the number of available gallium atoms overcomes this stabilising effect.

Table 3.1: Experimental data of the hydrothermal synthesis

Starting materials ¹		Yield /g	Na ₈ [Al _{1-y} Ga _y SiO ₄] ₆ (NO ₂) ₂	
NaAlO ₂ /g	NaGaO ₂ /g		Initial y	Refined y
1.00	0.00	0.75	0	0
1.00	0.40	0.91	21	17
1.00	0.50	1.20	25	20
1.00	0.60	1.17	28	22
1.00	0.80	1.13	34	30
0.60	1.00	0.94	52	37
0.50	1.00	1.21	57	47
0.30	1.00	0.84	69	55
0.20	1.00	0.85	77	60
0.15	1.00	0.82	81	63
0.10	1.00	0.76	87	70
0.10	1.60	0.95	91	85
0.10	2.13	1.66	93	90
0.00	2.00	1.59	100	100

¹2g Na₂SiO₃, 15g NaNO₂, 20 ml 2M NaOH, 48 h at 473 K in all cases.

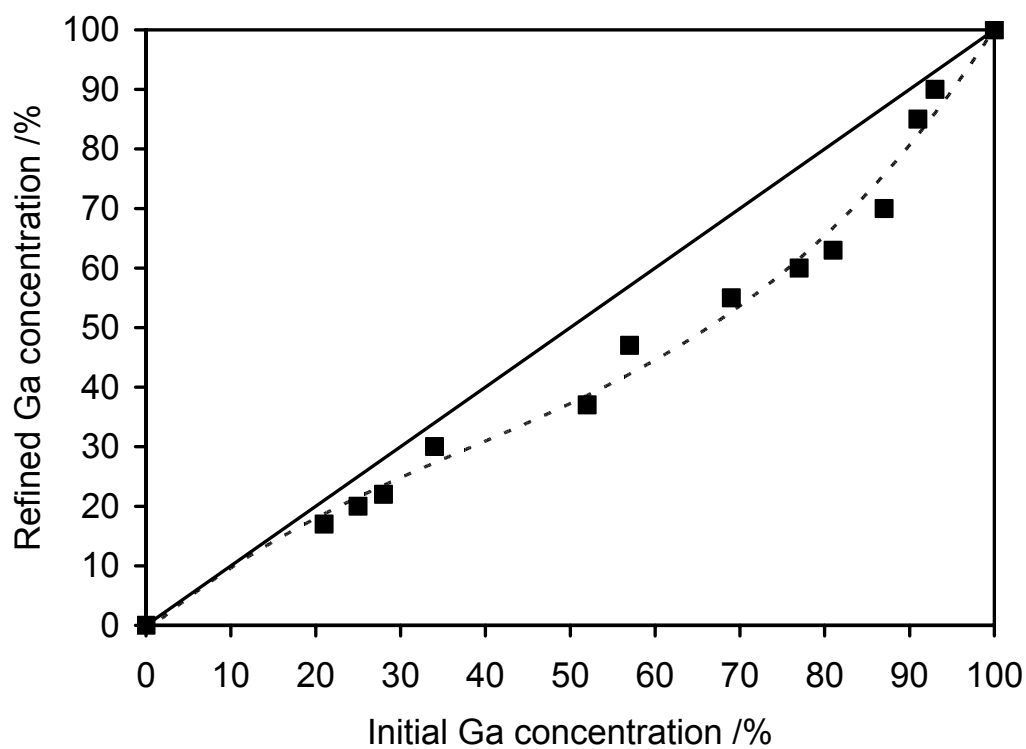


Figure 3.2: XRD refined Ga concentration vs. initial stoichiometry. The solid straight line represents concentration equivalence.

3.2.2 XRD INVESTIGATIONS AND RIETVELD REFINEMENTS

The XRD refined compositions along with several defining crystallographic parameters of the $\text{Na}_8[\text{Al}_{1-y}\text{Ga}_y\text{SiO}_4]_6(\text{NO}_2)_2$ sodalites are summarised in Table 3.2 (see Attachment). The important geometric parameters are plotted in Figure 3.1 and are listed in Tables 3.3 and 3.4. The graph shown in Figure 3.3a is a generic example for all Rietveld refinement results. The initial atomic positional sites and fractional coordinates for the X-ray data Rietveld refinements in the space group P-43n were taken from Sieger et al. [102]. The gallium and aluminium atoms were placed in the same crystallographic position (6c). The occupancy parameters of both atom types were constrained in such a way that the amount of gallium is one minus the amount of aluminium. For the refinement of the displacement parameters of these two atoms, one has to take into account that the gallium nucleus is significantly heavier than the aluminium nucleus. Therefore, the vibrational amplitude of gallium atoms and the resulting displacement parameter is expected to be lower than the corresponding behaviour of aluminium atoms. Nevertheless, we have refined the displacement parameters of these two types of atoms with constrained values. Calculations performed in the absence of linear constraints for these parameters lead to negative values for one atom and high positive values

Table 3.3: Selected interatomic distances [pm], angles [degree], average tilt (ϕ) [degree] and sixring window diameter (d_6) [pm]

T ¹ -site	Al/Ga-O	Si-O	Na-O(1)	O(1)-O(1)	α'_1/α''_1	α'_2/α''_2	γ	ϕ	d_6
[Al]	174.0(3)	162.6(3)	233.6(3)	374.4(3)	112.1(1)....4x 108.2(1)....2x	114.0(1) 107.3(1)	139.6(2)	21.6(1)	190.3(4)
[Al _{0.83(1)} Ga _{0.17(1)}]	175.0(5)	163.2(6)	233.4(3)	372.3(6)	112.1(2)....4x 108.2(2)....2x	114.0(2) 107.2(2)	138.5(4)	22.4(2)	189.6(4)
[Al _{0.80(1)} Ga _{0.20(1)}]	174.3(2)	163.9(2)	232.8(3)	372.2(3)	112.3(1)....4x 108.1(1)....2x	114.1(1) 107.2(1)	138.5(1)	22.4(1)	188.0(7)
[Al _{0.78(1)} Ga _{0.22(1)}]	174.6(2)	162.4(2)	233.9(3)	373.8(3)	112.1(1)....4x 108.2(1)....2x	114.1(1) 107.2(1)	139.3(1)	21.8(1)	190.0(4)
[Al _{0.70(1)} Ga _{0.30(1)}]	174.7(3)	163.8(3)	232.5(3)	371.3(4)	112.6(1)....4x 108.0(1)....2x	114.5(1) 107.0(1)	138.2(2)	22.4(1)	186.7(5)
[Al _{0.64(1)} Ga _{0.36(1)}]	176.8(2)	162.6(2)	232.2(3)	370.2(3)	112.6(1)....4x 107.9(1)....2x	115.0(1) 106.8(1)	137.6(1)	22.7(1)	185.5(4)
[Al _{0.53(1)} Ga _{0.47(1)}]	175.3(2)	164.1(2)	232.8(3)	371.2(3)	112.4(1)....4x 108.0(1)....2x	114.3(1) 107.1(1)	137.9(1)	22.8(1)	186.6(4)
[Al _{0.44(1)} Ga _{0.56(1)}]	177.2(2)	162.8(2)	232.6(3)	371.1(3)	112.5(1)....4x 108.0(1)....2x	115.0(1) 106.8(1)	137.4(1)	22.9(1)	186.5(4)
[Al _{0.40(1)} Ga _{0.60(1)}]	177.1(2)	163.4(2)	232.5(3)	370.1(3)	111.8(1)....4x 108.3(1)....2x	114.1(1) 107.2(1)	137.1(1)	23.6(1)	185.3(4)
[Al _{0.37(1)} Ga _{0.63(1)}]	177.3(3)	164.0(3)	232.3(3)	369.1(4)	111.8(1)....4x 108.3(1)....2x	114.1(1) 107.2(1)	136.6(2)	24.0(1)	184.2(5)
[Al _{0.30(1)} Ga _{0.70(1)}]	178.5(3)	163.7(3)	231.8(4)	368.0(5)	111.8(2)....4x 108.3(1)....2x	114.3(1) 107.1(2)	136.0(2)	24.4(2)	183.0(6)
[Al _{0.15(1)} Ga _{0.85(1)}]	179.9(2)	162.8(2)	232.1(3)	368.4(3)	111.2(1)....4x 108.6(1)....2x	114.0(1) 107.3(1)	135.8(1)	24.8(1)	183.4(4)
[Al _{0.10(1)} Ga _{0.90(1)}]	181.0(2)	162.3(2)	231.7(3)	367.0(3)	111.2(1)....4x 108.6(1)....2x	114.4(1) 107.1(1)	135.4(1)	25.0(1)	181.8(4)
[Ga]	182.7(3)	161.3(3)	231.7(4)	366.5(4)	111.2(1)....4x 108.6(1)....2x	114.9(2) 106.8(2)	134.9(2)	25.2(2)	181.2(5)

for the other atom along with an estimated standard deviation (e.s.d.) that was 49 times higher than anticipated. Since the silicon site (6d) was always obtained fully occupied, the possibility for a T-site composition such as $[(Al_{1-y}Ga_y)_zSi_{1-z}]$ ($0 < z < 1$) was discounted. This will be further discussed in the NMR section 3.2.3. When free displacement parameters were tried for nitrogen (N1) and nitrite oxygen (O2), incompatible output was obtained which mired the refinement. However, when the displacement parameter for sodium was tried along with the constrained values of the corresponding N(1) and O(2), the results did not hamper the occupancy factor of sodium. In all cases, the sodium occupancy fluctuation was within 1% deviation, whether it was treated as fixed or free. In the final run, sodium occupancy was fixed as fully occupied along with the respective charge required to balance the non-framework N(1) and O(2).

Table 3.4: Selective interatomic distances [pm] and angles [degree]

T1-site	Na-O(2)···3x	Na-O(2)···3x	Na-N	N-O(2) ^a	O(1)-O(2)	O(2)-N-O(2) ^b
[Al]	251(5)	263(6)	245.8(9)	125(3)	344(5)	108(2)
[Al _{0.83(1)} Ga _{0.17(1)}]	240(5)	261(5)	241.4(9)	129(2)	344(4)	103(2)
[Al _{0.80(1)} Ga _{0.20(1)}]	241(2)	272(3)	240.3(89)	122(9)	343(3)	107(7)
[Al _{0.78(1)} Ga _{0.22(1)}]	261(4)	262(4)	240.1(14)	113(14)	355(3)	112(5)
[Al _{0.70(1)} Ga _{0.30(1)}]	259(10)	261(11)	242.1(11)	118(4)	350(10)	112(4)
[Al _{0.66(1)} Ga _{0.36(1)}]	257(10)	264(7)	243.0(15)	112(10)	353(8)	113(7)
[Al _{0.53(1)} Ga _{0.47(1)}]	249(8)	276(12)	244.9(13)	112(9)	347(1)	116(6)
[Al _{0.44(1)} Ga _{0.56(1)}]	246(5)	270(6)	246.4(11)	116(4)	345(5)	114(4)
[Al _{0.40(1)} Ga _{0.60(1)}]	248(5)	263(3)	243.9(11)	117(3)	349(2)	113(1)
[Al _{0.37(1)} Ga _{0.63(1)}]	249(5)	253(6)	243.0(12)	118(5)	355(5)	110(3)
[Al _{0.30(1)} Ga _{0.70(1)}]	249(14)	256(14)	240.8(14)	118(3)	353(11)	112(4)
[Al _{0.15(1)} Ga _{0.85(1)}]	248(6)	249(6)	244.6(10)	121(2)	352(3)	111(1)
[Al _{0.10(1)} Ga _{0.90(1)}]	248(7)	248(7)	243.1(12)	119(3)	353(4)	110(3)
[Ga]	244(6)	250(6)	244.9(12)	117(4)	354(4)	111(3)

^adistances are corresponding to that angles^b

To some extent, NO_2^- dynamical disorder was studied along with possible sodium hopping. From these calculations, the refinement offered evidence that the NO_2^- group be redefined as a quasi rigid body inside the sodalite β -cage. During this refinement no linear restraints (bond angles, bond lengths) were used within this oxoanion, however, O(2) was covalently bonded to N(1). In contrast with other atoms, the high e.s.d. (estimated by conventional method [92]) of N(1) and O(2) positional coordinates merely define their exact positions. This conventional XRD method does not localise highly disordered low scattering atoms accurately. Therefore, the refined NO_2^- geometries do not represent true values, but an averaged internuclear separations and angles (Table 3.4).

The enlarged middle range of the mixed phases ($0 < y < 1$) XRD profiles (Figure 3.3b) did not show any indication of domains or domain boundaries. The half-width of the reflections implies that each sample is a single phase with similar average crystal size, and

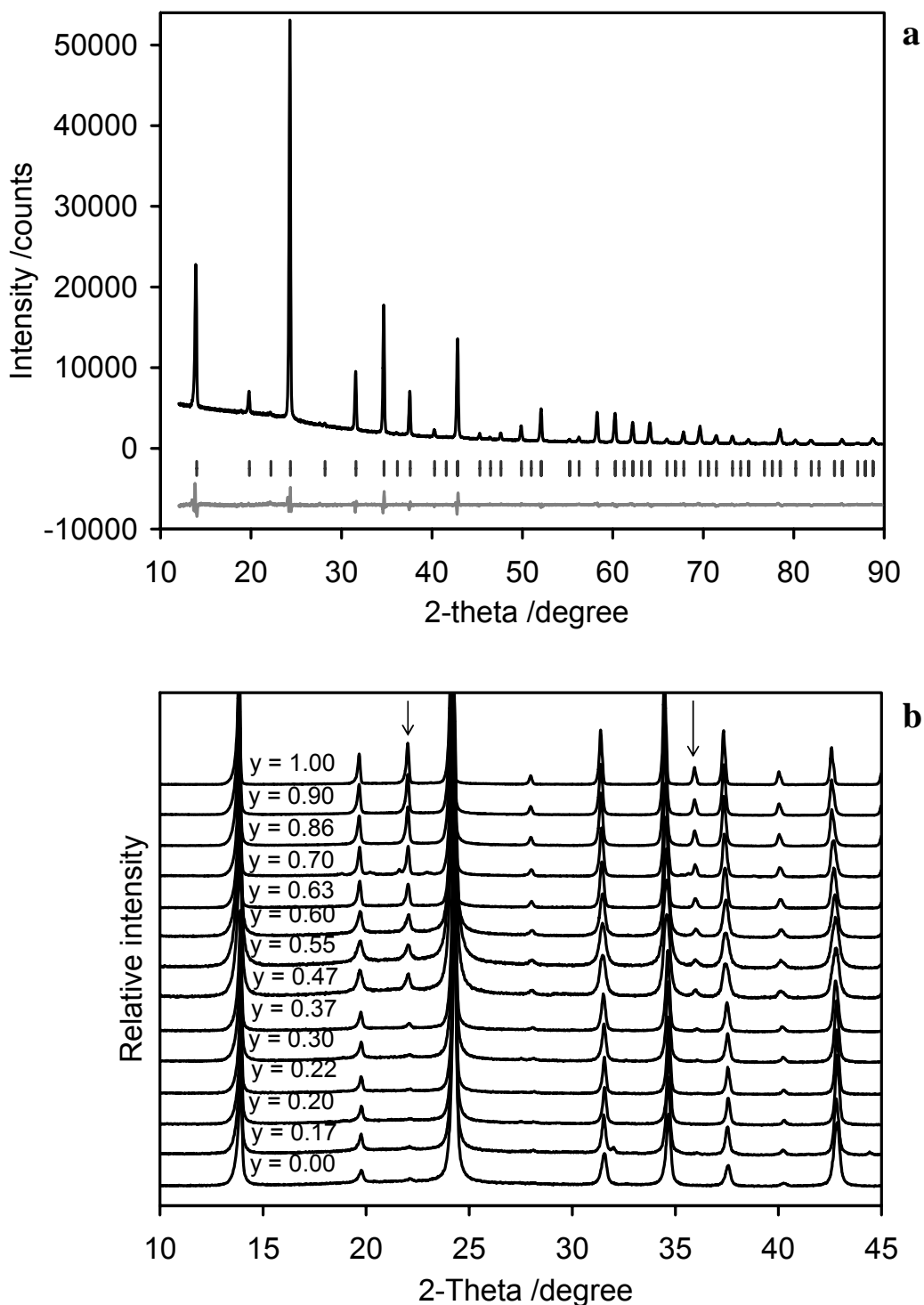


Figure 3.3: (a) Rietveld Plot of $\text{Na}_8[\text{Al}_{0.80(1)}\text{Ga}_{0.20(1)}\text{SiO}_4]_6(\text{NO}_2)_2$ sodalite with observed intensities (top graph), difference between observed and calculated intensities (lower graph) and possible Bragg reflections (middle graph). (b) X-ray powder diffraction patterns of $\text{Na}_8[\text{Al}_{1-y}\text{Ga}_y\text{SiO}_4]_6(\text{NO}_2)_2$ sodalites where the $[h + k + l = 2n + 1]$ reflections are shown with downward arrow.

statistical distribution of the gallium and aluminium throughout the whole crystalline phase.

Several structural trends were observed with increasing gallium concentration in the $\text{Na}_8[\text{Al}_{1-y}\text{Ga}_y\text{SiO}_4]_6(\text{NO}_2)_2$ system. The cell parameters increase with increasing gallium concentration (Figure 3.4a) at the trivalent T^1 -site of the framework. This linear behaviour is similar to those of the $\text{Na}_8[\text{Al}_{1-y}\text{Ga}_y\text{SiO}_4]_6(\text{Cl}/\text{Br})_2$, $\text{Na}_6[\text{Al}_{1-y}\text{Ga}_y\text{SiO}_4]_6(\text{H}_2\text{O})_8$ and $\text{Na}_{6+x}[\text{Al}_{1-y}\text{Ga}_y\text{SiO}_4]_6(\text{OH}\cdot\text{H}_2\text{O})_x(\text{H}_2\text{O})_{8-4x}$ sodalites [96]. The T^1 -O distances also increase with increasing gallium content (y), while the T^2 -O distances remain almost constant at 163.0 pm within 1.5σ (Figure 3.4b). This result indicates that the type of occupancy of the T^1 -site and its concentration determines the T^1 -O distance. Sodalites with one type of T-atom or a statistical distribution of more than one type of T-atom (identical T^1 -O and T^2 -O distances) results in the I-43m space group [70, 103]. Any deviation between T^1 -O and T^2 -O distances occurs due to different types of T-atoms and the structure can be described by the P-43n space group. A distinction could easily be seen through systematic absence in the X-ray diffraction. First, the presence of $[h + k + l = 2n+1]$ planes in our $\text{Na}_8[\text{Al}_{1-y}\text{Ga}_y\text{SiO}_4]_6(\text{NO}_2)_2$ system ensures the primitive space group and second the absence of any indication of superstructure or domains shows that AlO_4 and GaO_4 tetrahedra are statistically distributed in the T^1 -sites. Therefore the T^1 -O distance does not reflect either Al-O or Ga-O distances, but denotes an averaged distance of Al/Ga-O. The relative intensity of the $[h + k + l = 2n+1]$ planes increases with increasing 'y'. Therefore, it is possible to check the refined gallium concentration by calculating the relative intensity of the $[h + k + l = 2n+1]$ planes (Figure 3.3b). If the average crystal size remains similar one would also be able to determine the degree of partial ordering (formation of domains) of AlO_4 and GaO_4 tetrahedra from the FWHM. Nevertheless, the FWHM-behaviour indicates only a small fluctuation in the different samples, which can be explained by small variations in the average crystal size.

The increasing strain in the sodalite framework could be released through two possible pathways: by increasing (1) tilt angle [4, 29] and (2) tetragonal tetrahedra distortion [29]. Figure 3.5a shows a linear relationship between the tilt angle (φ) and T^1 -O distance, which increases with increasing gallium concentration. The O-T-O distortion ($\Delta\alpha_1 = \alpha'_1 - \alpha''_1$), in the presence of increasing gallium concentration, decreases in the T^1O_4 tetrahedra, but increases through discontinuities in the T^2O_4 tetrahedra ($\Delta\alpha_2 = \alpha'_2 - \alpha''_2$) as is shown in Figure 3.4c. In addition, the averaged $\Delta\alpha$ trend remains unchanged, which may indicate that the local TO_4 tetrahedra adapt preferred geometries with respect to the tilt to release the imposed strain. Additionally, distortion in one type of TO_4 could possibly be reduced by alternating with the second type of TO_4 by mutual adaptation.

With increasing tilt angle, the T-O-T (γ) angle must decrease (Table 3.3) because of the geometrical correlation of these parameters [29].

An additional correlation, $\rho \sim \cos(T-O-T) / [\cos(T-O-T) - 1]$, exists between the T-O-T angle and the degree of framework oxygen *s*-hybridisation (ρ) [104]. Megaw [105] reported that silicate linkage T-O-T oxygen prefers $\rho = 0.45$ ($\rho = 0.50 \equiv \gamma = 180^\circ \equiv sp$; $\rho = 0.33 \equiv \gamma = 120^\circ \equiv sp^2$; $\rho = 0.25 \equiv \gamma = 109.47^\circ \equiv sp^3$ and $\rho = 0.45 \equiv \gamma = 145^\circ \equiv sp^{1.23}$).

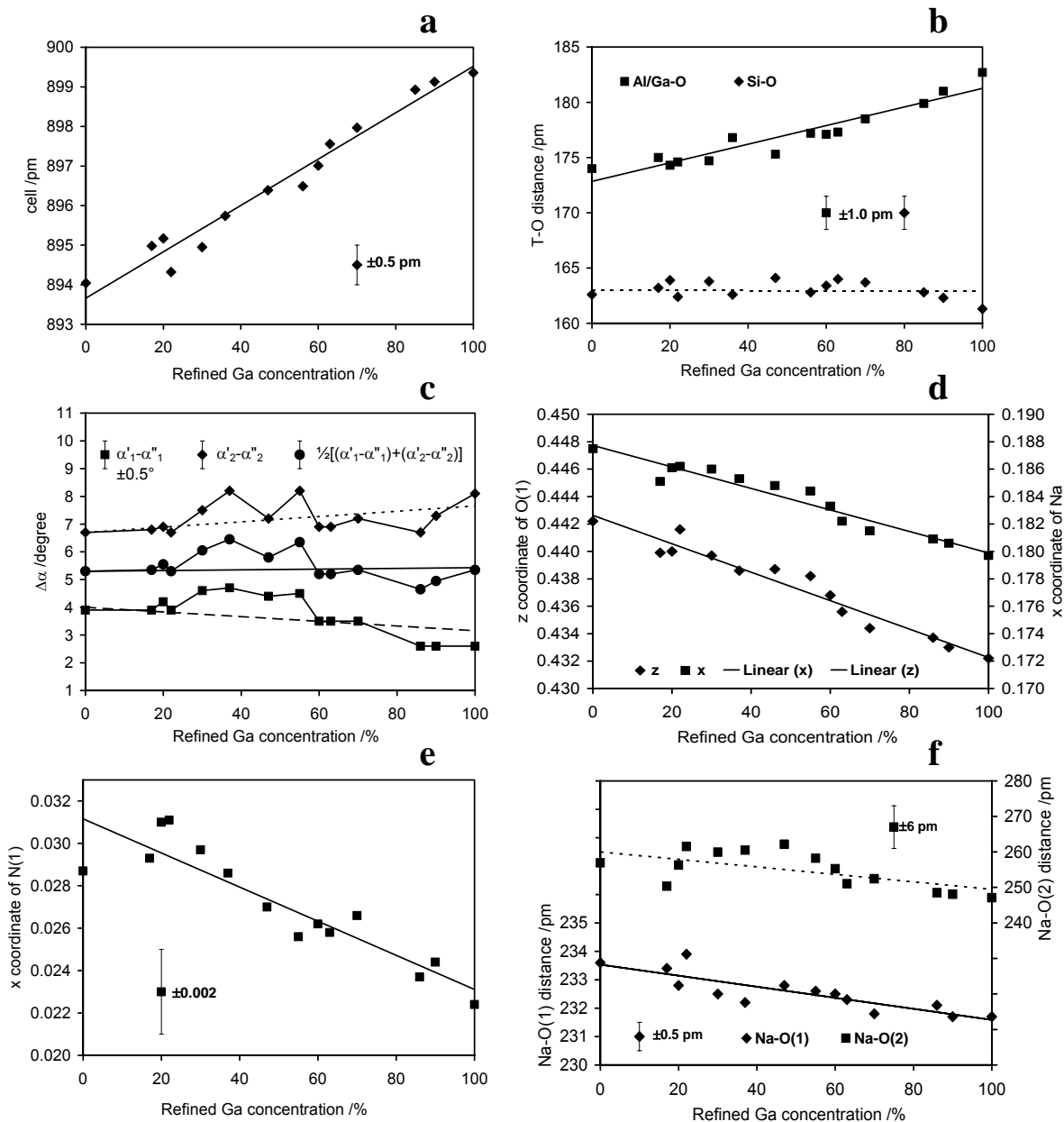


Figure 3.4: Structural parameters vs. refined Ga concentration (a) unit cell, (b) T-O distances, (c) tetragonal tetrahedra distortion of Al/GaO₄ (α_1) and SiO₄ (α_2) together with their average values, (d) fractional coordinate of the framework oxygen z parameter and Na (x,x,x), (e) fractional coordinate of N(1) (x,x,x), (f) Na-O distances. In all cases, trend lines have been fitted to the plotted data.

Figure 3.5b (ρ vs. average T-O distance) indicates that the stability of the T-O-T linkage and thus the stability of the sodalite framework gradually decreases with increasing T-O distance. The repulsion between the T-O bond electrons and the O(1) lone pair electrons probably increases or shifts resulting in a reduction in γ and thereby ρ . Extrapolation of the observed ρ values to 0.33, Figure 3.5b, will provide the theoretical makeup of the most distorted sodalite possible. This theoretical sodalite may not be synthesised because of the unusual T-O-T angle (120°) known to tectosilicates.

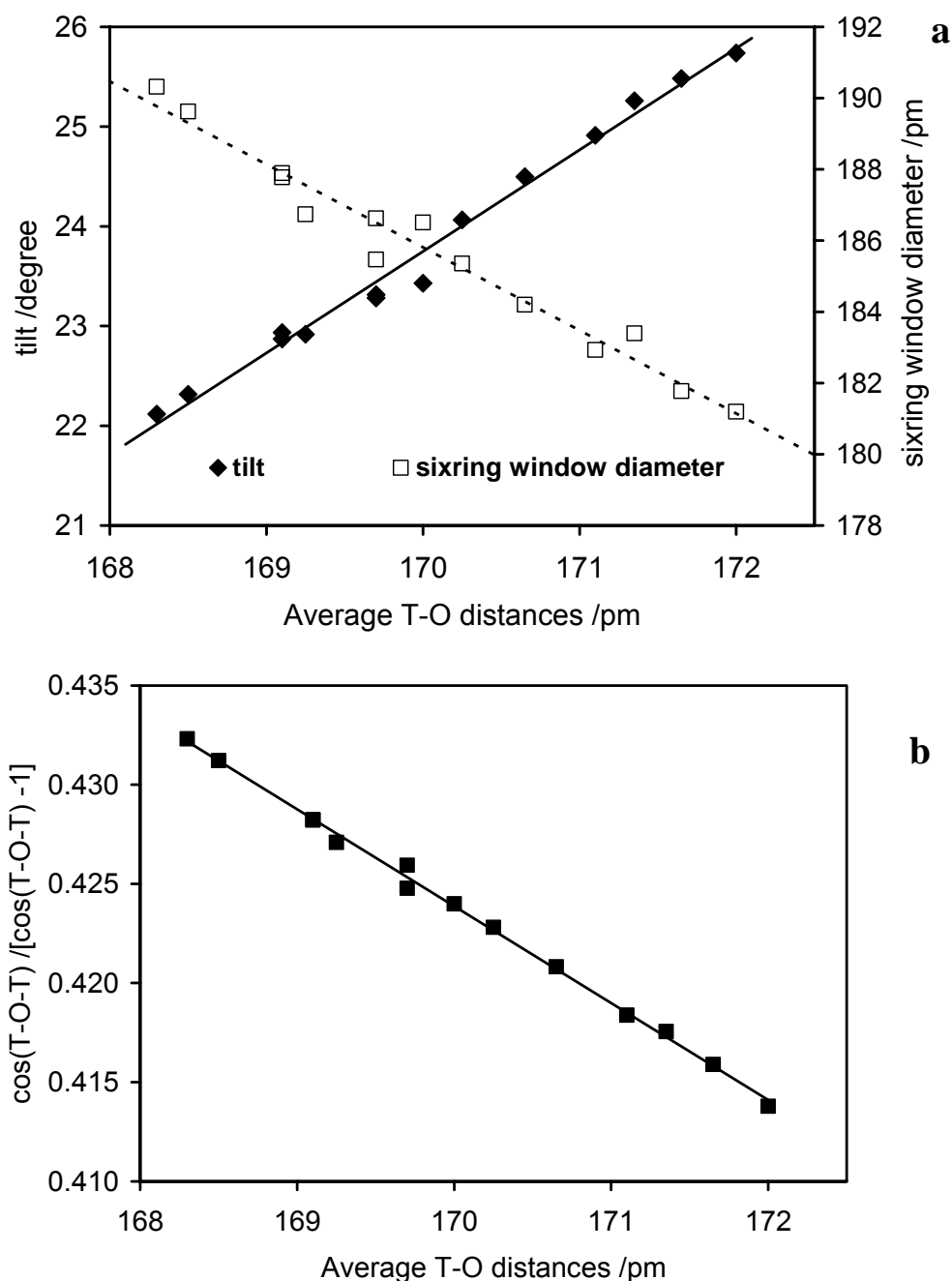


Figure 3.5: Structural parameters vs. T-O distances (a) tilt angle and six-ring window diameter, (b) degree of framework oxygen *s*-hybridisation (ρ)

The type (shape, size, charge) and location of the guest species largely determines the T-O-T angle for a particular framework. In general, the higher the guest volume, the greater the T-O-T angle at room temperature, i.e., $\text{Na}_8[\text{AlSiO}_4]_6\text{Cl}_2$: $\gamma = 138.1^\circ$, $\text{Na}_8[\text{AlSiO}_4]_6\text{Br}_2$: $\gamma = 140.4^\circ$, $\text{Na}_8[\text{AlSiO}_4]_6\text{I}_2$: $\gamma = 144.5^\circ$ [106]. Longer average T-O distances with relatively smaller guests could lead to lower T-O-T angles (higher deviation from $\rho = 0.45$) but the corresponding sodalite formation could not be easily determined. Consequently, the empty cage sodalite hydrothermal synthesis is rarely discussed because sodalites with empty cages can only exist after dehydration of a water containing sodalite [107].

The dimension of the six-ring window (d_6) is directly related to the framework oxygen position that is correlated to several structural features (T-O-T, T-O, tilt) for a particular cation (M) and guest species (Y). The effective cylindrical pathway (Figure 3.1b) was calculated from the equation: $d_6 = 2[d_o/\sqrt{3}-r_o]$ where d_o is the O(1)-O(1) bond length nearest to the bottleneck of the six-ring window and r_o is the oxygen radii (121 pm [108]). The six-ring window diameter decreases with increasing gallium content or average T-O distance (Figure 3.5a), and this is in agreement with the observation by Nenoff et al. [95] for different framework types.

With increasing amounts of gallium in the framework, both the framework oxygen 'z' coordinate magnitude and the Na 'x' coordinate decrease linearly (Figure 3.4d) even with increasing cell parameters. As a result, the Na-O(1) distance decreases with increasing 'y' (Figure 3.4f), which is mainly influenced by increasing tilt. This result may be assigned to the interaction between the framework atoms and non-framework atoms via electrostatic correlation. The refined NO_2^- geometries (Table 3.4) are in agreement with the Sieger et al. single crystal investigation (model I) [102] as well as the theoretical calculations of Fois et al. [99]. A centre ward repulsive force thus could be traced like that of reported structure investigation [96] as Na-O(2) distance (calculated average from two nearby possible Na-O(2) distances) decreases with decreasing Na-O(1) (Fig. 3.4f). But for a possible highly disordered dynamics of the NO_2^- group, O(2) position fractional coordinates could not be localised properly. The average deviation was ~ 6 pm within a total range of ~ 15 pm, which made the position of the NO_2^- group difficult to resolve. In other words, it provides poor conformation to claim the shortening of Na-O(2) distances. In the same way, the NO_2^- volume (possible spherical space where NO_2^- dynamics thought to be occurred within) compaction /expansion can not be drawn from the N-O(2) distances except an idea from the trend of the nitrogen 'x' coordinate (Figure 3.4e). Fois et al. [99] showed that NO_2^- in nitrite sodalite is actually in a rotational state, where the nitrite ion changes the orientation of its molecular axis with respect to the crystallographic axis, and that this rotation occurs around the centre of the β -cage. This motion is fast (~ 100 femtoseconds calculated by first-principle molecular dynamics simulation) compared to typical scattering experiments data collections (\sim hours).

3.2.3 MAS NMR INVESTIGATIONS

In the ^{29}Si MAS NMR spectra (Figure 3.6a), a single peak at -86.4 ppm (FWHM = 1.6 ppm, $x\text{Gauss}/(1-x)\text{Lorentz} = 0.03$) was observed for $\text{Na}_8[\text{AlSiO}_4](\text{NO}_2)_2$. This chemical shift appeared to be located between the corresponding chemical shifts observed by Engelhardt et al. (-85.6 ppm) [110] and Johnson et al. (-86.6 ppm) [106]. As well, this chemical shift also agreed with the relationship, $\delta/\text{ppm} = 1.89 - 0.631*(\text{T-O-T})/^\circ$, proposed by Weller and Wong [111] for aluminosilicate sodalites. The calculated chemical shift that was obtained for the pure aluminosilicate sodalite ($y = 0$) in this study was -86.2 ppm. However, the pure gallosilicate sodalite, $\text{Na}_8[\text{GaSiO}_4](\text{NO}_2)_2$, showed a corresponding $\delta(^{29}\text{Si})$ at -80.0 ppm (FWHM = 0.94 ppm, $x\text{Gauss}/(1-x)\text{Lorentz} = 0.55$), similar to the observed value of -79.8 ppm [106]. The single peak observed for both end members indicates a single silicon environment. Partial isomorphous substitution in the trivalent T¹-site leads to five possible environments around the SiO_4 tetrahedra: $\text{SiO}_4(\text{Ga}_4)$, $\text{SiO}_4(\text{Ga}_3\text{Al})$, $\text{SiO}_4(\text{Ga}_2\text{Al}_2)$, $\text{SiO}_4(\text{GaAl}_3)$ and $\text{SiO}_4(\text{Al}_4)$ in the $\text{Na}_8[\text{Al}_{1-y}\text{Ga}_y\text{SiO}_4](\text{NO}_2)_2$ sodalite for $0 < y < 1$. Therefore, five corresponding signals were observed in Figure 3.6a for the varying Ga/Al ratios. Table 3.5 summarises the peak position, halfwidth and integrated intensity for each of these intermediate sodalites. By comparing the intensity of these five peaks, one can prove that the AlO_4 and GaO_4 tetrahedra are statistically distributed throughout the entire crystalline matrix for the whole series ($0 < y < 1$).

Table 3.5: ^{29}Si MAS NMR fit results. The chemical shift (δ /ppm), the halfwidth (FWHM /ppm) and the integrated peak intensity (I_{int}) divided by 10^4 are given together with the calculated gallium concentration.

Ga% (XRD)	$\text{SiO}_4(\text{Ga}_4)$			$\text{SiO}_4(\text{Ga}_3\text{Al})$			$\text{SiO}_4(\text{Ga}_2\text{Al}_2)$			$\text{SiO}_4(\text{GaAl}_3)$			$\text{SiO}_4(\text{Al}_4)$			Ga% (NMR)
	$\delta(^{29}\text{Si})$	FWHM	I_{int}	$\delta(^{29}\text{Si})$	FWHM	I_{int}	$\delta(^{29}\text{Si})$	FWHM	I_{int}	$\delta(^{29}\text{Si})$	FWHM	I_{int}	$\delta(^{29}\text{Si})$	FWHM	I_{int}	
0													-86.36	1.62	24.4	0
20(1)	-79.36	1.85	7.9	-81.11	1.14	13.3	-82.98	1.53	50.9	-84.76	1.30	70.2	-86.50	1.48	156.1	20(2)
22(1)	-79.63	1.35	4.0	-81.01	1.25	9.7	-82.73	1.25	19.1	-84.46	1.17	37.9	-86.31	1.13	98.2	18(2)
37(1)	-79.50	1.36	28.2	-81.31	1.19	44.3	-83.13	1.51	62.7	-84.86	1.24	56.2	-86.55	1.59	99.8	37(2)
47(1)	-79.77	1.57	49.4	-81.40	1.13	21.8	-83.03	1.51	29.5	-84.69	1.25	27.1	-86.39	1.44	61.3	46(2)
60(1)	-79.72	1.11	87.2	-81.51	1.05	45.8	-83.27	1.35	35.8	-84.77	1.16	28.5	-86.47	1.21	43.2	61(2)
70(1)	-79.88	0.93	153.2	-81.67	0.95	32.3	-83.21	1.18	28.9	-84.94	1.28	34.8	-86.62	1.27	41.9	69(2)
100(1)	-80.00	0.94	25.4													100(2)

Assuming a complete statistical distribution of the aluminium and gallium atoms throughout the sodalite matrix, one would expect an orderly shift in the intensities of the Q₄ peaks seen in the ^{29}Si NMR spectra for the entire sodalite series ($0 < y < 1$). A shift in the intensities of the Q₄ peaks is clearly visible in the aluminogallosilicate chloride sodalite series (Figure 3.6b taken from [112]). However, in contrast to the expected results for a statistical distribution, behaviour inconsistent with such a distribution was observed. In the case of 20% incorporation of gallium into the aluminosilicate sodalite, the ^{29}Si MAS NMR spectrum appears as was expected for a statistical distribution of Al and Ga at the T¹-site. For the aluminosilicate sodalite containing 45% gallium content (47% calculated from X-ray, Table 3.5, Figure 3.6a),

the intensity of the $\text{Si}(\text{OGa})_4$ and $\text{Si}(\text{OAl})_4$ peaks are significantly higher than those of the other three configurations. This result provides clear evidence for a non-statistical distribution, indicating that there are aluminium and gallium enriched domains in the crystals. However, no evidence of these domains could be detected in the X-ray patterns. Therefore, it must be assumed that these domains are smaller than the coherence length of the X-ray radiation but large enough to be detected by MAS NMR technique.

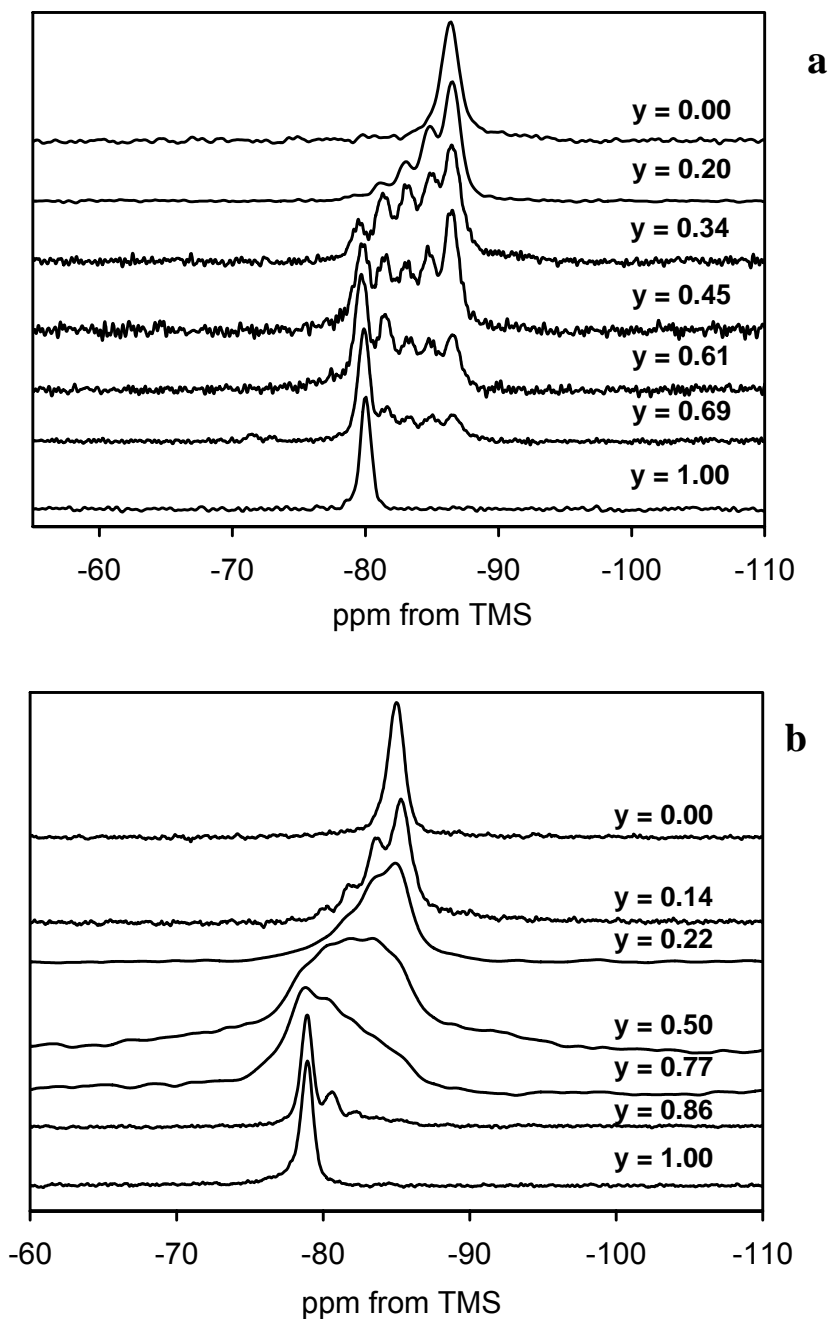


Figure 3.6: ^{29}Si MAS NMR of $\text{Na}_8[\text{Al}_{1-y}\text{Ga}_y\text{SiO}_4]_6(\text{NO}_2)_2$ (a) and $\text{Na}_8[\text{Al}_{1-y}\text{Ga}_y\text{SiO}_4]_6\text{Cl}_2$ (b), taken from [47]); ‘y’ was calculated from NMR fit results.

One may note that it looks like we can observe a higher strain parameter in the X-ray reflection profiles of the samples of around 50% gallium content in the slightly broader reflex bottoms (Figure 3.3b). If this is true, the fluctuation in the tetragonal tetrahedra distortion (Figure 3.4c) is not given by errors during the parameter calculations could be resolved as a second hint for a higher strain, close to the 50% gallium containing samples, which decreases towards both end members. The same effect could be seen from the stoichiometric relation given in Figure 3.2. The highest deviation from the initial gallium concentration could be found at a refined gallium concentration of about 50%. But these observations need to be confirmed through further investigations. Additionally, the ^{29}Si MAS NMR spectra suggests that $\text{Si}/\text{Al}_{1-y}\text{Ga}_y = 1$ in the framework which agrees with the XRD results of fully occupied silicon positions in each phase. Five distinct peaks were observed in the ^{29}Si MAS NMR spectra and were fit within e.s.d's (Table 3.5). It could also be shown that each aluminium substitution with gallium in the $\text{SiO}_4(\text{Al})_4$ species lead to an approximate downfield shift of 1.3 ppm. By determining the area of these five peaks in the ^{29}Si MAS NMR spectra one could calculate the Ga/Al ratio. In this study the peaks in each spectra were fitted using the 'dmfit2003' [93] program and their corresponding Ga/Al ratios were determined. The degree of halfwidth deviation of each peak was within reasonable error, confirming that the calculations from the fit were reliable. The calculated Ga/Al ratios resulting from ^{29}Si MAS NMR are in good agreement with those determined from the XRD refined results (Table 3.5).

3.2.4 FTIR INVESTIGATIONS

Infrared spectra in the mid-infrared range (MIR, 370 cm^{-1} to 4000 cm^{-1}) were recorded for the entire series. In all cases, a sharp absorption band corresponding to the NO_2^- group was observed at 1267 cm^{-1} (Figure 3.7a). In general, the characteristic OH^- and H_2O bands were absent, although, in a few samples very weak bands of H_2O were observed. These bands were attributed to traces of surface water, since any formation of basic /hydro nitrite sodalite $\text{Na}_8[\text{Al}_{1-y}\text{Ga}_y\text{SiO}_4]_6(\text{OH}\cdot\text{H}_2\text{O})_x(\text{NO}_2)_{2-x}$ [100] could be easily confirmed through deviations in cell parameters. NO_3^- , as an oxidised form of NO_2^- , was not found in any phase. Therefore the template composition as was confirmed by the X-ray data, was the same for all of the sodalites in this study.

Asymmetric T-O-T stretching (ν_{as} T-O-T), symmetric T-O-T stretching (ν_{s} T-O-T) and bending O-T-O (δ O-T-O) modes were observed from 370 cm^{-1} to 1200 cm^{-1} (Figure 3.7a). The ν_{as} T-O-T stretching bands were observed with several maxima within a broad range between 800 cm^{-1} and 1200 cm^{-1} for $0 \leq y \leq 1$. Due to a large FWHM value (50 cm^{-1}) and mode overlapping, the exact positions of the different bands in this region were difficult to resolve. However, Figure 3.7c confirmed the presence of one, three and two maxima that are related to $y = 0$, $0 < y < 1$ and $y = 1$, respectively. These three bands were better resolved for y

~ 0.50 which clearly indicates the presence of three different T-atoms in the framework by showing three corresponding stretching modes. Although a shift could be supposed, it was poorly resolved. Three bands of $\nu_s T^{IA}-O-T^2$ (732 cm^{-1} , 708 cm^{-1} , 665 cm^{-1} and $T^{IA} = \text{Al}$, $T^2 = \text{Si}$), and five bands of $T^{IG}-O-T^2$ (634 cm^{-1} , 639 cm^{-1} , 643 cm^{-1} , 576 cm^{-1} , 553 cm^{-1} where $T^{IG} = \text{Ga}$) were observed for the end members of the alumosilicate and gallosilicate framework, respectively. Both the $\nu_s T^{IA}-O-T^2$ mode (Set-A) and $\nu_s T^{IG}-O-T^2$ mode (Set-G) were seen for $0 < y < 1$ and their positions change with a very small shift from one end member to the other (Figure 3.7b). The intensity of Set-A decreases with increasing gallium concentration in the T^1 -site, while the intensity of Set-G increases. Therefore Set-A/G intensity ratio is a function of Al/Ga concentration. It should be noted that additional bands of $\nu_s T^{IA}-O-T^{IG}$ were not observed and therefore the extended Loewenstein's aluminium avoidance rule [37] was not violated in the mixed Al/Ga framework. These results are in complete agreement with corresponding alumogallosilicate hydro, hydro-hydroxy, chloride and bromide sodalites [96].

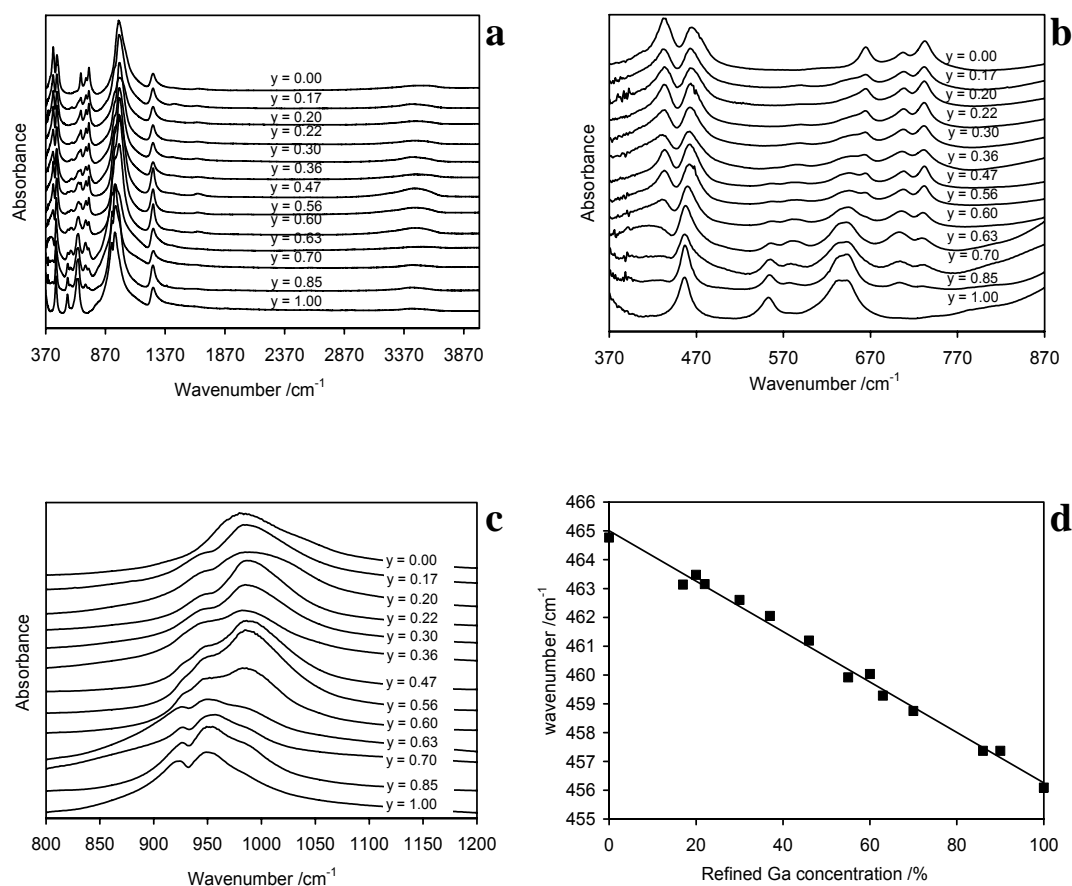


Figure 3.7: (a) FTIR of $\text{Na}_8[\text{Al}_{1-y}\text{Ga}_y\text{SiO}_4]_6(\text{NO}_2)_2$, (b) enlarged '(a)' between 370 cm^{-1} to 870 cm^{-1} , (c) enlarged '(a)' between 800 cm^{-1} to 1200 cm^{-1} , (d) wavenumber [$\delta(\text{O-T-O})$] vs. refined Ga concentration.

Two δ O-T-O bands were observed for the aluminosilicate sodalite framework [109] although only one band is observed for the gallosilicate system. One of these δ O-T-O bands was observed at 432 cm^{-1} for the pure aluminosilicate framework. As the gallium concentration increased, this band gradually decreased in intensity and shifted to lower wavenumbers and finally disappeared in the pure gallosilicate matrix (Figure 3.7b). The second δ O-T-O band was observed at 465 cm^{-1} and although it retained its intensity, the band shifted to lower wavenumbers along with increasing gallium concentration. Using this linear relationship (Figure 3.7d), one could check the Al/Ga ratio in the framework from the regression curve: $\text{Ga \%} = 5271.04 - 11.335W$ ($R^2 = 0.992$, $W = \text{wavenumber /cm}^{-1}$). Since the halfwidth of this band was $\sim 20\text{ cm}^{-1}$, a value almost double that of the total shift, this equation cannot be used to gain any significant data on gallium concentrations from the infrared spectra. However, one can clearly see the high correlation between the position of this mode and the refined gallium concentration from the X-ray powder data. Therefore, this is indirect proof for the correctness of using the refined gallium content as the real compositional parameter.

3.3 CONCLUSION

Partial substitution of aluminium by gallium revealed an extensive isomorphic miscibility in the $\text{Na}_8[\text{Al}_{1-y}\text{Ga}_y\text{SiO}_4]_6(\text{NO}_2)_2$ sodalite system. Each composition for $0 < y < 1$ is isotopic to the end members ($y = 0$ or 1). The Ga/Al ratio was controlled by selective initial stoichiometry in the hydrothermal synthesis. The gallium concentration in the framework was always lower than the theoretical maximum concentration calculated from the starting precursors. For the structural parameters, several linear relationships were observed depending on the increasing concentration of Ga atoms in the framework, including the lattice parameter changes from 893.5 pm to 898.9 pm for the aluminosilicate to gallosilicate sodalite, respectively; the tilt of the framework tetrahedral; the six-ring window diameters and the Al/Ga-O distances. The Si-O distances were determined to be constant for the whole series at 163.0 pm ($\sigma \sim 1.0$). The Al/Ga-O-Si linkage stability was derived on the basis of the framework oxygen *s*-hybridisation. The fractional coordinate of both nitrogen and oxygen of NO_2^- were observed within high deviation (max. up to third decimal). Therefore the position of those atoms could hardly be localised. The NO_2^- geometry does not bear the true N-O(2) distance and O(2)-N-O(2) angle rather possible internuclear separations and positions only. Out of these the NO_2^- was assumed to be in high disordered dynamics or in a rotational state and this rotation occurs around the centre of the β -cage. The calculation of gallium concentration from the position of the δ O-T-O bending mode may possibly be an easy and fast technique if one could clearly resolve the peak maximum. The possible domain formation can be checked by further single crystal investigations. Raman spectroscopy would be interesting studies for this nitrite sodalite series with increasing cell parameter along with the sixring tuning.

4 GALLIUM SUBSTITUTED ALUMOSILICATE CHLORIDE AND BROMIDE SODALITES

4.1 INTRODUCTION

Substitution of T-atom within the sodalite host framework is known in the natural minerals, i.e. helvine [4]. Complete isomorphous substitution in the framework T-sites of sodalites has long been a study of much interest in zeolite chemistry [8, 70, 86, 87]. Partially substituted gallium zeolite structures have been shown to be catalytically important [97]. Cathodochromic behaviour was studied as a function of cell parameter within the same template where the cell parameters were varied by partial substitution of T-atoms [63]. From these important points of view, partial T-sites substitution in the sodalite framework could lead to carry much interest in material science of controlled change in the framework properties as well as of pore selectivity in an orderly manner. The structural modifications of chloride and bromide sodalites will lead to change the physical-chemical properties by tuning the sixring aperture of the β -cage (Figure 4.1). In a recent conference contribution partial T-site substituted sodalites [96] were reported. On this basis we report here the synthesis and characterisation with detailed structural features of gallium substituted aluminosilicate $\text{Na}_8[\text{Al}_{1-y}\text{Ga}_y\text{SiO}_4]_6(\text{Cl}/\text{Br})_2$ sodalites ($0 < y < 1$) along with the corresponding end members ($y = 0$ or 1).

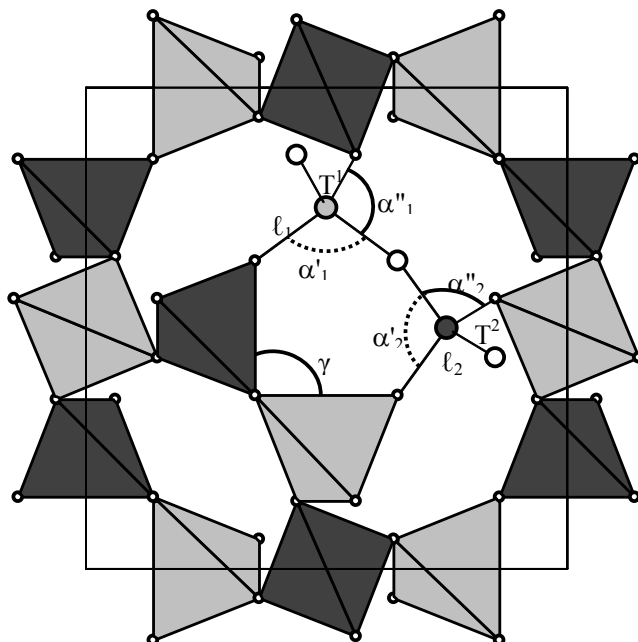


Figure 4.1: (a) Sodalite β -cage in $\langle 100 \rangle$ direction along with the Al/GaO_4 (T^1O_4) and SiO_4 (T^2O_4) tetrahedra. α' and α'' are the O-T-O angle of TO_4 tetrahedron linked with four-membered and six-membered ring, respectively. l_1 , l_2 are the corresponding T^1 -O and T^2 -O distances and ' γ ' represents the T-O-T angle.

4.2 RESULTS AND DISCUSSION

4.2.1 SYNTHESIS

The results of the hydrothermal syntheses are summarised in Table 4.1. Three different synthesis routes were performed in the chloride sodalite system (Figure 4.2) to control the Al/Ga ratio in the framework $[Al_{1-y}Ga_ySiO_4]$ ($0 < y < 1$) from the initial stoichiometry. Using $NaAlO_2$ and $NaGaO_2$ as source materials for aluminium and gallium, respectively, together with 8M NaOH solution (Route A, Figure 4.2) shows that the refined gallium concentration in the framework is significantly different from the initial gallium feed. Probably the used 8M alkaline concentration is too high for the crystallisation of a gallium enriched sodalite due to high solubility of sodium gallate in the reaction solution. Additionally, gallosilicate chloride sodalite could not be produced (within the starting materials amount, Table 4.1) via this route. For instance, even 50% gallium in the initial stoichiometry produces a poor gallium content of 4% in the alumogallosilicate sodalites (Table 4.1) whereas corresponding 100% initial feed produce no sodalite rather than a clear alkaline solution. Furthermore, the amount of yields seems to be a function of initial aluminium amount (Table 4.1, Route A). In contrast to Route A, using 8M NaOH solutions together with binary oxide sources of aluminium and gallium

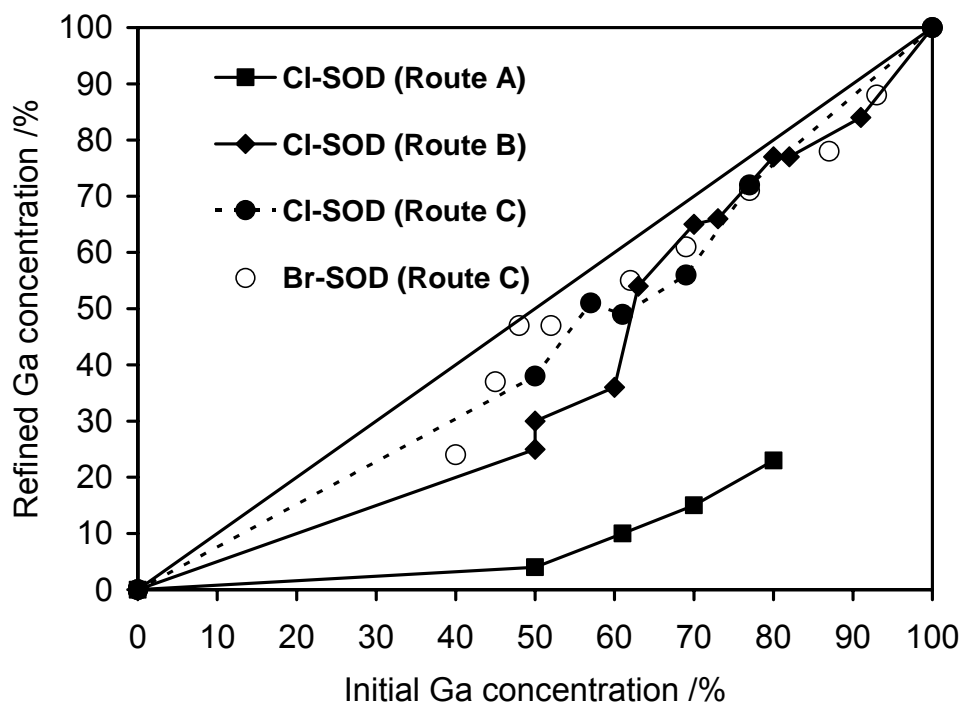


Figure 4.2: Refined Ga concentration from X-ray data vs. initial stoichiometry. The solid straight line represents concentration equivalence. The reaction routes are named according to the starting materials described in Table 4.1.

(γ - Al_2O_3 and Ga_2O_3) (Route B) the refined gallium concentration in the framework approaches more closely to the equivalence line (Figure 4.2) and the total yields (Table 4.1) are higher. On the other hand, using NaAlO_2 and NaGaO_2 together with 2M NaOH (Route C) shows the nearest refined gallium concentration to the initial feed although the amount of synthesised samples are smaller compared to Route B. A dominating role of aluminium could be assumed by comparing the initial feed of aluminium and the amount of products. Due to the maximum gallium content in the framework compared to the rest two routes, we selected Route C for the synthesis of bromide sodalites. The refined gallium concentrations in the bromide sodalites are found almost similar to those of the corresponding chloride sodalites. Nevertheless, the gallium concentration in the sodalite products was always observed to be lower than in their initial stoichiometry [90, 96].

Table 4.1: Experimental data of the hydrothermal synthesis

Experiment	Starting materials ¹					$\text{Na}_8[\text{Al}_{1-y}\text{Ga}_y\text{SiO}_4]_6(\text{Cl}/\text{Br})_2$		
	Al_2O_3 /g	Ga_2O_3 /g	NaAlO_2 /g	NaGaO_2 /g	NaOH /mol/l	Yield /g	Initial y	Refined y
Route A Cl-SOD			0.00	1.00	8.0			
			0.14	0.86	8.0	0.33	0.80	0.23
			0.22	0.78	8.0	0.34	0.70	0.15
			0.30	0.70	8.0	0.65	0.61	0.10
			0.40	0.60	8.0	0.67	0.50	0.04
		1.00	0.00	8.0	1.21	0.00	0.00	
Route B Cl-SOD	0.00	1.54			8.0	0.32	1.00	1.00
	0.08	1.54			8.0	1.85	0.91	0.84
	0.17	1.38			8.0	1.94	0.82	0.77
	0.17	1.23			8.0	1.32	0.80	0.77
	0.25	1.22			8.0	1.98	0.73	0.66
	0.25	1.07			8.0	1.35	0.70	0.65
	0.34	1.07			8.0	1.91	0.63	0.54
	0.33	0.92			8.0	1.42	0.60	0.36
	0.35	0.65			8.0	1.41	0.50	0.30
	0.42	0.77			8.0	1.48	0.50	0.25
	1.00	0.00		8.0	1.50	0.00	0.00	
Route C Cl-SOD			0.00	1.00	2.0	0.15	1.00	1.00
			0.20	1.00	2.0	0.80	0.77	0.72
			0.30	1.00	2.0	0.83	0.69	0.56
			0.40	0.60	2.0	0.85	0.50	0.38
			0.40	0.80	2.0	0.92	0.57	0.51
			0.40	0.96	2.0	0.85	0.61	0.49
		1.00	0.00	2.0	1.50	1.00	1.00	
Route C Br-SOD			0.00	1.00	2.0	0.96	1.00	1.00
			0.05	1.00	2.0	1.02	0.93	0.88
			0.10	1.00	2.0	1.62	0.87	0.78
			0.20	1.00	2.0	1.66	0.77	0.71
			0.30	1.00	2.0	1.76	0.69	0.61
			0.40	1.00	2.0	1.90	0.62	0.55
			0.50	1.00	2.0	1.67	0.57	0.55
			0.60	1.00	2.0	1.82	0.52	0.47
			0.70	1.00	2.0	2.02	0.48	0.47
			0.80	1.00	2.0	1.86	0.45	0.37
		0.90	1.00	2.0	1.51	0.42	0.34	
		1.00	1.00	2.0	1.29	0.40	0.24	
		1.00	0.00	2.0	1.20	0.00	0.00	

¹2g Na_2SiO_3 , 10g NaCl / NaBr , 48 h at 473 K in all cases

4.2.2 XRD INVESTIGATIONS AND RIETVELD REFINEMENTS

The result of X-ray data Rietveld refinement comprises various crystallographic data and related geometrical parameters (Figure 4.1), which are summarised in Table 4.2 (see Attachment) and Table 4.3, respectively. The low residual values in almost all cases indicate a good quality of fit as well as sodalite single phase. For the refinements of $\text{Na}_8[\text{Al}_{1-y}\text{Ga}_y\text{SiO}_4]_6(\text{Cl}/\text{Br})_2$ for various 'y' values the starting parameters were taken from the structure of $\text{Na}_8[\text{AlSiO}_4]_6\text{Cl}_2$ [27] and $\text{Na}_8[\text{AlSiO}_4]_6\text{Br}_2$ [113] placing Al and Ga on the same crystallographic site 6c in space group P-43n. Occupancy parameters of sodium and the halides fluctuate within 1% and were fixed in the final cycle as fully occupied. Independent occupancy parameter refinements of all T-atoms (Al, Ga, Si) for the framework compositions $[\text{Al}_{1-y}\text{Ga}_y\text{SiO}_4]$ show incompatible results between aluminium and gallium while silicon site (6d) was observed to be fully occupied. Therefore an occupancy linear constraint was chosen between aluminium and gallium summing the content of both atom types to be always one. The silicon site was refined as fully occupied and further evidence will be available in the NMR section. The gallium nucleus is much heavier than the aluminium one. As an obvious consequence the vibrational amplitude and the resulting displacement parameter are expected to be lower than the corresponding behaviour of aluminium atoms. Calculations using no linear displacement constraints between aluminium and gallium lead to negative values for one and high positive values for the other atom type. In contrast, using displacement parameter constraints improve the residual values. We therefore refined the displacement parameters of these two atom (Al/Ga) types constrained with equivalent values. Examples of the good agreement between the observed and calculated powder patterns together with the position of possible reflections are given in Figures 4.3a and Figure 4.3b for one compound of the chloride and bromide containing sodalite series, respectively.

In the XRD pattern the relative intensity of the $[h + k + l = 2n+1]$ planes increase (Figure 4.4) with increasing 'y' and one could further check the refined gallium concentration by calculating the intensity of the $[h + k + l = 2n+1]$ planes.

Additional structural parameters were observed which correlate with the compositional 'y' values. The lattice parameter increases linearly with increasing gallium concentration (Figure 4.5a) in both chloride and bromide sodalite series. The systematic cell expansion could also be seen from the linear decrease of the z coordinate of the framework oxygen with increasing Ga concentration (Figure 4.5b) in the framework.

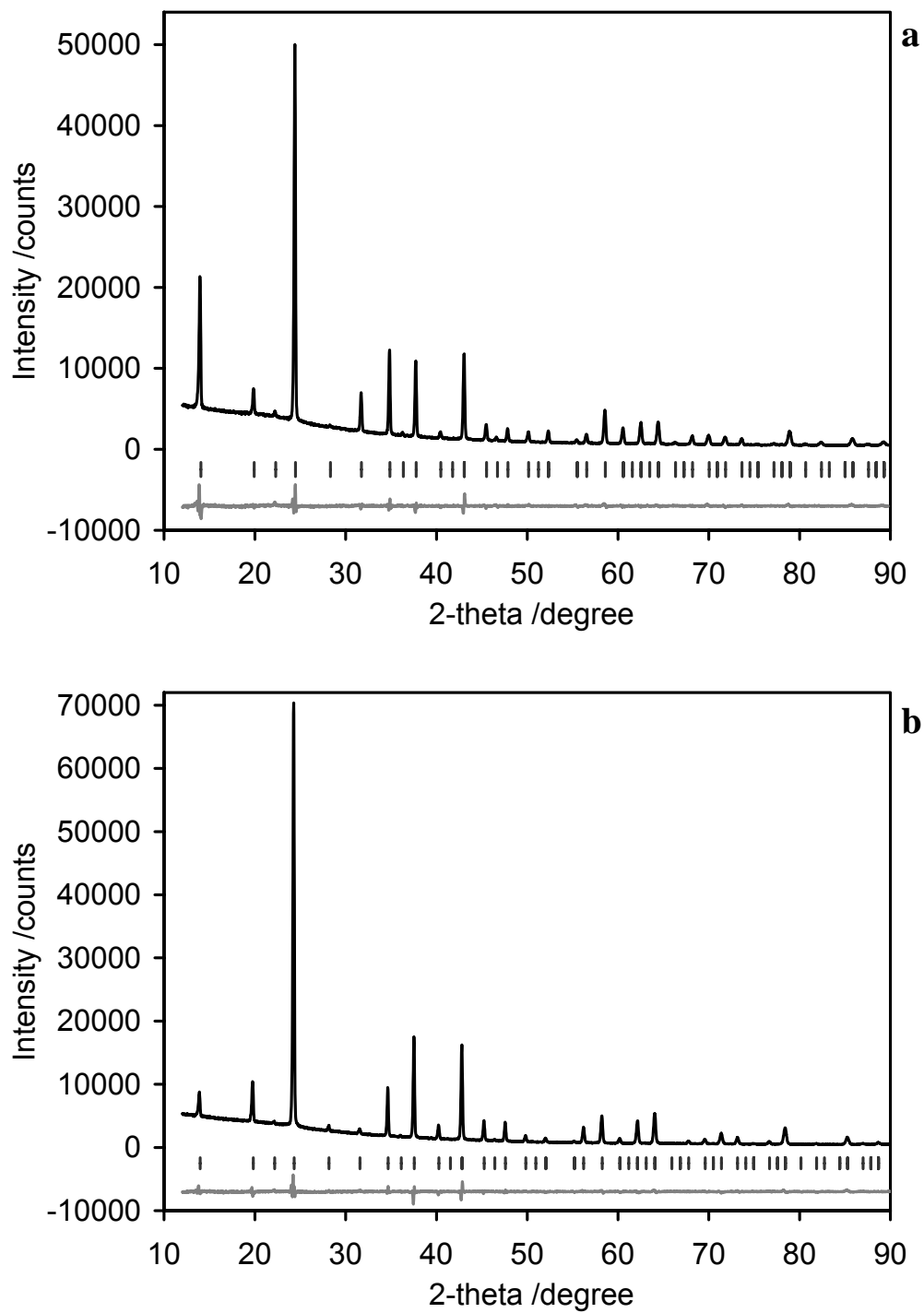


Figure 4.3: Rietveld plot of $\text{Na}_8[\text{Al}_{0.70(1)}\text{Ga}_{0.30(1)}\text{SiO}_4]_6\text{Cl}_2$ (a), $\text{Na}_8[\text{Al}_{0.76(1)}\text{Ga}_{0.24(1)}\text{SiO}_4]_6\text{Br}_2$ (b) sodalites with observed intensities (top part) difference between observed and calculated intensities (lower part) and positions of possible Bragg reflections (middle part).

Table 4.3: Interatomic distances [pm] and angles [degree] of alumogallosilicate chloride and bromide sodalite series and the corresponding end members

Ga% ¹	Al/Ga-O	Si-O	Na-O(1)	Na-Cl	O(1)-O(1)	$\alpha'_1 \cdots 2x$	$\alpha''_1 \cdots 4x$	$\alpha'_2 \cdots 2x$	$\alpha''_2 \cdots 4x$	γ	Avs. tilt
0	174.4(2)	162.0(2)	234.4(1)	274.0(1)	368.5(2)	111.3(1)	108.6(1)	113.4(1)	107.6(1)	137.8(1)	23.3(1)
4	174.8(3)	162.0(3)	233.9(3)	273.8(2)	368.4(4)	110.6(1)	108.9(1)	112.7(1)	107.9(1)	137.5(2)	23.9(1)
10	174.2(4)	163.0(4)	233.5(3)	273.8(2)	367.2(5)	111.4(2)	107.7(1)	113.2(2)	108.6(2)	137.2(3)	23.8(1)
15	175.3(4)	162.2(4)	233.7(3)	272.8(2)	367.2(4)	111.0(1)	108.7(1)	113.2(2)	107.6(1)	137.1(3)	24.0(1)
23	175.0(3)	163.1(3)	232.9(3)	272.9(2)	365.8(4)	111.5(1)	108.5(1)	113.5(1)	107.5(1)	136.6(2)	24.2(1)
25	175.4(2)	163.1(3)	233.3(3)	274.0(2)	367.3(3)	110.9(1)	108.8(1)	112.9(1)	107.8(1)	136.8(1)	24.4(1)
30	176.0(2)	162.6(2)	233.6(3)	274.2(2)	366.9(3)	111.6(1)	108.4(1)	113.9(1)	107.3(1)	136.8(1)	24.0(1)
36	175.7(4)	163.5(3)	232.9(4)	273.4(4)	366.5(4)	111.0(1)	108.7(1)	113.0(1)	107.8(1)	136.3(2)	24.7(1)
38	175.9(2)	163.2(2)	233.7(3)	273.5(2)	366.8(3)	111.5(1)	108.5(1)	113.6(1)	107.5(1)	136.6(1)	24.2(1)
49	176.4(4)	163.7(4)	233.1(3)	272.9(2)	365.4(4)	111.7(2)	108.4(1)	113.8(1)	107.3(1)	135.9(3)	24.6(1)
51	176.7(2)	163.4(2)	233.5(2)	272.4(1)	365.8(3)	111.5(1)	108.5(1)	113.7(1)	107.4(1)	136.0(1)	24.6(1)
56	177.3(2)	163.1(2)	232.6(2)	271.8(1)	364.6(3)	111.3(1)	108.6(1)	113.7(1)	107.4(1)	135.5(1)	25.0(1)
72	178.2(2)	163.4(2)	232.3(3)	270.6(2)	363.9(3)	110.9(1)	108.7(1)	113.4(1)	107.5(1)	134.9(1)	25.7(1)
77	178.8(2)	162.8(2)	232.7(3)	270.4(3)	364.2(3)	111.0(1)	108.7(1)	113.7(1)	107.4(1)	134.9(1)	25.5(1)
84	179.7(3)	162.4(3)	232.4(3)	270.4(2)	363.8(4)	110.8(2)	108.8(1)	113.8(1)	107.4(2)	134.7(2)	25.8(2)
85	180.4(3)	162.6(3)	232.3(3)	269.1(2)	362.8(4)	110.9(1)	108.8(1)	113.9(1)	107.3(1)	134.1(2)	26.1(1)
100	182.6(3)	161.8(3)	230.9(4)	268.4(3)	360.4(4)	111.0(1)	108.7(1)	114.6(1)	107.0(2)	133.0(2)	26.8(2)

Ga% ²											
0	174.2(3)	162.3(3)	234.7(2)	288.4(1)	375.2(3)	111.8(1)	108.2(2)	113.8(1)	107.4(1)	139.8(1)	21.5(1)
24	174.7(6)	163.2(6)	233.8(2)	289.1(1)	374.0(2)	112.0(1)	108.3(1)	113.9(2)	107.3(2)	139.1(2)	22.0(1)
34	174.6(3)	164.2(3)	233.3(3)	286.2(2)	371.8(3)	112.2(1)	108.1(1)	114.0(1)	107.3(1)	138.2(2)	22.7(1)
37	175.4(3)	163.9(3)	233.1(3)	286.6(2)	371.6(4)	112.2(2)	108.1(1)	114.1(1)	107.2(2)	138.0(2)	22.8(2)
47	175.6(3)	163.8(3)	232.5(3)	288.0(2)	371.3(3)	112.4(1)	108.0(1)	114.4(1)	107.1(1)	137.9(2)	22.7(1)
47	175.7(3)	163.6(3)	233.1(3)	286.8(2)	371.6(4)	112.2(2)	108.1(1)	114.2(1)	107.2(2)	138.0(2)	22.8(2)
55	175.3(2)	164.9(2)	232.8(2)	284.5(1)	370.8(3)	111.8(1)	108.4(1)	113.5(1)	107.5(1)	137.4(1)	23.5(1)
55	175.9(3)	164.4(3)	232.5(3)	285.9(2)	370.6(3)	112.1(1)	108.2(1)	114.0(1)	107.3(1)	137.4(1)	23.3(1)
61	176.7(2)	164.2(2)	232.4(2)	283.5(1)	369.8(3)	111.6(1)	108.4(1)	113.6(1)	107.4(1)	136.9(1)	23.9(1)
71	177.9(3)	163.6(3)	232.2(3)	283.6(2)	369.8(3)	111.2(1)	108.6(1)	113.6(1)	107.5(1)	136.6(2)	24.2(1)
78	179.2(3)	163.1(3)	231.6(3)	283.8(2)	368.9(4)	111.2(1)	108.6(1)	114.0(1)	107.3(1)	136.1(1)	24.5(1)
88	180.7(2)	162.7(2)	231.2(3)	283.5(2)	368.2(3)	111.1(1)	108.7(1)	114.1(1)	107.2(1)	135.6(1)	24.9(1)
100	182.7(2)	160.6(2)	231.7(3)	283.2(2)	368.8(4)	110.8(1)	108.8(1)	114.5(1)	107.0(1)	135.6(1)	24.9(1)

^{1,2}chloride and bromide sodalite, respectively.

Frameworks composed of T atoms with similar ionic radii would have greater structural integrity and sodalite with alternate short and long T-O bonds gives rise to more unstable and highly strained structure [114]. In our two series the interatomic distances ℓ_1 (Al/Ga-O distances) increase with increasing gallium content (Figure 4.5c) while ℓ_2 (Si-O distances) are observed almost constant at ~162.8(4) pm and 163.4(4) pm for chloride and bromide sodalite, respectively, within 2.5σ . Interestingly, ℓ_1 increases slightly linear up to a gallium content of about 50% and then degree of increase is much higher but again linear. On the other hand, ℓ_2

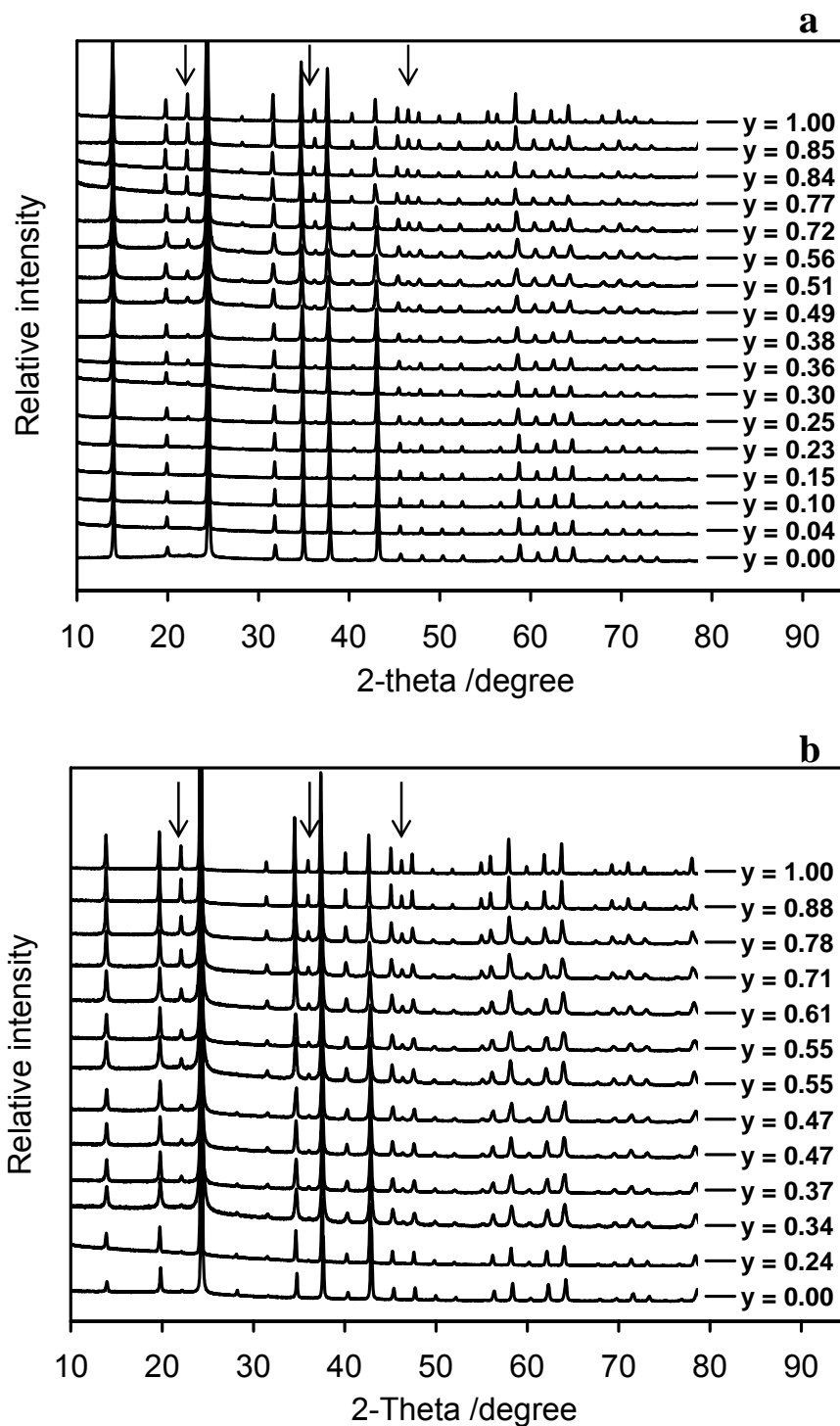


Figure 4.4: X-ray powder diffraction patterns of $\text{Na}_8[\text{Al}_{1-y}\text{Ga}_y\text{SiO}_4]_6\text{Cl}_2$ (a) and $\text{Na}_8[\text{Al}_{1-y}\text{Ga}_y\text{SiO}_4]_6\text{Br}_2$ (b) sodalites. Reflections shown by downward arrows belong to the $[h+k+l = 2n+1]$ planes.

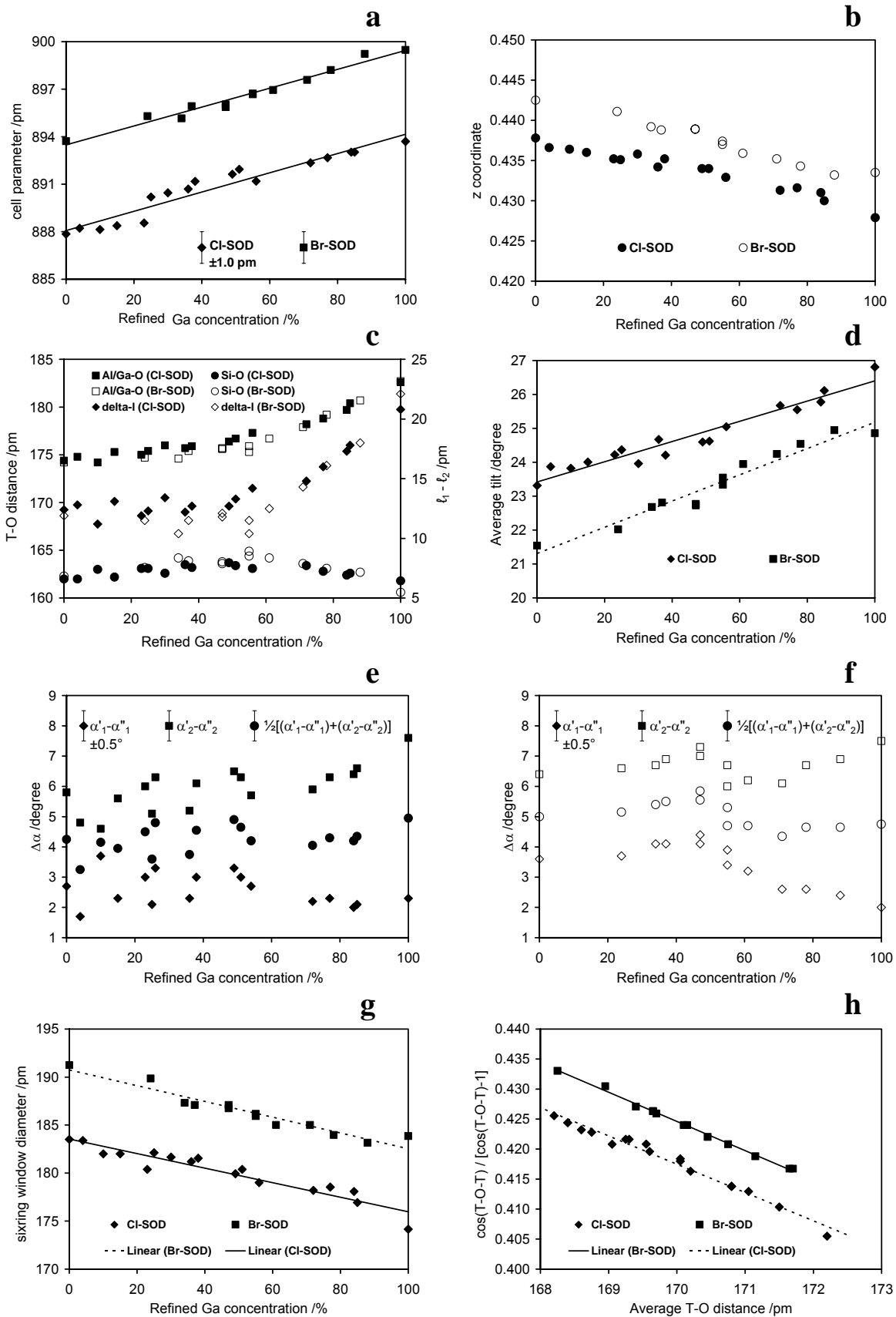
seems also to increase up to 50% gallium concentration and then decreases back to the values of the gallium less compound. If one takes the difference between the two distances ($\Delta\ell = \ell_1 - \ell_2$) it seems to be constant for compounds with less than around 50% gallium on the aluminium positions. For phases with higher gallium content $\Delta\ell$ increases linearly. This behaviour could be observed for both, the chloride and bromide series (Figure 4.5c).

For different structural strains the sodalite family members adapt different preferable space groups [30] and for this purpose the tilt [28, 29] of the TO_4 tetrahedra plays an important role. Depmeier [29] showed that any exerted strain could be reduced by two possible mechanisms: (a) by increasing tilt angle (φ) or (b) by increasing O-T-O angles termed as tetragonal tetrahedra distortion [29]. As given in the literature [28, 29, 33, 114], the tilt angles (φ) are calculated according to $\tan(\varphi_{\text{Si}}) = (0.5-z) / x$ and $\tan(\varphi_{\text{Al/Ga}}) = (0.5-z) / y$, where x , y and z are the framework oxygen position fractional coordinates. In our two sodalite systems the average tilt increases (Figure 4.5d) with increasing gallium incorporation in the T^1 -site.

The O-T-O angles (α) of TO_4 tetrahedra enclosed by the four-membered rings (α'_1 and α'_2 , Figure 4.1) are greater than the ideal tetrahedral value (109.47°) and angles enclosed by the six-membered rings (α''_1 and α''_2) are correspondingly smaller than the ideal value [115] (Table 4.3). α' and α'' correlate to each other via $109.47^\circ = (2\alpha' + 4\alpha'') / 6$ and the difference between α' and α'' represents the tetragonal tetrahedra distortion ($\Delta\alpha$). In the chloride and bromide sodalite series the $\Delta\alpha$ does not show any significant appearance correlated with 'y' value. However, in the T^1O_4 tetrahedra the O-T-O distortion ($\Delta\alpha_1 = \alpha'_1 - \alpha''_1$) seems to be decreased while in the T^2O_4 tetrahedra the corresponding distortion ($\Delta\alpha_2 = \alpha'_2 - \alpha''_2$) increased (Figure 4.5e, f) through discontinuities with increasing gallium concentration.

The dimension of the sixring window (d_6) (the effective cylindrical pathway) is calculated from the relation: $d_6 = 2[d_0/\sqrt{3} - r_o]$ where d_0 is the O(1)-O(1) nearest distances at the bottleneck of the sixring window and r_o is the oxygen radii (121 pm [108]) (see section 3.2.2). The sixring window diameter decreases with increasing gallium content (Figure 4.5g) in an agreement with the observation by Nenoff et al. [95] for different framework types.

The hybridisation of the bridging oxygen changes with corresponding variation of the T-O-T (γ) angles as well as the T-O bonds [127]. In view of preferable silicate T-O-T angle (145° [105]), the bridging oxygen hybridisation could be explained as sp^n where n is between one and two. Oxygen possesses a preferable hybridisation with regard to γ which is linear with average T-O distance. From the relation, $\rho \sim \cos(\text{T-O-T}) / [\cos(\text{T-O-T}) - 1]$, proposed by Hinze [104] one could draw the linear correlation between average T-O distance and the degree of framework oxygen s -hybridisation, ρ (Figure 4.5h). The linear decreasing behaviour



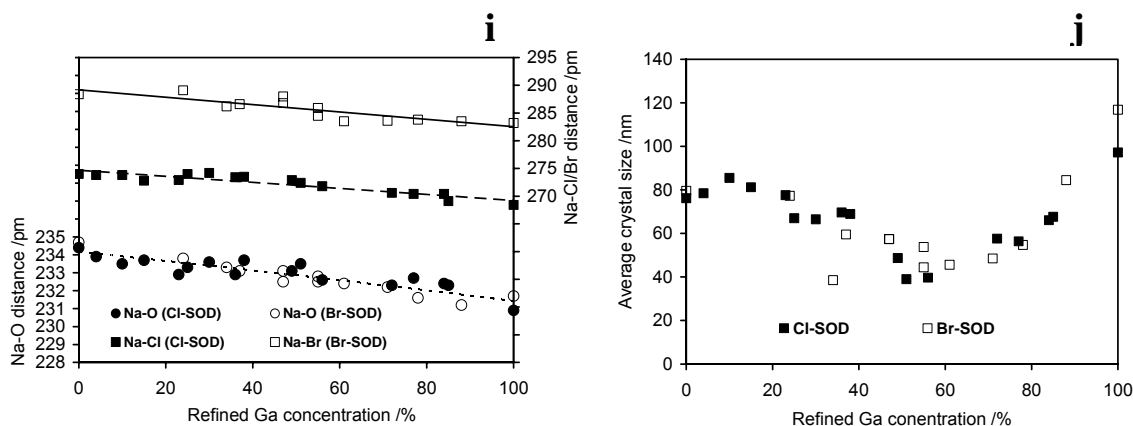


Figure 4.5: Structural parameters vs. refined Ga concentration (a) unit cell, (b) framework oxygen z coordinate, (c) T-O distances, (d) average tilt angles, (e) tetragonal tetrahedra distortion in chloride sodalite, (f) tetragonal tetrahedra distortion in bromide sodalite, (g) sixring window diameter, (h) degree of framework oxygen s-hybridisation vs. average T-O distance, (i) Na-O and NaCl/NaBr distances and (j) average crystal size.

given in Figure 4.5h indicates the increasing deviation from $\rho = 0.45$ and thereby decreasing the T-O-T linkage stability with progressive gallium content in the systems. Additionally, the theoretical ‘ ρ ’ magnitude can be calculated for any mixed halide sodalites [21] as well as the T-O-T linkage stability for respective sodalites. The linear correlation between Na-O and Na-Y (halide) distances to the gallium concentration (Figure 4.5i) appears as the structural correlation between the framework and the guest species. The simultaneous shortening of Na-Cl/Br and Na-O distances indicates that the framework oxygen approaches nearer to sodium and the augmenting repulsive force pushes sodium towards the centre of the β -cage.

Calculating the average crystal size L of the different compounds out of the halfwidth of the phases using the Scherrer equation one can clearly see a decrease of L with increasing gallium concentration up to about 50%. With further increasing gallium content L increases first slowly but finally to nearly the same value as for the other end members (Figure 4.5j). This is at least a hint for the decreasing stability of the sodalite framework if one T atom is occupied by more than one atom type. If the degree of mixing atoms on this site is at a maximum value ($y = 0.5$), we observe the lowest stability of the sodalites framework concerning crystal formation which is then expressed in the lowest average crystal size of the crystals. This effect should correspond to the difference of the two atomic radius. This seems to be truer for the samples plotted in Figure 4.5j are from different synthesis routes and show all the same effect.

4.2.3 MAS NMR INVESTIGATIONS

A series of ^{29}Si MAS NMR spectra were measured in the systems $\text{Na}_{6+x}[\text{Al}_{1-y}\text{Ga}_y\text{SiO}_4]_6(\text{Cl}/\text{Br})_x$. For the chloride compounds with $y = 1$ and $y = 0$, single peak with a chemical shift $\delta(\text{Si})$ of -78.9 ppm and -85.0 ppm were observed (Figure 4.6a), respectively. Corresponding chemical shifts of -80.2 ppm and -86.2 ppm were found in the bromide sodalites. The results of these end members are in agreement with the reported range [106, 110] within e.s.d.'s. In accordance with the Loewenstein rule [37] (or extended the Loewenstein rule for gallium instead of aluminium) these samples consist of perfect ordering of $\text{Si}(\text{OAl})_4$ and $\text{Si}(\text{OGa})_4$ species in the sodalite framework. Partial isomorphous substitution in the trivalent T^1 site leads to a result of different Ga/Al ratio in the framework of chloride and bromide sodalites. Therefore SiO_4 tetrahedra could be found within five possible environments: $\text{SiO}_4(\text{Ga})_4$, $\text{SiO}_4(\text{Ga}_3\text{Al})$, $\text{SiO}_4(\text{Ga}_2\text{Al}_2)$, $\text{SiO}_4(\text{GaAl}_3)$ and $\text{SiO}_4(\text{Al})_4$. Five corresponding signals were observed for different Ga/Al ratio in the as synthesised sodalites and their respective peak positions were summarised in Table 4.4 together with the calculated FWHM and integrated intensity. In both the chloride and bromide series no more than five peaks were observed in any case. This result suggests a $\text{Si}/\text{Al}_{1-y}\text{Ga}_y = 1$ ratio in both series and agrees with X-ray results for fully occupied silicon position throughout the series. In the chloride sodalite series, five distinct peaks were observed between -78.5 ppm and -85.3 ppm, with an estimated

Table 4.4: Fit results of ^{29}Si MAS NMR spectra. The chemical shift (δ /ppm), the halfwidth (FWHM /ppm) and the integrated peak intensity (I_{int} /counts) divided by 10^4 are given together with the calculated gallium concentration. The estimated standard deviations are 1 in the last digit for all values if not given.

Ga% (XRD)	$\text{SiO}_4(\text{Ga}_4)$			$\text{SiO}_4(\text{Ga}_3\text{Al})$			$\text{SiO}_4(\text{Ga}_2\text{Al}_2)$			$\text{SiO}_4(\text{GaAl}_3)$			$\text{SiO}_4(\text{Al}_4)$			Ga% (NMR)
	$\delta(^{29}\text{Si})$	FWHM	I_{int}	$\delta(^{29}\text{Si})$	FWHM	I_{int}	$\delta(^{29}\text{Si})$	FWHM	I_{int}	$\delta(^{29}\text{Si})$	FWHM	I_{int}	$\delta(^{29}\text{Si})$	FWHM	I_{int}	
0													-84.97	1.33	1101.7	0
10(1)	-78.53	1.00	0.5	-80.06	0.98	40.6	-81.74	1.04	133.9	-83.56	1.43	492.3	-85.34	1.61	988.9	13(2)
23(1)	-78.14	1.82	8.1	-79.96	2.02	17.9	-81.66	2.19	60.4	-83.50	2.27	158.2	-85.12	1.90	173.8	22(2)
49(1)	-78.51	2.17	37.3	-80.25	1.81	38.5	-81.88	1.92	45.6	-83.54	1.75	41.6	-85.15	1.91	38.7	49(2)
56(1)	-78.48	2.19	56.2	-80.36	2.24	63.6	-82.04	2.20	42.5	-83.56	2.12	38.5	-85.15	2.00	30.5	58(2)
72(1)	-78.66	2.91	117.7	-80.55	2.02	44.7	-82.14	1.78	30.1	-83.71	1.75	24.5	-85.22	1.38	13.7	75(2)
84(1)	-78.89	0.87	630.4	-80.61	0.88	158.5	-82.24	0.94	61.3	-83.72	0.95	36.9	-85.32	0.93	26.7	86(2)
100	-78.89	0.97	1049.4													100
0													-86.18	2.66	386.0	0
34(1)	-79.09	2.73	24.6	-80.85	2.50	36.9	-82.73	2.50	45.0	-84.25	2.58	53.0	-86.13	2.58	86.1	36(2)
55(1)	-80.00	2.66	76.4	-81.92	2.50	47.3	-83.60	2.58	42.6	-85.01	2.58	41.1	-86.58	2.57	59.2	54(2)
78(1)	-80.05	2.66	111.8	-81.78	2.35	47.0	-83.14	2.27	32.4	-84.75	2.27	23.7	-86.59	2.11	13.6	75(2)
100	-80.19	2.27	299.9													100

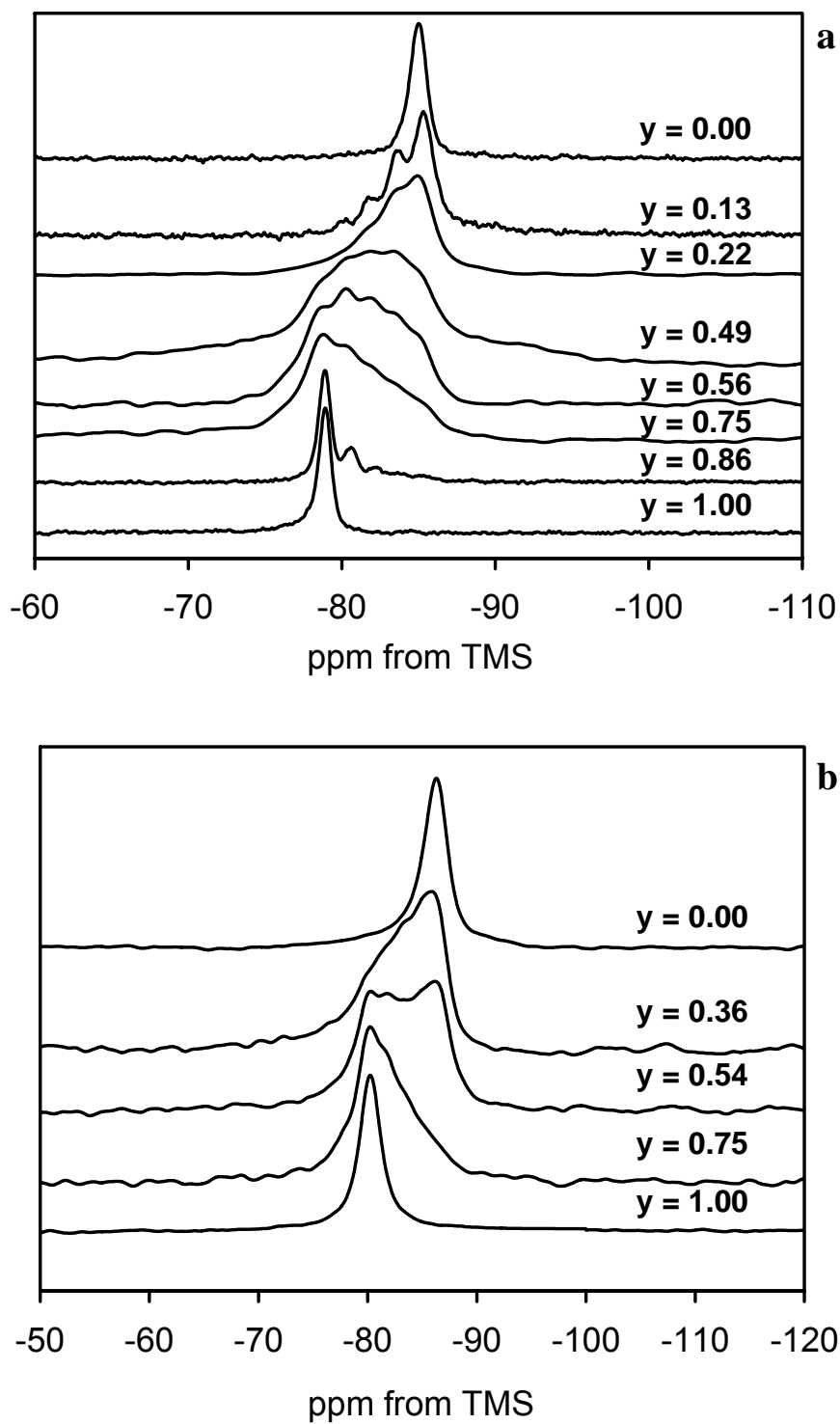


Figure 4.6: ^{29}Si MAS NMR spectra of $\text{Na}_8[\text{Al}_{1-y}\text{Ga}_y\text{SiO}_4]_6\text{Cl}_2$ (a) and $\text{Na}_8[\text{Al}_{1-y}\text{Ga}_y\text{SiO}_4]_6\text{Br}_2$ (b) sodalites. The given 'y' values were calculated from NMR spectra fit results.

average negative increase of about 1.36 ppm (all $\delta(\text{Si})$ should be considered from TMS). This result suggests that each aluminium substitution with gallium in the $\text{SiO}_4(\text{Al})_4$ species leads about 1.36 ppm downfield shift and vice versa. The corresponding results were observed in the bromide sodalite series within a range of -80.2 ppm to -86.8 ppm (Figure 4.6b) with an estimated average variation of about 1.32 ppm; i.e., 1.32 ppm for each aluminium substitution with gallium in the $\text{SiO}_4(\text{Al})_4$ species and vice versa. From the inspection of the intensity of these five peaks one can prove the statistical distribution of AlO_4 and GaO_4 tetrahedra in the whole crystalline samples throughout the series ($0 < y < 1$). From the shape of the intensity maximum of a curve representing the summarised intensity of the five different Q_4 signal, from one end member to the other, one could expect a complete statistical distribution of aluminium and gallium atoms throughout the whole crystal in the chloride series (Figure 4.6a). In contrast to this, we observe a slightly different behaviour in the bromide sodalite $\text{Na}_8[\text{Al}_{0.45(1)}\text{Ga}_{0.55(1)}\text{SiO}_4]_6\text{Br}_2$. The intensities of $\text{Si}(\text{OGa})_4$ and $\text{Si}(\text{OAl})_4$ peaks are higher as for the other three configurations. This is a clear hint for a non-statistical distribution, means possible domain formation of aluminium and gallium enriched parts in the crystals. This result may be compared with $\text{Na}_8[\text{Al}_{1-y}\text{Ga}_y\text{SiO}_4]_6(\text{NO}_2)_2$ with $y \sim 0.50$ (see section 3.2.3). We did not clearly observe any hint for this domain formation from XRD studies. Therefore we assume that possible domains are smaller than the coherence length of the X-ray radiation but big enough to be detected by MAS NMR technique. Nevertheless, more data points could possibly prove this hint by further investigations. However, from these five distributions in the spectral profile one could be able to calculate the Ga/Al ratio. In our study, five peaks of each composition were fitted using 'dmfit2003' [93] program and their corresponding Ga/Al ratios were accounted from the Gaussian /Lorentzian peak area. The calculated Ga/Al ratios resulting from ^{29}Si MAS NMR are in good agreement with the refined values from the Rietveld calculations (Table 4.4).

4.2.4 FTIR INVESTIGATIONS

According to Iiishi et al. [116] absorptions arising from the vibration of the non framework cations and the framework oxygen's occur below 250 cm^{-1} in some feldspars of aluminosilicate frameworks and later the same results were observed by Godber and Ozin [117] in some halogenide sodalites. The main infrared absorption bands for aluminosilicate, alumogermante, gallosilicate, gallogermanate and many other cubic sodalites framework are in the range of $300\text{-}1200 \text{ cm}^{-1}$ [118, 119] and the position of each individual band depends on the type of T-atoms and the encapsulated guest species. Between 1200 cm^{-1} and 4000 cm^{-1} the possible vibrations of some template molecules and water could be seen. As expected, the asymmetric T-O-T stretching (ν_{as} T-O-T), symmetric T-O-T stretching (ν_{s} T-O-T) and O-T-O bending (δ O-T-O) modes were observed in the mid infrared region (Figure 4.7) for our

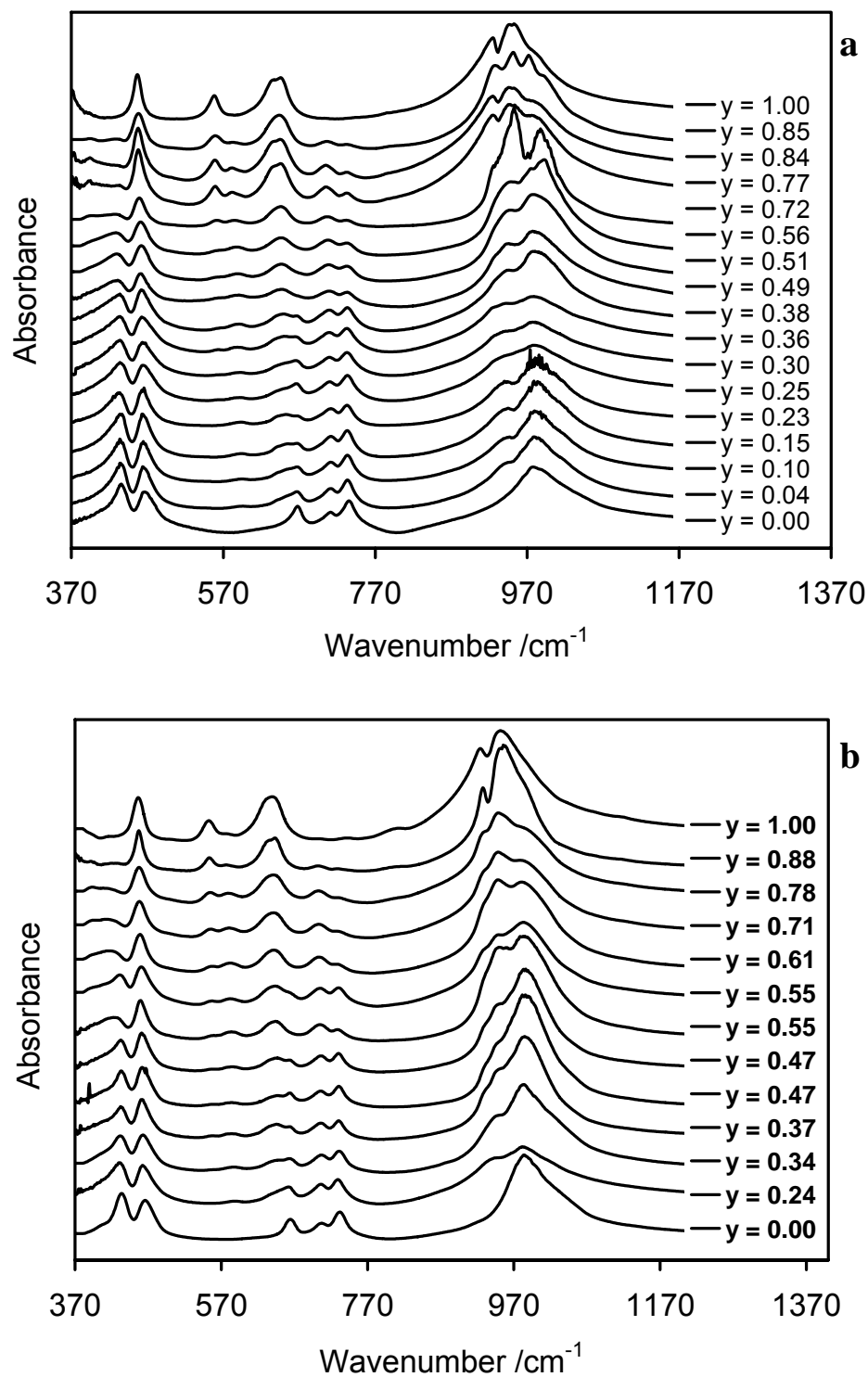


Figure 4.7: (a) FTIR spectra of Na₈[Al_{1-y}Ga_ySiO₄]₆Cl₂ (a) and Na₈[Al_{1-y}Ga_ySiO₄]₆Br₂ sodalites. The given 'y' values were calculated from XRD data refinements.

system $\text{Na}_{6+x}[\text{Al}_{1-y}\text{Ga}_y\text{SiO}_4]_6(\text{Cl}/\text{Br})_x$. More than one band was observed for ν_{as} T-O-T with several maxima within a broad range of 800 cm^{-1} to 1200 cm^{-1} for $0 \leq y \leq 1$. For $y = 0$ and $y = 1$, three bands of $\nu_s \text{T}^{1\text{A}}\text{-O-T}^2$ (736 cm^{-1} , 712 cm^{-1} , 668 cm^{-1} and $\text{T}^{1\text{A}} = \text{Al}$, $\text{T}^2 = \text{Si}$), and three bands of $\text{T}^{1\text{G}}\text{-O-T}^2$ (647 cm^{-1} , 582 cm^{-1} , 558 cm^{-1} where $\text{T}^{1\text{G}} = \text{Ga}$) were observed in chloride sodalite, respectively. The corresponding results of $\nu_s \text{T}^{1\text{A}}\text{-O-T}^2$ (732 cm^{-1} , 707 cm^{-1} , 664 cm^{-1}) and $\text{T}^{1\text{G}}\text{-O-T}^2$ (639 cm^{-1} , 578 cm^{-1} , 552 cm^{-1}) for the bromide compounds were observed for $y = 0$ and $y = 1$, respectively, with a downward shift of the modes for the comparative bigger anion in bromide sodalite which is in agreement (max. 20 cm^{-1} downward shift) with Godber and Ozin [117].

Interestingly in both the chloride and the bromide series, we observed only a very small shift of the ν_s T-O-T mode from the position of one end member to the other. Starting with the ν_s Si-O-Al vibrations we observe a small shift to lower wavenumbers and a decrease of the intensity of all of the three first clearly observed modes with increasing gallium concentration in the sodalite framework. In combination with the decreasing intensity of the $\nu_s \text{T}^{1\text{A}}\text{-O-T}^2$ modes, the intensity of $\nu_s \text{T}^{1\text{G}}\text{-O-T}^2$ modes increase. Additionally, we observe for both sets of vibrations an ‘internal’ change of intensities which is correlated to the geometrical change like lattice parameter and tilt angle. Whereas the later behaviour is known for expanding sodalites [33] (and there is no difference between the expansion caused by increasing temperature or framework T-atom substitution) the corresponding intensity changes for the different ν_{as} T-O-T vibration sets seems to be very interesting concerning information of the framework composition. The decrease intensity of the ν_s Si-O-Al modes with increasing gallium concentration indicates that the total amount of this type of vibrations decreases. In contrast, the amount of ν_{as} Si-O-Ga vibrations increase with increasing gallium content that results the increasing intensities of these bands. Taking this behaviour as a basic observation one can derive a local origin of these vibrations separated from the neighbouring one which is then a short range order vibration involving only one T^1 , one T^2 and one oxygen atom.

In contrast to this, the δ O-T-O mode seems to be a long range vibration summing the statistical vibration of three T-atoms (Si, Al and Ga) in the sodalite framework. Here we observe a linear shift of the δ O-Si/Al-O mode from 463 cm^{-1} to 455 cm^{-1} for the δ O-Si/Ga-O mode. On the other hand one has to take a second explanation into account. It could be possible that there is more than one mode observable which could not be resolved. If so, and the intensity of the first mode (lower wavenumber) increases with increasing gallium content whereas the intensity of the second mode decreases, one could also observe a shift to lower wavenumbers for the summarised signal. Nevertheless, the linear correlation of the gallium concentration with the wavenumber of this band, which is slightly different for the chloride and bromide sodalite series (Figure 4.8), was used to establish an equation for the recalculation of the gallium concentration. This will give the possibility to estimate the

composition of this sodalite types with an easy and fast IR measurement. The two proposed equations are: $Ga \% = 4717.64 - 10.112W_{Cl}$ ($R^2 = 0.992$) and $Ga\% = 4334.96 - 9.315W_{Br}$ ($R^2 = 0.984$) (W = wavenumber) for the chloride and bromide sodalite series, respectively. Since the halfwidth of this band is $\sim 20\text{ cm}^{-1}$, which is almost double of the total shift, the equation has only significance for the calculation of gallium concentration from an infrared spectrum if one could clearly resolve the maximum of the mode. On the other hand, one can clearly see the high correlation between the position of this mode and the refined gallium concentration of the X-ray powder data. Therefore these observations are indirect proof for the correctness of the used refined gallium content of the sodalite framework as the correct compositional parameter.

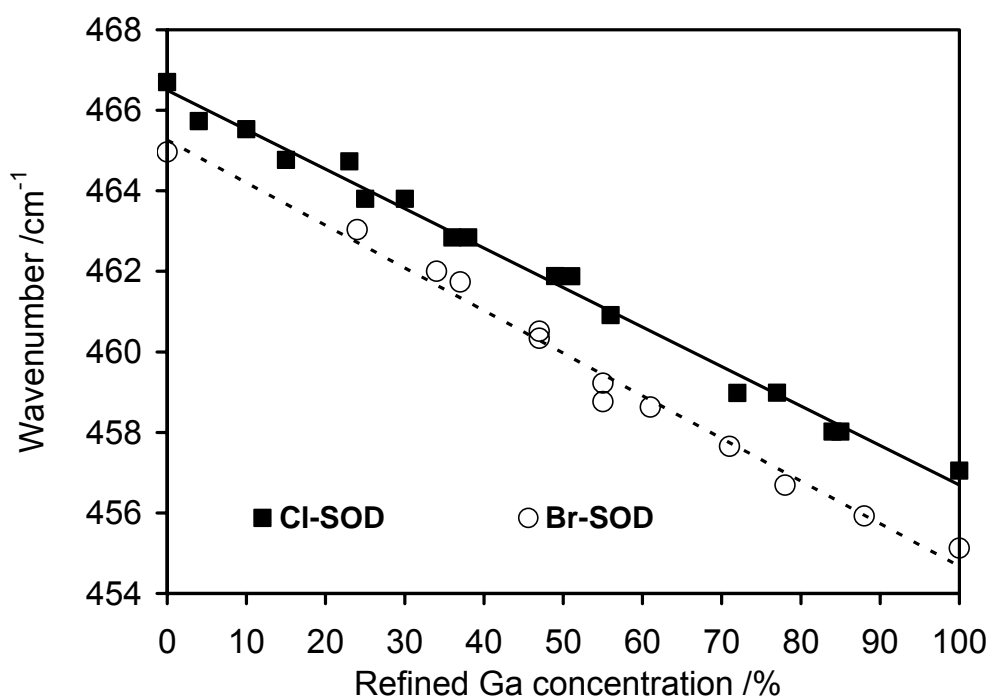


Figure 4.8: Position of the O-T-O bending mode [δ (O-T-O)] vs. Ga concentration for the aluminosilicate sodalite series and the corresponding end members. Ga concentrations were taken from XRD results. The calculated linear correlations are also plotted.

A second bending mode was observed in the aluminosilicate sodalites at 436 cm^{-1} and 434 cm^{-1} for the chloride and bromide compound, respectively. It decreases in intensity with increasing gallium concentration and disappears completely in the pure gallosilicate compounds. This observation is in agreement with the given number of bending modes with two-three and one for the aluminosilicate and gallosilicate framework, respectively, as proposed by Henderson and Taylor [109]. The disappearance of this bending mode together with the appearance and disappearance of the ν_{as} T-O-T mode strongly implies that for the ‘shifting’ bending mode around 460 cm^{-1} may have a combined change in intensity might also be true.

4.3 CONCLUSION

In the $\text{Na}_8[\text{AlSiO}_4]_6(\text{Cl/Br})_2$ sodalite system, the aluminium position was progressively substituted with gallium progressively. The synthesised products represent the new composition $\text{Na}_8[\text{Al}_{1-y}\text{Ga}_y\text{SiO}_4]_6(\text{Cl/Br})_2$ ($0 \leq y \leq 1$). Simultaneous presence of aluminium and gallium in the same site added a new sodalite member in their respective mineral families. Gallium concentrations for different compositions calculated using X-ray powder data Rietveld refinements and ^{29}Si MAS NMR spectroscopy shows good agreement. Structural correlations are observed as a function of gallium incorporation on the T^1 -site. The lattice parameters increase linearly from $[\text{AlSiO}_4]_6$ to $[\text{GaSiO}_4]_6$ framework matrix. The Al/Ga-O distance is found as an average magnitude, which increases with increasing gallium concentration while the Si-O distance remains almost constant at 162.8 pm ($\sigma \sim 2.0$) and 163.4 pm ($\sigma \sim 3.0$) for the chloride and bromide sodalite, respectively. The increasing average tilt of the framework Al/GaO₄ and SiO₄ tetrahedra lead to Na-O and Na-Cl/Br distances shortening as consequences of increasing gallium content or increasing average T-O distances or decreasing T-O-T angles. The degree of framework oxygen *s*-hybridisation is found linearly correlated to the average T-O distances showing that the T-O-T linkage (tetrahedra linkage) is less stable with increasing gallium concentration. In the X-ray diffraction patterns no clear hints for the domain formation of aluminium and gallium enriched parts in the crystals were observed. Nevertheless, the ^{29}Si MAS NMR clearly shows a non statistical distribution of the different Si-(OT¹₄) surroundings for $\text{Na}_8[\text{Al}_{0.45(1)}\text{Ga}_{0.55(1)}\text{SiO}_4]_6\text{Br}_2$. In the other investigated compounds in the bromide sodalite series as well as all compositions in the chloride containing samples the NMR results indicate a statistical distribution of aluminium and gallium throughout the crystals. These two series sodalite materials would be very interesting to study photochromism and cathochromism with progressive incorporation of gallium in the framework as well as tuning of the sixring window within ~ 10 pm. Furthermore, the structural modifications could change prospective physical-chemical properties for the advanced zeolite materials [47].

5 GALLIUM SUBSTITUTED ALUMOSILICATE HYDRO-HYDRXY AND HYDRO SODALITES

5.1 INTRODUCTION

Typical zeolitic reactions are possible in sodalites as they undergo (cationic /anionic) ion exchange reactions [38, 100, 107], subject to the typical size restrictions imposed by the sixring inter-cavity windows. Empty cage sodalite would be one of the best choices to study packaged insulators, semiconductors and metals [46] within the framework. For such many studies the selectivity of the sixring pore dimensions of the β -cage (Figure 5.1) is very important. Empty cage $\text{Na}_6[\text{T}^1\text{T}^2\text{O}_4]_6$ sodalites could readily be achieved from the corresponding $\text{Na}_6[\text{AlSiO}_4]_6(\text{H}_2\text{O})_8$ [41], $\text{Na}_6[\text{GaSiO}_4]_6(\text{H}_2\text{O})_8$ [70], $\text{Na}_6[\text{GaGeO}_4]_6(\text{H}_2\text{O})_8$, $\text{Na}_6[\text{AlGeO}_4]_6(\text{H}_2\text{O})_8$, and $\text{Na}_6[\text{ZnAsO}_4]_6(\text{H}_2\text{O})_8$ [95] by dehydration. On the other hand, basic hydro sodalites $\text{M}_{6+x}[\text{T}^1\text{T}^2\text{O}_4]_6(\text{OH})_x(\text{H}_2\text{O})_n$ [43, 68, 86, 120] and the hydrogen dihydroxide sodalite $\text{M}_{6+x}[\text{T}^1\text{T}^2\text{O}_4]_6(\text{H}_3\text{O}_2)_x$ [25] left much dispute concerning the mutual magnitude between 'x' and 'n', and the enclathrated guest compositions. Tielen et al. [89] reviewed the

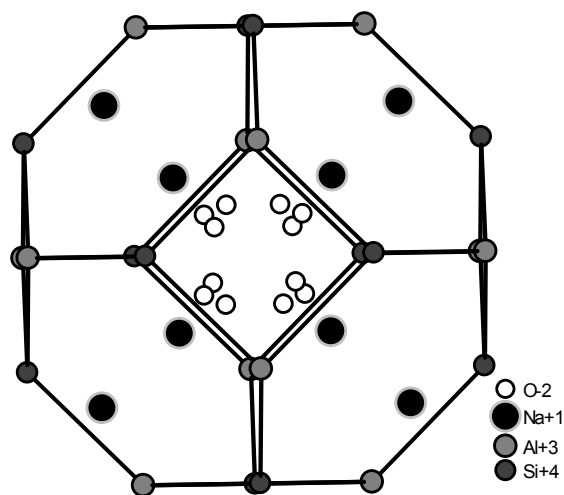


Figure 5.1: (a) β -cage of hydro-hydroxy sodalite with possible orientations of non framework oxygen O(2) either from OH^- or H_2O .

catalytic implications of the isomorphic substitution of gallium in some zeolites resulting from the lattice contraction /expansion and Brønsted acid strength. Therefore partial and /or full T-site substitution of aluminium with gallium in the alumosilicate sodalite system may reveal an extensive isomorphic miscibility in the $\text{Na}_{6+x}[\text{Al}_{1-y}\text{Ga}_y\text{SiO}_4]_6(\text{Y})_x(\text{H}_2\text{O})_{8-4x}$ sodalite system for various 'x', 'y' and 'Y' magnitudes. The consequent structural modifications in sodalite, as a model compound, could play a vital role in potential applications. The present study is concerned with the synthesis and characterisation of two new series of $\text{Na}_{6+x}[\text{Al}_{1-y}\text{Ga}_y\text{SiO}_4]_6(\text{OH}\cdot\text{H}_2\text{O})_x(\text{H}_2\text{O})_{8-4x}$ and $\text{Na}_6[\text{Al}_{1-y}\text{Ga}_y\text{SiO}_4]_6(\text{H}_2\text{O})_8$ sodalites.

5.2 RESULTS AND DISCUSSION

5.2.1 SYNTHESIS

Alumosilicate sodalite crystallisation ($y = 0$) prefers high alkaline media (16M NaOH [41, 122]), while in the gallosilicate system ($0 < y \leq 1$) low concentration must be used [46, 62]. Therefore a borderline concentration (8M NaOH solution, Table 5.1) was selected for alumogallosilicate systems. As described in literature for different framework types [90, 96, 121] we also observe the refined gallium concentration in the hydro-hydroxy sodalite framework lower than the calculated initial stoichiometry (Figure 5.2).

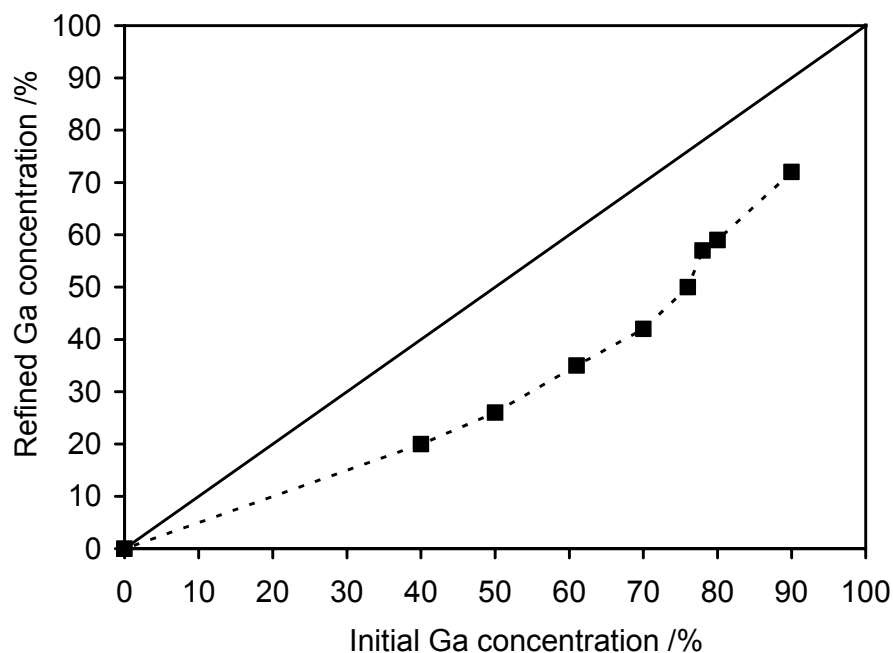


Figure 5.2: XRD refined Ga concentration vs. initial stoichiometry of hydro-hydroxy sodalite. The solid straight line represents concentration equivalence.

The reason could be assigned from the solubility product of gallium oxide which is higher than that of aluminium oxide within the used alkaline concentration. Therefore relatively a less participation of gallium could be expected in the crystallisation equilibrium. With increasing aluminium concentration in the alumogallosilicate sodalite it is expected that the system prefers higher alkaline concentration than 8M for higher alumosilicate $[\text{AlSiO}_4]_6$ framework units compared with gallosilicate counterpart ($[\text{GaSiO}_4]_6$). But the alkaline solution higher than 8M would be less preferable for gallosilicate units to be found in the alumogallosilicate framework. We observed a very slow change of refined gallium concentration with respect to initial gallium stoichiometry (Figure 5.2) up to a initial feed of about 50%. Further increase of initial gallium feed the refined framework gallium content

comes near to the equivalence line. This behaviour could be assigned from the total amount of initial materials ($\text{Al}_2\text{O}_3 + \text{Ga}_2\text{O}_3$). Additionally, this result possibly indicates that aluminium plays the dominating role in the tectosilicate crystallisation for comparatively a less strained sodalite β -cage [114]. During the exchange procedure (see section 2.1) from hydro-hydroxy sodalite to hydro sodalite an increasing pH value of the solution was observed. The rising pH was being neutralised by adding low concentrated acetic acid drop wise to maintain the pH between 5.5 and 6.0 until constant pH was observed in the solution. The gradual pH development in the mixture in course of time clearly indicates that at least one acid-base neutralisation reaction takes place. Additionally, this result supports that $\text{OH}^-/\text{H}_2\text{O}$ exchange is a dynamic equilibrium between inside and outside the β -cage through the window channel which is accelerated by employing additional acid within the above pH condition. Therefore the autoclave exchange [123] employing only in water is slower than the method using low concentrated acid. Cancrinite co-crystallisation was observed as an obvious part of the hydro-hydroxy sodalite production as a function of reaction time (Figure 5.3a) and could easily be reduced by selecting appropriate reaction period. Hydro-hydroxy sodalites produced at a period of four hours were purer samples compared to six hours synthesis but we chose the later for better crystallinity. As a result a small amount (max. ca. 2%) of cancrinite was produced along with each hydro-hydroxy sodalite and a correlation was observed between the amount of cancrinite and the refined framework gallium concentration (Figure 5.3b). Nevertheless, no cancrinite was traced in any of the corresponding hydro sodalites. Probably a carbonate directed cancrinite was produced from the aerial carbonation and /or impurities of NaOH and destroyed in the exchange method employed in an acidic medium. Therefore cancrinite seems to be less stable than sodalite within this pH range. In each of the corresponding hydro sodalite the framework composition does not change even in the intermediate period of the exchange experiment where a broad distribution of encapsulated $(\text{OH}\cdot\text{H}_2\text{O})^-$ and OH^- or H_2O guest species is possible.

Table 5.1: Hydrothermal synthesis (2g Na_2SiO_3 and 8M 20 ml H_2O was used in each synthesis for 6 hours) of hydro-hydroxy sodalite. Ga concentration (/%) was calculated from the initial stoichiometry and XRD data Rietveld refinement.

Al_2O_3 /g	Ga_2O_3 /g	Yield /g	Initial Ga	Refined Ga in H-H-SOD	Refined Ga in H-SOD
					100 ^a
0.17	2.75	1.83	90	72(1)	75(1)
0.35	2.50	1.76	080	59(1)	57(1)
0.35	2.25	1.63	78	57(1)	56(1)
0.35	2.00	1.57	76	50(1)	45(1)
0.35	1.50	1.42	70	42(1)	42(1)
0.35	1.00	1.29	61	35(1)	36(1)
0.35	0.66	1.10	50	26(1)	25(1)
0.35	0.43	1.02	40	20(1)	20(1)
			0	0 ^b	0

^aobtained from $\text{Na}_8[\text{GaSiO}_4]_6\text{I}_2$. ^bsynthesised from 2.0 g kaolinite together with 16M 20 ml NaOH for 120 h.

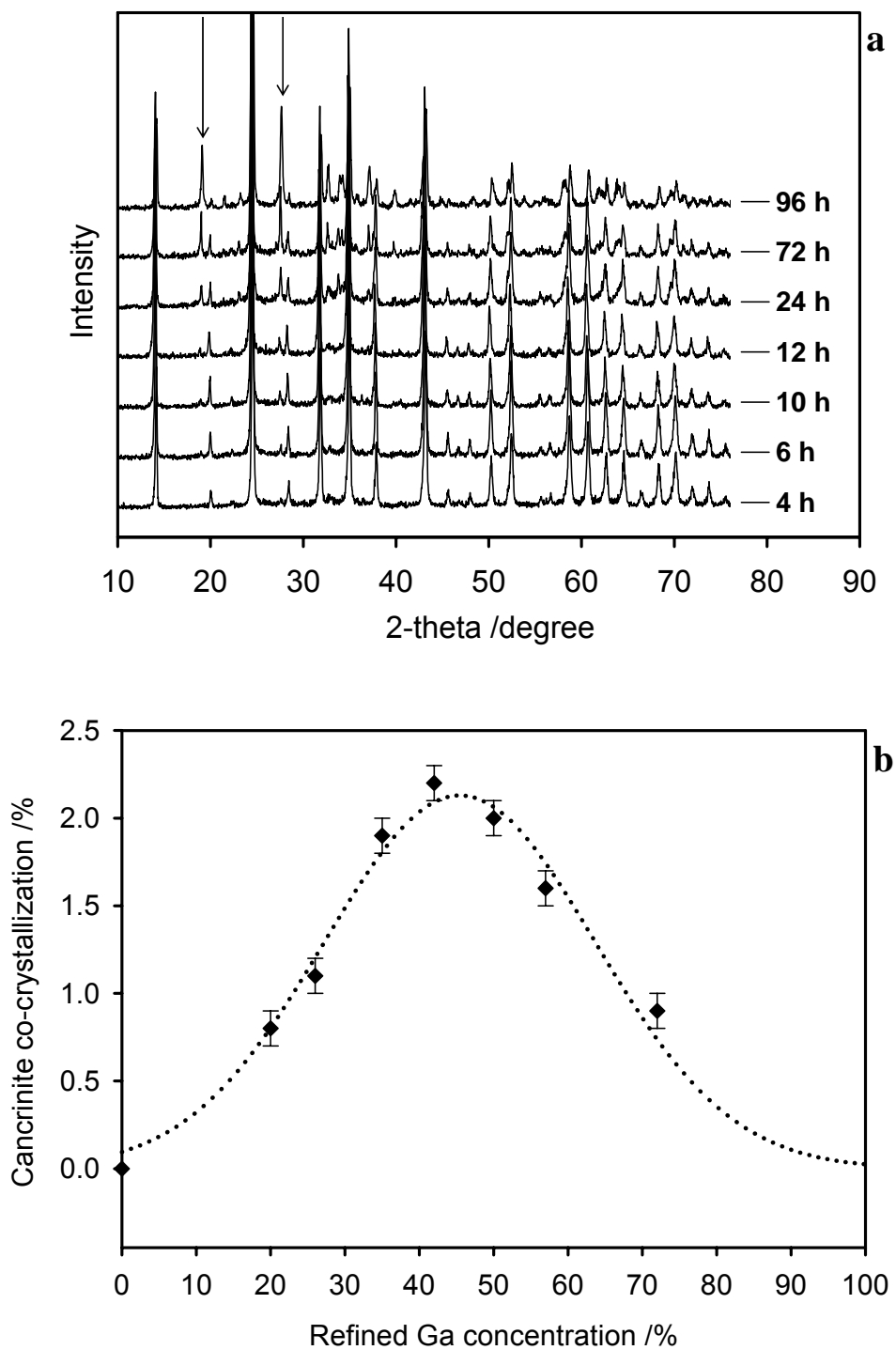
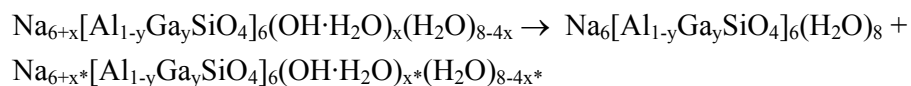


Figure 5.3: (a) XRD patterns of as synthesized hydro-hydroxy sodalites along with cancrinite phase. The downward arrows show the reflections coming from cancrinite. (b) Cancrinite formation is shown as a function of refined gallium concentration.

5.2.2 XRD INVESTIGATIONS AND RIETVELD REFINEMENTS

The XRD data refined compositions together with pertaining crystallographic parameters and geometries are summarised in Table 5.2 (see Attachment) and Table 5.3, respectively, and some terminologies are taken from Figure 4.1 (section 4.1). For the refinement of $\text{Na}_{6+x}[\text{Al}_{1-y}\text{Ga}_y\text{SiO}_4]_6(\text{OH}\cdot\text{H}_2\text{O})_x(\text{H}_2\text{O})_{8-4x}$ (H-H-SOD) and $\text{Na}_6[\text{Al}_{1-y}\text{Ga}_y\text{SiO}_4]_6(\text{H}_2\text{O})_8$ (H-SOD) the starting parameters were taken from the structure of $\text{Na}_8[\text{AlSiO}_4]_6(\text{OH})_2(\text{H}_2\text{O})_2$ [124] and $\text{Na}_6[\text{AlSiO}_4]_6(\text{H}_2\text{O})_8$ [41], respectively, placing both aluminium and gallium on the same crystallographic site and detailed explanations were given in section 3.2.2 for the isotopic sodalite framework. In the H-H-SOD system, placing non framework oxygen O(2) (oxygen either from water or hydroxide) at the centre of the β -cage gives incompatible high displacement parameters which indicates that the high symmetry sodalite β -cage centre may be empty. Therefore the choice of the starting parameters were correct placing O(2) slightly off-centred on the 24i (x, y, z) general position. It seems that O(2) adapts a variety of off-centred positions within the cage with respect to the tetrahedrally occupied sodium cation. For the positional lower local symmetry (24i) O(2) possess a high degeneracy and it is rather difficult to distinguish between the oxygen from OH^- and H_2O in the β -cage. Therefore we used the guest composition as $\{(\text{OH}\cdot\text{H}_2\text{O})_x(\text{H}_2\text{O})_{8-4x}\}^-$. For $0 < y < 1$, the amount of H_2O (~1.3) and $(\text{OH}\cdot\text{H}_2\text{O})^-$ (~1.7) along with each sodalite composition were observed almost constant within e.s.d.'s throughout the series. In contrast, one end member was found as $\text{Na}_{7.1(1)}[\text{AlSiO}_4]_6(\text{OH}\cdot\text{H}_2\text{O})_{1.1(1)}(\text{H}_2\text{O})_{3.5(1)}$ with a higher water content sodalite which can be compared with Felsche et al. [68]. In the leaching of NaOH with H_2O in hydroxy sodalites the following exchange occurs and as a result, a multiphase XRD pattern could be obtained for infinite distribution of 'x' until it equals to zero.



where $x^* < x$. Out of the exchange procedure we refined an intermediate sample with $y = 0.26(1)$. A double phase (Figure 5.4a) was observed and refined with a good quality of fit ($R_{\text{wp}} = 0.054$, $R_p = 0.042$) except a deviation in cell parameters (891.92(4) pm and 885.82 pm for H-H-SOD_{inter} and H-SOD_{inter} sodalite, respectively) in the intermediate phase) from their corresponding end members (Table 5.2, see Attachment). But the small and orderly manner of the residual values assure that those two refined phases are the main components and possible uncalculated other phases are trace in amount and could be infinite in number. Additionally, this result indicates that even in the intermediate phases the Al/Ga ratios in the framework do not change. Besides, the quality of other single phase refinements could be seen in Figures 5.4b and 5.4c of H-H-SOD and H-SOD, respectively.

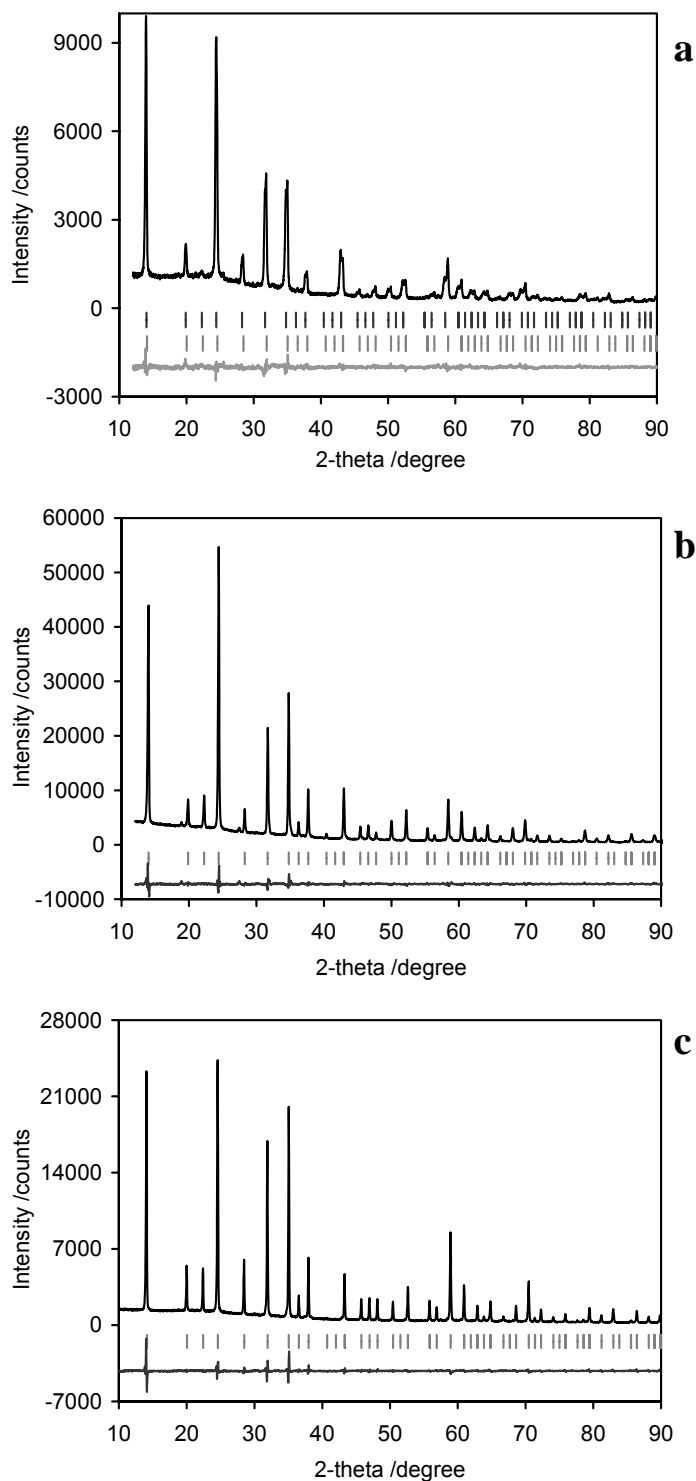


Figure 5.4: Rietveld plot of $\text{Na}_{7.7(1)}[\text{Al}_{0.74(1)}\text{Ga}_{0.26(1)}\text{SiO}_4]_6(\text{OH}\cdot\text{H}_2\text{O})_{1.7(1)}(\text{H}_2\text{O})_{1.3(1)}$ along with $\text{Na}_8[\text{Al}_{0.75(1)}\text{Ga}_{0.25(1)}\text{SiO}_4]_6(\text{H}_2\text{O})_8$ (a), $\text{Na}_{7.7(1)}[\text{Al}_{0.28(1)}\text{Ga}_{0.72(1)}\text{SiO}_4]_6(\text{OH}\cdot\text{H}_2\text{O})_{1.7(1)}(\text{H}_2\text{O})_{1.3(1)}$ (b) and $\text{Na}_8[\text{Al}_{0.75(1)}\text{Ga}_{0.25(1)}\text{SiO}_4]_6(\text{H}_2\text{O})_8$ (c) sodalites with observed intensities, difference between observed and calculated intensities and possible positions of Bragg reflections.

Table 5.3: Interatomic distances [pm], angles [degree] of H-H-SOD (upper part) and H-SOD (lower part)

T ¹ -site	Al/Ga-O	Si-O	Na-O(1)	Na-O(2)	O(1)-O(2)	O(2)-O(2)	α''_1/α'_1	α''_2/α'_2	γ	φ
[Al]	174.0(3)	161.6(3)	239.8(4)	264(2)	298(3)	301(3) ^h 257(3) ^a	108.2(1) ...4x 112.0(1) ...2x	107.2(1) 114.1(1)	139.1(1)	22.0(4)
[Ga _{0.20(1)} Al _{0.80(1)}]	174.6(2)	163.1(2)	234.5(3)	262(3)	326(3)	246(4) ^h 222(4) ^a	108.2(1) ...4x 112.0(1) ...2x	107.3(1) 114.0(1)	137.3(1)	23.4(1)
[Ga _{0.26(1)} Al _{0.74(1)}]	175.0(3)	164.7(3)	232.9(4)	261(7)	314(9)	264(12) ^h 224(13) ^a	107.7(1) ...4x 113.1(1) ...2x	106.8(1) 114.9(1)	135.6(2)	24.2(1)
[Ga _{0.35(1)} Al _{0.65(1)}]	175.8(3)	164.6(3)	232.3(3)	261(7)	321(9)	253(13) ^h 220(12) ^a	108.1(1) ...4x 112.2(1) ...2x	107.2(1) 114.2(1)	135.4(2)	24.8(2)
[Ga _{0.42(1)} Al _{0.58(1)}]	176.7(3)	164.5(3)	233.5(3)	258(3)	322(4)	253(6) ^h 215(5) ^a	108.0(1) ...4x 112.5(1) ...2x	107.0(1) 114.6(1)	135.0(1)	25.0(1)
[Ga _{0.50(1)} Al _{0.50(1)}]	177.4(3)	164.9(3)	231.6(4)	259(6)	324(8)	249(10) ^h 213(9) ^a	107.8(1) ...4x 112.8(1) ...2x	106.8(1) 115.0(1)	134.2(1)	25.4(2)
[Ga _{0.57(1)} Al _{0.43(1)}]	178.4(2)	163.7(2)	233.2(3)	256(3)	324(4)	251(5) ^h 210(5) ^a	108.2(1) ...4x 112.2(1) ...2x	106.9(1) 114.8(1)	134.3(1)	25.5(1)
[Ga _{0.59(1)} Al _{0.41(1)}]	178.7(2)	164.2(2)	231.2(1)	259(7)	324(9)	251(12) ^h 217(11) ^a	108.2(1) ...4x 112.0(1) ...2x	107.0(1) 114.6(1)	134.0(1)	25.9(1)
[Ga _{0.72(1)} Al _{0.28(1)}]	179.4(2)	163.4(2)	234.5(3)	253(4)	326(5)	250(6) ^h 221(5) ^a	108.6(1) ...4x 111.4(1) ...2x	107.2(1) 114.2(1)	133.9(1)	26.1(1)

[Al]	174.0(1)	163.0(1)	238.9(3)	258.4(4)	302.3(3)	294.0(4)	108.6(1) ...4x 111.3(1) ...2x	107.7(1) 113.1(1)	136.3(1)	24.6(1)
[Ga _{0.20(1)} Al _{0.80(1)}]	175.5(1)	162.1(1)	239.1(1)	255.8(1)	301.7(1)	294.0(1)	107.4(1) ...4x 113.6(1) ...2x	108.5(1) 111.4(1)	135.6(1)	25.0(1)
[Ga _{0.25(1)} Al _{0.75(1)}]	175.4(4)	163.9(4)	240.2(6)	251.7(1)	299.3(5)	295.3(5)	107.9(1) ...4x 112.7(1) ...2x	106.9(1) 114.8(1)	134.2(1)	25.5(2)
[Ga _{0.35(1)} Al _{0.65(1)}]	177.2(1)	163.0(1)	238.7(5)	253.9(6)	297.3(2)	304.2(3)	108.4(4) ...4x 111.6(1) ...2x	107.2(4) 114.1(1)	133.6(1)	26.4(1)
[Ga _{0.42(1)} Al _{0.58(1)}]	177.8(2)	163.0(2)	240.7(3)	248.7(4)	302.0(4)	296.2(5)	108.7(1) ...4x 111.1(1) ...2x	107.5(1) 113.7(1)	133.3(1)	26.7(1)
[Ga _{0.45(1)} Al _{0.55(1)}]	177.6(3)	163.2(3)	245.6(4)	243.2(4)	297.8(4)	304.4(4)	108.6(1) ...4x 111.2(1) ...2x	107.4(1) 113.7(1)	133.1(1)	26.9(1)
[Ga _{0.56(1)} Al _{0.44(1)}]	178.4(3)	164.6(3)	244.1(4)	243.2(4)	298.7(4)	305.7(4)	108.7(1) ...4x 111.0(1) ...2x	107.5(1) 113.4(1)	131.9(1)	27.9(2)
[Ga _{0.57(1)} Al _{0.43(1)}]	178.9(2)	162.3(3)	240.3(6)	249.0(6)	298.5(4)	302.4(5)	108.6(1) ...4x 111.3(1) ...2x	107.2(1) 114.1(1)	132.7(1)	27.1(2)
[Ga _{0.75(1)} Al _{0.25(1)}]	181.0(2)	162.9(2)	237.8(4)	248.9(4)	300.4(3)	302.6(4)	109.0(1) ...4x 110.6(1) ...2x	107.4(1) 113.8(1)	131.1(1)	28.5(1)
[Ga]	183.0(2)	160.5(2)	244.5(4)	244.7(4)	295.2(3)	318.1(4)	109.3(1) ...4x 109.7(1) ...2x	107.7(1) 113.0(1)	131.3(1)	28.8(1)

^hhighest, ^aaverage

In the XRD pattern the relative intensity of the $[h + k + l = 2n+1]$ planes increase (Figure 5.5) with increasing ‘y’ and one could further check the refined gallium concentration by calculating the intensity of the $[h + k + l = 2n+1]$ planes.

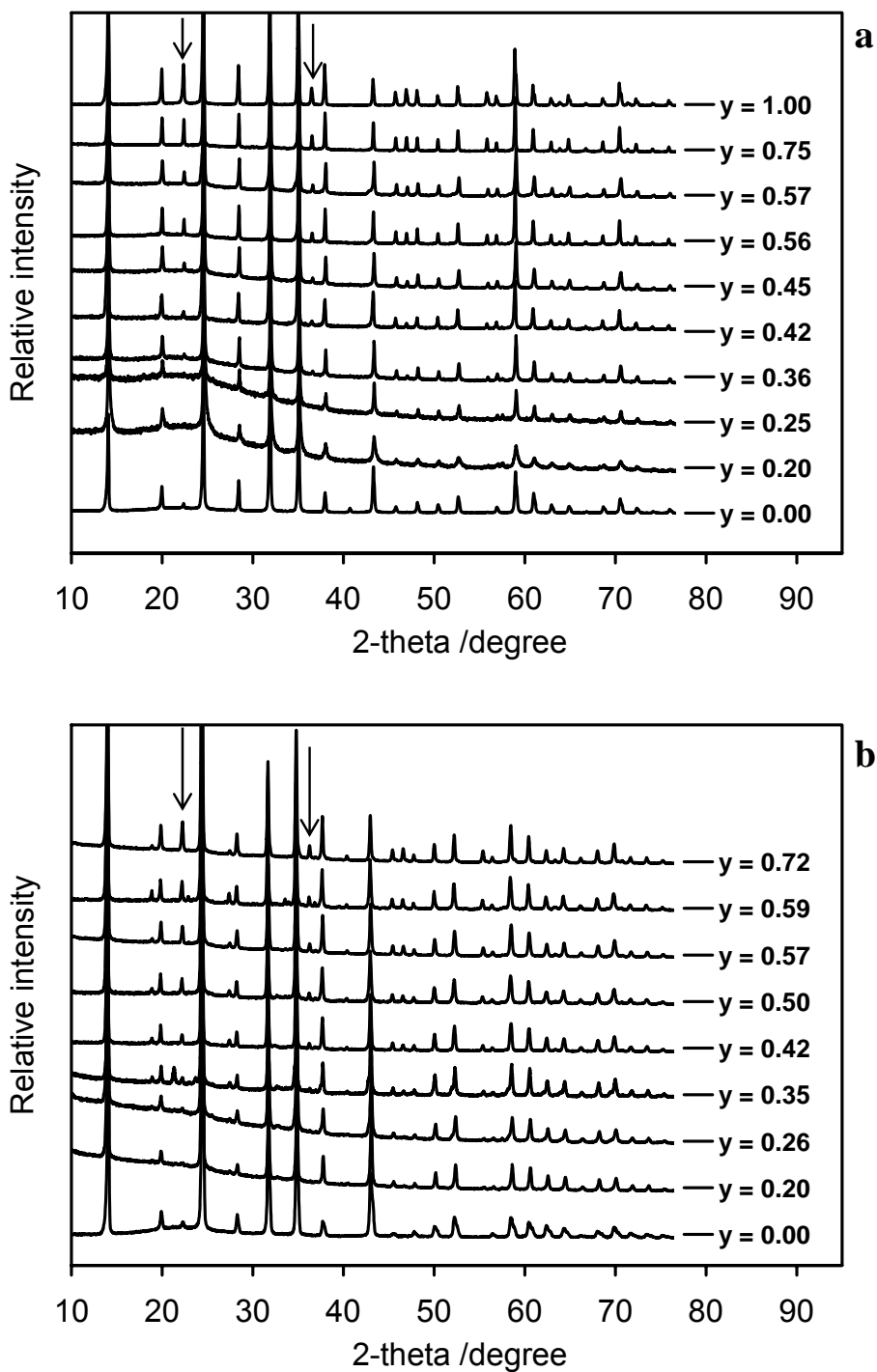


Figure 5.5: X-ray powder diffraction patterns (a) hydro-hydroxy and (b) hydro sodalites. The downward arrows belong to $[h + k + l = 2n+1]$ plane reflections.

Several structural parameters were observed correlated with the compositional ‘y’ values of H-H-SOD. The lattice parameter increases linearly with increasing gallium concentration (Figure 5.6a). Since the amount of the refined guest species (the ‘x’ value) is almost constant within σ throughout the series, and the XRD experiments were performed at room temperature, all other factors can easily be excluded and trivalent T-site electron concentration is solely responsible for this sort of change. This linear trend can be compared with $\text{Na}_8[\text{Al}_{1-y}\text{Ga}_y\text{SiO}_4]_6(\text{Cl}/\text{Br})_2$ [112], $\text{Na}_8[\text{AlSi}_x\text{Ge}_{1-x}\text{O}_4]_6\text{Br}_2$ [90] and $\text{Na}_8[\text{Al}_{1-y}\text{Ga}_y\text{SiO}_4]_6(\text{NO}_2)_2$ (see section 3.2.2) sodalite framework types. Additionally, it implies that the enclathrated guest species $\{(\text{OH}\cdot\text{H}_2\text{O})_x(\text{H}_2\text{O})_{8-4x}\}^-$ acts like that of discrete Cl^- or Br^- anions as a spacer inside the β -cage. Interestingly we did not observe any significant cell expansion in the corresponding H-SOD series with increasing gallium concentration. The fractional coordinate of O(2) and Na occupying the same crystallographic site (8e) decrease with increasing gallium content in the framework as well as the O(1) z coordinate decreases (Table 5.2). As a result, the Na-O(2) distance decreases along with O(2)-O(2) distance enlargement (Figure 5.6b). As a consequence the Na-O(1) and O(1)-O(2) distances remain almost constant resulting from the increasing O(2)-Na-(O2) angles. Therefore the strength of the possible hydrogen bonds [14] between O(1) and O(2) is believed to be partially responsible for the constant lattice parameter. The cell parameter does not change (Figure 5.6a) even when aluminum is fully substituted by the large T-atom gallium [95, 70] in the framework. This shrinkage could also be attributed from the so called tilt mechanism which will be discussed.

In our two series, the Al/Ga-O distances (ℓ_1) increase linearly with increasing gallium (Figure 5.6c) for its higher ionic radii while the Si-O distances (ℓ_2) were observed almost constant at 163.8 pm ($\sigma \sim 3 \sigma$) and 162.9 pm ($\sigma \sim 2.5 \sigma$) for hydro-hydroxy and hydro sodalite series, respectively. Therefore both the H-SOD and H-H-SOD series gain a progressive structural strain for increasing deviation between ℓ_1 and ℓ_2 distances because sodalites with alternate short and long T-O bonds give rise to more unstable and highly strained structure [114]. This possible increasing strain is released by increasing tilt angle (φ) [29, 34] in both H-SOD and H-H-SOD series. The increasing tilt was observed as a function of gallium concentration (Figure 5.6d) in both series, which is higher for H-SOD compared with its H-H-SOD counterpart. Since the H-SOD β -cage centre is empty within an extended off-centred volume and there is three sodium in contrast with four sodium in the H-H-SOD, the reduction of cage volume via tilt mechanism in H-SOD is more influential. Here it is notable that the empty cage sodalite $\text{Na}_6[\text{AlSiO}_4]_6$ [41] only exists at higher temperature and the cell volume thermally increases via reduction of tilt angle. From the above observation the flexibility of the H-SOD framework could easily be understood. On the other hand, the tetragonal tetrahedra distortion ($\Delta\alpha = \alpha' - \alpha''$ [29]) was observed exactly in opposite manner in these two sodalite types to release the framework strain as a secondary pathway. In the H-H-Sod the

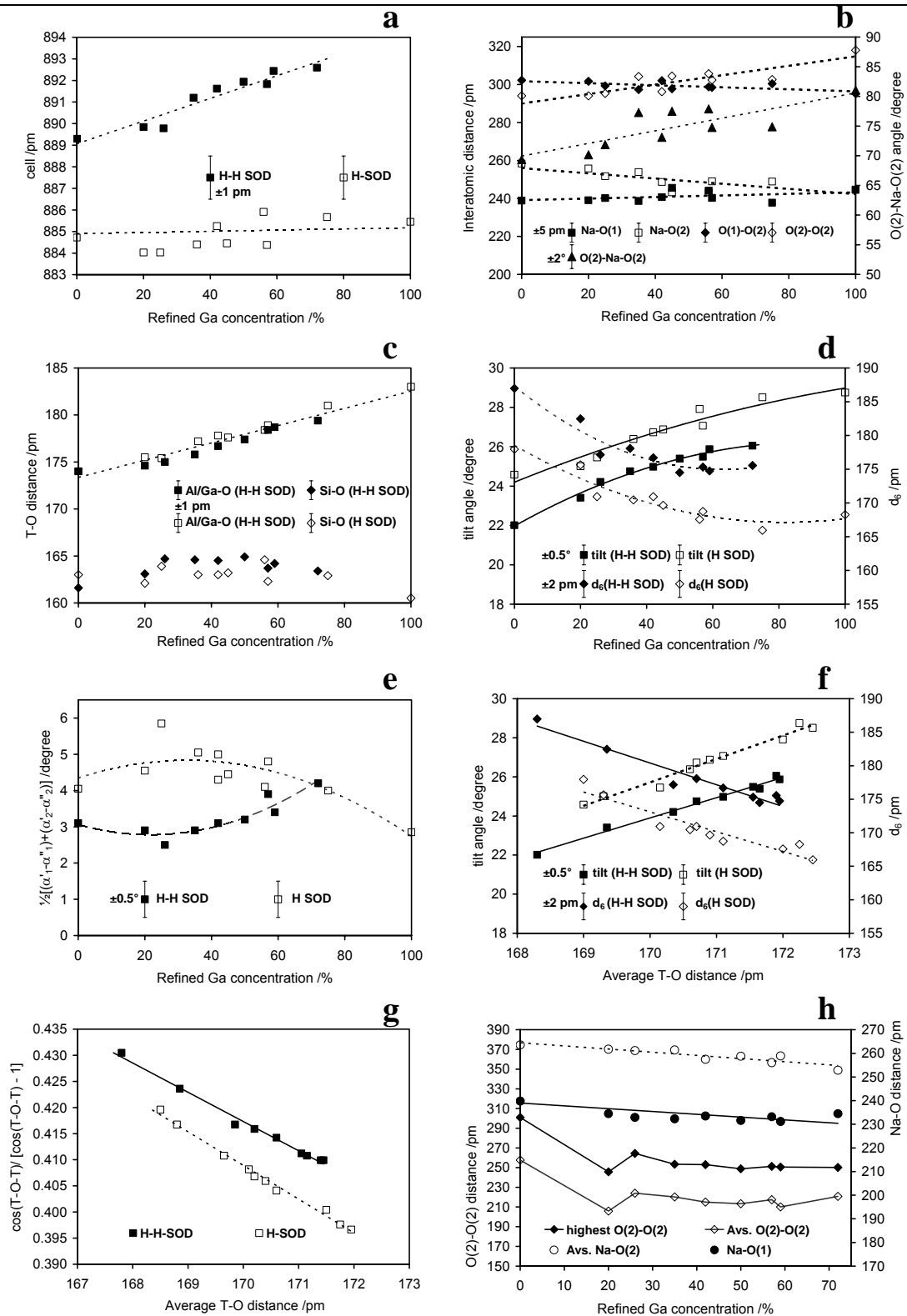


Figure 5.6: Structural parameters vs. refined Ga concentration. (a) cell parameter, (b) interatomic distances and angles among Na and O(1) and O(2) in H-SOD, (c) T-O distances, (d) tilt angle and sixring window diameter (d_6), (e) average tetragonal tetrahedra distortion, (f) tilt angle and sixring window diameter (d_6) vs. T-O distances, (g) degree of s-hybridisation, (h) interatomic distances among Na, O(1) and O(2) in H-H-SOD.

average tetragonal tetrahedra distortion $((\Delta\alpha_1 + \Delta\alpha_2)/2)$ increases, while it decreases in the H-SOD, through a second order polynomial (Figure 5.6e). In the H-SOD three sodium atoms hop within four possible available positions and thereby relaxed enough to take a suitable position in the cage as there is no central anionic attraction force to reduce its hopping rate. Additionally, $O(1)\cdots H\cdots O(2)$ bridging in the H-SOD structure possibly plays a role on the local geometry of TO_4 tetrahedra. Therefore $\Delta\alpha$ in the H-SOD system may differ from that of H-H-SOD.

The sixring window diameter (d_6) was calculated ($d_6 = 2[d_o/\sqrt{3} - r_o]$) where d_o is the O(1)-O(1) distances at nearest the bottleneck of the sixring window (Figure 5.7) and r_o is the oxygen radii (121pm [108]). d_6 decreases fast up to a gallium concentration of about 50% and then about to constant within 1.2 pm in both series with increasing gallium content. This behaviour could be assigned from the correlation between the tilt angle and the sixring aperture. The tilt angle increases until a maximum electrostatic compaction among those particular three framework oxygen O(1) and thereby the reduction of the effective window aperture. On the other hand, both the tilt angle and the sixring window diameter were observed linear with the average T-O distances (Figure 5.6f).

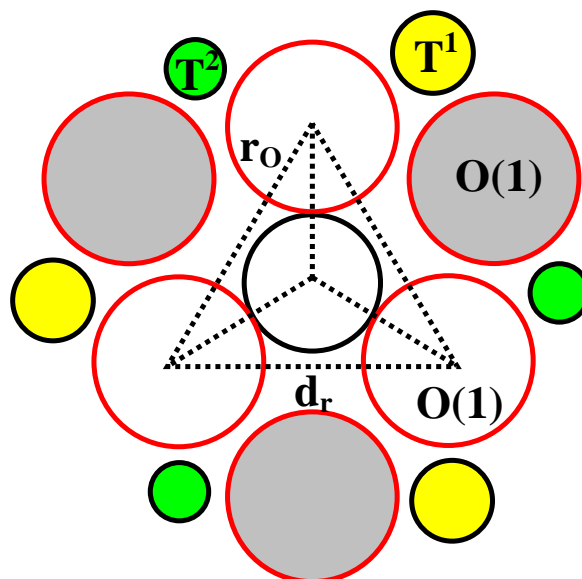


Figure 5.7: Calculation of sixring window diameter from three parallel framework oxygen O(1) where r_o and d_o are the atomic radii of O(1) and O(1)-O(1) nearest distance, respectively.

Framework oxygen adapts preferable s -hybridisation to offer the T-O-T angle (γ) to the structure. The degree of framework oxygen s -hybridisation (ρ) [104] decreases with increasing gallium content (Figure 5.6g) and the correlation seems to be as that of ϕ and d_6 . The gradual increasing deviation of ' ρ ' from the preferable silicate linkage value 0.45 [105]

further indicates the increasing T-O-T linkage strain adapted by the gallium enriched sodalites.

This part of the discussion is mainly concerned with the guest species of the H-H-SOD series. With increasing gallium concentration the z coordinate of O(1) decreases (Table 5.2) and as result Na-O(1), Na-O(2) and O(2)-O(2) distances decrease (Figure 5.6h). From the O(1)···Na···O(2) ···O(2) correlations an increasing centre directed force could be assumed with progressive gallium incorporation in the framework. Therefore the O(2)-made truncated tetrahedra gains compaction gradually and that is clear from the decreasing of O(2)-O(2) distances.

Wiebcke et al. [14] explained a strong linear hydrogen bonding between the longest O(2)-O(2) distances (236 pm) from X-ray and neutron data studies. They did not encounter the other possible O(2)-O(2) distances created from high degree of disorder of the H_3O_2^- guest species. Considering this observation the possibilities of strong hydrogen bonding between the longest O(2)-O(2) distances can not be drawn from our alumogallosilicate and alumosilicate H-H-SOD types for not optimistic O(2)-O(2) distances [125]. On the other hand, taking the average O(2)-O(2) distances this sort of hydrogen bonding could be predicted in our H-H-SOD systems for $0 \leq y < 1$. Consequently, the strength of hydrogen bonding could apparently be observed with decreasing O(2)-O(2) distances with increasing gallium content in the framework (Figure 5.6h). Therefore in one of the end members $\text{Na}_{7.1(1)}[\text{AlSiO}_4]_6(\text{OH}\cdot\text{H}_2\text{O})_{1.1(1)}(\text{H}_2\text{O})_{3.5(1)}$ sodalite system (which is believed not to be an as-synthesised sodalite rather a secondary product produced via uncontrollable aqueous exchange during exchange process) the strength of this sort of strong hydrogen bonding [14] is the least. This result also indicates that increasing water diffusion into the β -cage may diminish the possibilities of this linear strong hydrogen bonding among the off-centred non framework oxygen. For relatively a higher H_2O content the $\{(\text{OH}\cdot\text{H}_2\text{O})_{1.1(1)}(\text{H}_2\text{O})_{3.5(1)}\}^-$ truncated tetrahedron could poorly be explained for the highest O(2)-O(2) distances of the series. Therefore a further O(2)-O(2) elongation could be predicted for more incoming oxygen atoms via H_2O in the exchange process due to preferable spatial accommodation. Probably this off-centring phenomenon is associated with driving one sodium atom off the cage and thereby a preferable new crystallographic site (8e) is chosen by O(2) atoms in pure hydro sodalites. As a further consequence, higher dynamics of sodium is expected in H-SOD within a vacant centre and non charged H_2O compared with H-H-SOD which is in agreement with ^{23}Na MAS NMR data (FWHM = 1.9 KHz and 3.5 Hz for H_3O_2^- and H_2O enclathrated sodalites, respectively) reported by Engelhardt et al. [110]. Hydrogen could not be refined with the conventional XRD studies. The high degeneracy and disordered dynamics of hydrogen were proposed by several literatures with respect to time average. Therefore the

source of hydrogen could hardly be detected in our H-H-SOD and we thereby further propose the guest species as $\{(\text{OH}\cdot\text{H}_2\text{O})_x(\text{H}_2\text{O})_{8-4x}\}^-$ rather than discrete OH^- or H_2O or even H_3O_2^- .

The average crystal size (L) for the both series was calculated by using Scherrer equation. L was observed with a slight increasing behaviour with increasing gallium concentration in H-H-SOD, while the trend is sharper in the H-SOD series (Figure 5.8). Nevertheless, the hydro sodalites are not as synthesised samples and the degree of crystallinity and average crystal size also depend on the conditions of the exchange procedure.

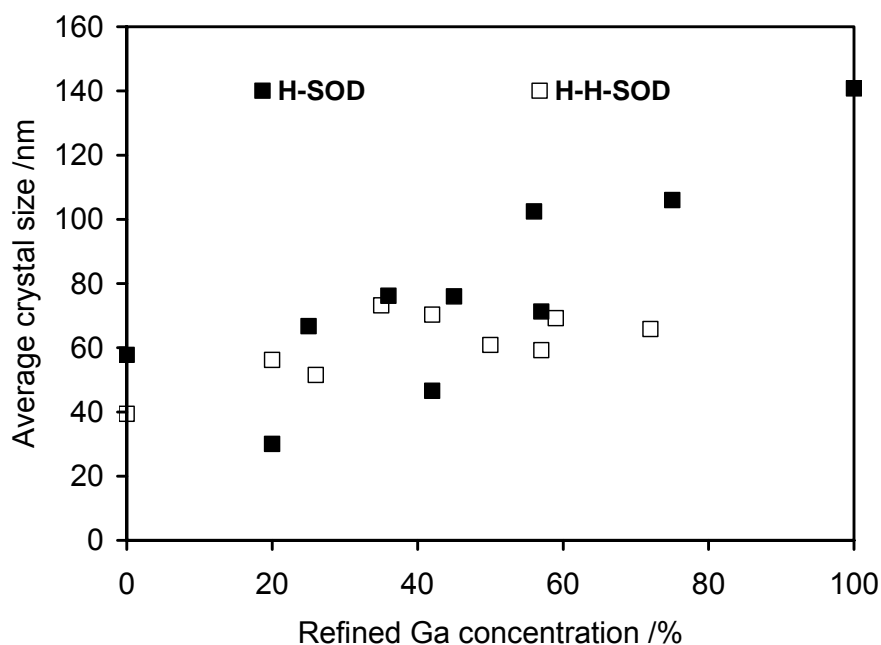


Figure 5.8: Average crystal size vs. refined gallium concentration.

5.2.3 MAS NMR INVESTIGATIONS

In the ^1H MAS NMR spectra of the H-H-SOD series, two peaks at 3.5(5) ppm and 1.0(2) ppm were observed which could be assigned to H_2O and OH^- , respectively, in the sodalite cavity (Figure 5.9a). A sample of $\text{Na}_{6+x}[\text{AlSiO}_4]_6(\text{OH}\cdot\text{H}_2\text{O})_x(\text{H}_2\text{O})_{8-4x}$ composition was produced and dried without washing, which contains a lot of surface NaOH as well as CO_3^{2-} . This sample (H-H-SOD*) shows an extra broad peak at ~ 15.8 ppm (Figure 5.9a) which can be compared with the chemical shift (16.3 ppm) of central proton of the strong hydrogen bond in the H_3O_2^- species of Wiebcke et al. [14]. Although we observed a convenient O(2)-O(2) average distance to explain the existence of the H_3O_2^- species, no corresponding ^1H NMR peak was observed.

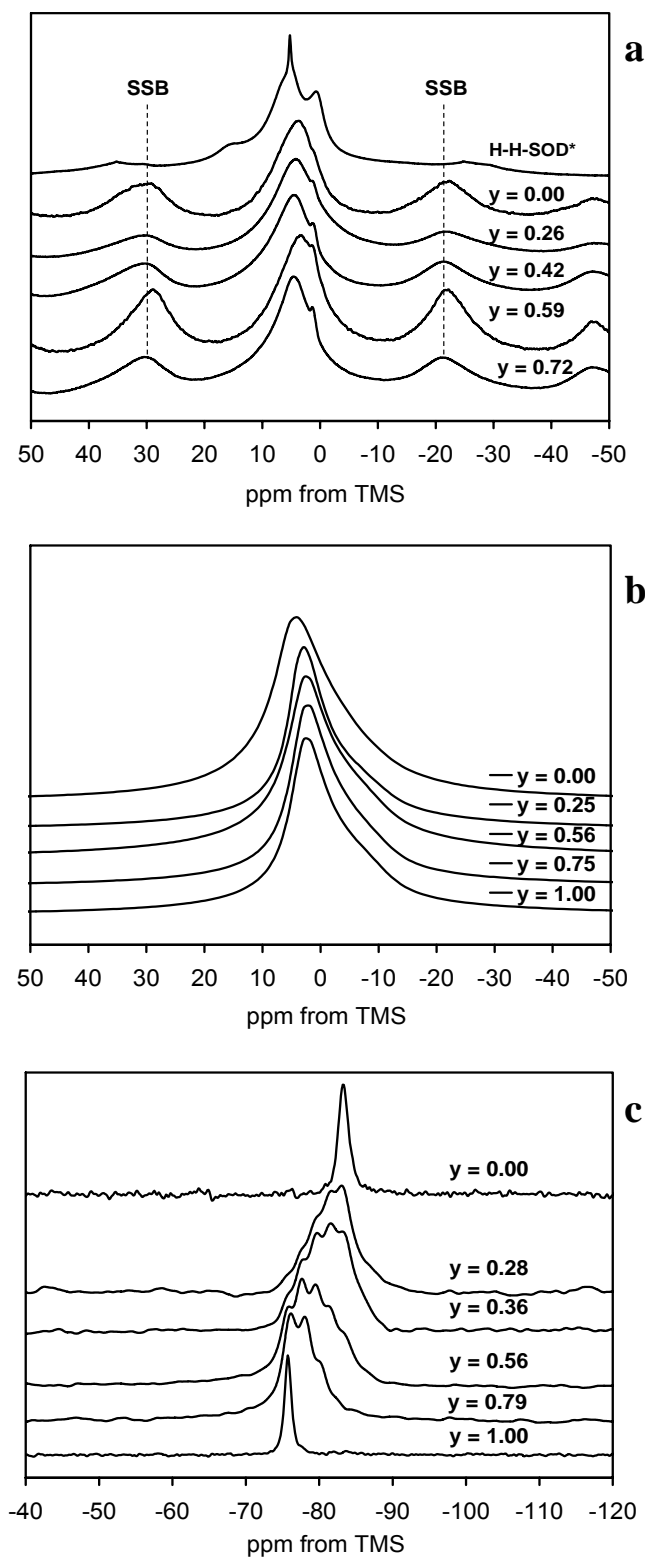


Figure 5.9: ^1H MAS NMR spectra of H-H-SOD (a) and H-SOD (b) where the 'y' values were calculated from XRD results and SSB denotes spinning sidebands. ^{29}Si MAS NMR spectra of H-SOD (c) where the 'y' values were calculated from ^{29}Si MAS NMR spectra.

In contrast, we observed only a single peak at ~ 4.2 ppm (Figure 5.9b) for each H-SOD sample throughout the series irrespective of the ‘y’ magnitude. The relative high broadening of the peak could be assigned from the statistical distribution of hydrogen of four H₂O per cage, which may be influenced by the hopping of the three sodium atoms inside the β -cage on the NMR timescale.

Table 5.4: ²⁹Si MAS NMR fit results of Na₈[Al_{1-y}Ga_ySiO₄]₆(H₂O)₈. The chemical shift (δ /ppm), the halfwidth (FWHM /ppm) and the integrated peak intensity (I_{int} /counts) divided by 10⁴ are given together with the calculated gallium Conc.

SiO ₄ (Ga ₄)			SiO ₄ (Ga ₃ Al)			SiO ₄ (Ga ₂ Al ₂)			SiO ₄ (GaAl ₃)			SiO ₄ (Al ₄)			(y)	(y)
δ	FWHM	I_{int}	δ	FWHM	I_{int}	δ	FWHM	I_{int}	δ	FWHM	I_{int}	δ	FWHM	I_{int}	NMR	XRD
												-83.31	1.69	24.14	0	0
-75.84	3.10	1.20	-77.47	2.72	1.90	-79.56	2.82	7.85	-81.48	2.61	14.92	-83.35	2.90	61.46	28(1)	26(2)
-75.53	3.13	22.55	-77.88	2.66	44.49	-79.68	2.82	78.06	-81.55	2.82	92.80	-83.35	2.72	133.07	32(1)	35(2)
-75.65	2.31	12.71	-77.48	2.46	41.53	-79.63	2.77	73.53	-81.75	2.65	76.80	-83.83	2.57	68.21	36(1)	42(2)
-75.48	2.43	118.52	-77.57	2.60	191.45	-79.65	2.66	175.17	-81.62	2.28	96.03	-83.66	2.69	84.99	56(1)	56(2)
-75.94	2.27	169.91	-78.10	2.15	139.21	-80.22	2.11	59.27	-82.24	2.19	12.82	-84.08	2.00	6.15	79(1)	75(2)
-75.74	1.09	77.17													100	100

The ²⁹Si MAS NMR spectra (Figure 5.9c) show single peaks at -83.3 ppm and -75.7 ppm for Na₆[AlSiO₄]₆(H₂O)₈ and Na₆[GaSiO₄]₆(H₂O)₈ sodalites, respectively. According to an extended Loewenstein rule [37] these two phases consist perfect ordering of Si(OAl)₄ and Si(OGa)₄ species in the sodalite frameworks. The halfwidth of Na₆[AlSiO₄]₆(H₂O)₈ sodalite was observed higher than that of Na₆[GaSiO₄]₆(H₂O)₈ sodalite which is in agreement with other corresponding sodalite systems, i.e., Na₈[AlSiO₄]₆Cl₂ (1.20 ppm), Na₈[GaSiO₄]₆Cl₂ (0.97 ppm), Na₈[AlSiO₄]₆Br₂ (2.67 ppm), Na₈[GaSiO₄]₆Br₂ (2.22 ppm) [112], Na₈[AlSiO₄]₆I₂ (1.48 ppm), Na₈[GaSiO₄]₆I₂ (1.36 ppm) [126], Na₈[AlSiO₄]₆(NO₂)₂ (1.62 ppm) and Na₈[GaSiO₄]₆(NO₂)₂ (0.92 ppm) [section 3]. Probably this phenomenon could be attributed to different cell parameters except aluminosilicate and gallosilicate hydro sodalites where the cell parameter deviation between these two end members cannot be encountered (Table 5.2). It is possibly from different degree of crystallinity of the samples and a corresponding idea could be predicted from Figure 5.8. Partial isomorphous substitution in the trivalent T-site leads to a result of different Ga/Al ratio. Therefore SiO₄ tetrahedra could be surrounded by five possible environments: SiO₄(Ga)₄, SiO₄(Ga₃Al), SiO₄(Ga₂Al₂), SiO₄(GaAl₃) and SiO₄(Al)₄ for 0 < y < 1. Five corresponding signals were observed (Figure 5.9c) for different Ga/Al ratio in the sodalites and their respective peak positions together with halfwidth and integrated intensity were summarised in Table 5.3. Throughout the series, no more than five peaks were observed or calculated. This result suggests Si/Al_{1-y}Ga_y = 1 ratio in the framework and also agrees with the XRD results of fully occupied silicon position in each phase. According to peak shape and corresponding integrated intensity these five species are statistically distributed (see section 3.2.3) in the whole crystalline samples. Five distinct peaks were observed between -76.0(1) ppm to -84.0(1) ppm with an estimated average negative increase of about 1.6 ppm (all δ (Si) should be considered from TMS). Therefore each Al substitution with Ga in the SiO₄(Al)₄

species leads about 1.6 ppm downfield shift and vice versa. From the distinct five peaks of each composition were fitted using ‘dmfit2003’ [93] program and their corresponding Ga/Al ratios were accounted from the Gaussian /Lorentzian peak areas. In some profiles, adjacent peak maxima were hardly distinguished for merging but careful attention was paid to the average halfwidth for each spectra fitting. The calculated Ga/Al ratio resulting from ^{29}Si MAS NMR is in good agreement with the XRD refined results (Table 5.3).

5.2.4 FTIR INVESTIGATIONS

The main infrared absorption bands for aluminosilicate, alumogermante, gallosilicate, gallogermanate and many other cubic sodalites are in the range of $300\text{-}1200\text{ cm}^{-1}$ [109, 118, 119] and the position of each individual band depends on type of T-atoms and the encapsulated guest species. The IR spectroscopic results are given in Figure 5.10. A sharp absorption band at 3636 cm^{-1} of hydroxide was observed in H-H-SOD series, which was absolutely absent in the corresponding H-SOD series. The bending mode of water at $\sim 1650\text{ cm}^{-1}$ along with a broad band between 3100 cm^{-1} and 3600 cm^{-1} was observed in both H-SOD and H-H-SOD series. A weak characteristic CO_3^{2-} band at $\sim 1420\text{ cm}^{-1}$ (but not another characteristic CO_3^{2-} band at $\sim 880\text{ cm}^{-1}$ which was observed in H-H-SOD* sample) was seen which was probably from the cancrinite impurities cocrystallised during synthesis and washed away during exchange to corresponding H-SOD.

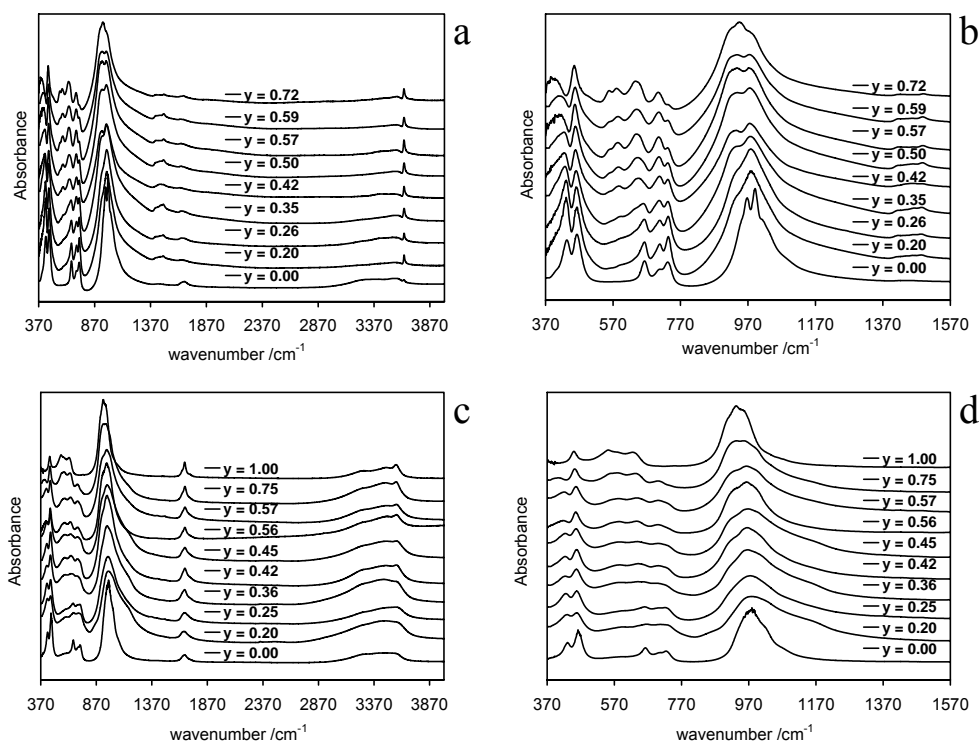


Figure 5.10: FTIR spectra of (a) H-H-SOD, (b) enlarged 5.10a, (c) H-SOD and (d) enlarged 5.10c.

The asymmetric T-O-T stretching (ν_{as} T-O-T), symmetric T-O-T stretching (ν_s T-O-T) and bending O-T-O (δ O-T-O) modes were observed in the mid infrared region. More than one band was observed for ν_{as} T-O-T with several maxima within a broad range between 800 cm^{-1} and 1200 cm^{-1} for $0 \leq y \leq 1$. Three bands of ν_s T^{IA} -O-T² (728 cm^{-1} , 707 cm^{-1} , 663 cm^{-1} and $T^{IA} = Al$), and three bands of T^{IG} -O-T² (628 cm^{-1} , 582 cm^{-1} , 553 cm^{-1} where $T^{IG} = Ga$) were observed in hydro sodalite for $y = 0$ and 1, respectively. The corresponding results of ν_s T^{IA} -O-T² (731 cm^{-1} , 706 cm^{-1} , 662 cm^{-1}) and T^{IG} -O-T² (638 cm^{-1} , 582 cm^{-1} , 556 cm^{-1}) were observed for $y = 0$ and 1, respectively, were obtained for H-H-SOD. Any significant shift of ν_s T^{IA} -O-T² band set was not observed between H-SOD and H-H-SOD though there is distinct difference between their cell parameters. In both series, we do not observe a shift of the ν_s T-O-T mode from the position of one end member to the other. With the decreasing intensity of the set of ν_s T^{IA} -O-T² mode, the intensity of ν_s T^{IG} -O-T² set increases with increasing gallium concentration. This result completely agrees with the same behaviour shown by aluminosilicate chloride /bromide [112] and nitrite sodalites (see section 3.2.4) where a detailed explanation is available. One of the δ O-T-O bands was observed at 431 cm^{-1} for $y = 0$ in both series and gradually went to lower wavenumber along with decreasing intensity with increasing gallium concentration (Figure 5.10b, d) and finally disappeared for pure gallosilicate matrix. On the other hand, the second δ O-T-O band was observed at $\sim 462\text{ cm}^{-1}$ and 463 cm^{-1} for $y = 0$ for H-SOD and H-H-SOD, respectively. This band shifts to lower wavenumber along with almost constant intensity with increasing 'y'. The above observation is in agreement with the given number of bending modes (2-3 and 1 for the aluminosilicate and gallosilicate framework, respectively,) by Henderson and Taylor [109]. This linear trend between wavenumber and 'y' was undertaken to calculate the gallium concentration. This will

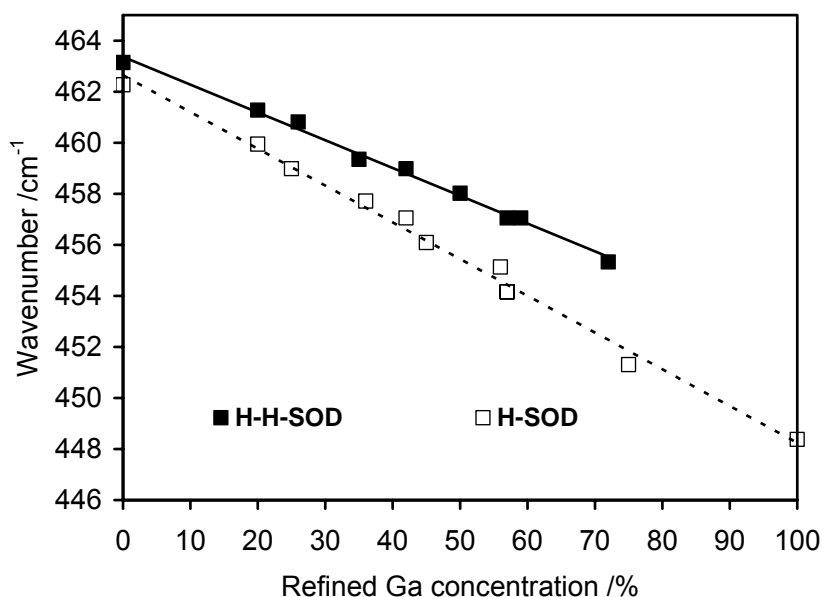


Figure 5.11: Position of O-T-O bending mode (δ O-T-O) vs. refined Ga concentration.

give the possibility to estimate the framework composition of this sodalite types with an easy and fast IR technique. The two proposed equations are: $Ga \% = 3188.259 - 6.890W_H$ ($R^2 = 0.996$) and $Ga\% = 4227.803 - 9.123W_{H-H}$ ($R^2 = 0.996$) (W = wavenumber) for the H-SOD and H-H-SOD, respectively. Nevertheless, the two equations bears the significance of linear correlation (Figure 5.11) between the position of O-T-O bending mode and the framework composition rather than to calculate gallium concentration within reasonable accuracy since the halfwidth of that peak is almost twice of the total shift range (see section 3.2.4, 4.2.4).

5.3 CONCLUSION

Gallosilicate hydro-hydroxy sodalite could not be produced without using template in the mentioned reaction conditions. In contrast, even 20% aluminium containing alumogallosilicate sodalite was obtained from the same types of starting materials and reaction conditions. It probably indicates a vital role of aluminium in the crystallisation of alumogallosilicate sodalites. The framework composition does not change throughout the leaching of NaOH with H₂O for the conversion of hydro-hydroxy sodalite to corresponding hydro sodalite. This is also true even for the partially leached intermediate products. Additionally, the exchange method by using low concentrated acid is fast compared with the conventional autoclave exchange process. Various structural features were distinguished from hydro to hydro-hydroxy sodalites throughout this study. The lattice parameter of hydro-hydroxy sodalite increases from 889.3 pm to 892.6 pm with increasing gallium concentration in the framework, while in the hydro sodalite series the cell parameter does not change from one end member to other and remains constant at about 884.8 pm within 2σ . Both aluminium and gallium were found in the same crystallographic site 6c and Al/Ga-O distance cannot be distinguished from Al-O and Ga-O distances in the alumogallosilicate sodalite system. Al/Ga-O distances increase with increasing gallium content in the framework. The Si-O distances was observed almost constant at 163.8 pm (within 3σ) and 162.9 pm (within 2.5σ) for hydro-hydroxy and hydro sodalite, respectively. Besides, other structural parameters have also been observed as a function of compositional 'y' value, i.e., Na-O distance, T-O-T angle, tilt angle, tetragonal tetrahedra distortion, sixring window, and framework oxygen *s*-hybridisation. The average crystal size (*L*) has also been calculated from the halfwidth of [211] reflections of sodalite X-ray patterns. *L* increases with increasing gallium content in the framework in H-SOD series. Probably this is an indication of producing gallosilicate hydro sodalite single crystals in a low alkaline solution [95]. Additionally, gallium concentration was calculated from the NMR fit spectra, which is in agreement with the results obtained from XRD studies. A temperature-pressure investigation along with partial framework T-site substitution would be very interesting for the fine tuning of the sixring aperture of sodalite β -cage.

6 SUMMARY

6.1 ENGLISH

KEY WORDS: Gallium substitution, Sodalite, Synthesis and Characterisation

Partial substitution of aluminium by gallium revealed an extensive isomorphic miscibility in the $\text{Na}_{6+x}[\text{Al}_{1-y}\text{Ga}_y\text{SiO}_4]_6\text{Y}_x(\text{H}_2\text{O})_{8-4x}$ sodalite systems where $0 < x < 2$ and $0 < y < 1$ and $\text{Y} = \text{NO}_2^-$, Cl^- , Br^- or $(\text{OH}\cdot\text{H}_2\text{O})_x^-$. Each composition for $0 < y < 1$ is isotypic to the end members ($y = 0$ or 1). The Ga/Al ratio was controlled by selective initial stoichiometry in the hydrothermal synthesis. For the nitrite, chloride and bromide sodalite series, NaAlO_2 and NaGaO_2 were used for the source materials of aluminium and gallium, respectively, while Al_2O_3 and Ga_2O_3 were found favourable for the corresponding hydro-hydroxy sodalite production. In all cases Na_2SiO_3 was used as silicon source. There were significant differences in synthesis conditions with and without templates. $\text{Na}_8[\text{Al}_{1-y}\text{Ga}_y\text{SiO}_4]_6(\text{NO}_2)_2$, and $\text{Na}_8[\text{Al}_{1-y}\text{Ga}_y\text{SiO}_4]_6(\text{Cl}/\text{Br})_2$ sodalites were synthesised at 48 hours using low concentrated alkaline solutions of 2M NaOH. In contrast, 8M NaOH was used in preparing $\text{Na}_8[\text{Al}_{1-y}\text{Ga}_y\text{SiO}_4]_6(\text{OH}\cdot\text{H}_2\text{O})_8(\text{H}_2\text{O})_{8-4x}$ sodalites at only 6 hours reaction period. Gallosilicate hydro-hydroxy sodalite could not be produced by the used reaction conditions. Pure gallosilicate hydro sodalite was produced by treating gallosilicate iodide sodalite together with deionised water at 473 K in autoclave at autogenous pressure. Hydro sodalites $\text{Na}_6[\text{Al}_{1-y}\text{Ga}_y\text{SiO}_4]_6(\text{H}_2\text{O})_8$ of corresponding 'y' values were obtained from hydro-hydroxy sodalites by exchange experiments in aqueous solution within a controlled pH range of 5.5 to 6.5. The framework composition does not change throughout the leaching of NaOH with H_2O for the conversion of hydro-hydroxy sodalite to corresponding hydro sodalite. This is true even for the partially leached intermediate products. Additionally, the exchange method by using low concentrated acid is fast compared with the conventional autoclave exchange process. The gallium concentration in the framework was always lower than the theoretical maximum concentration calculated from the starting precursors. During X-ray powder data refinement, gallium and aluminium atoms were found in the same crystallographic position (6c) in P-43n space group. The silicon site (6d) was always obtained fully occupied. Each refinement ensures a common $[\text{Al}_{1-y}\text{Ga}_y\text{SiO}_4]_6$ framework type for $0 < y < 1$. Both aluminium and gallium are statistically distributed in the T^1 -sites. Therefore the T^1 -O distances do not reflect either Al-O or Ga-O distances, but an averaged distance of Al/Ga-O. The lattice parameters increase linearly from aluminosilicate nitrite (893.5 pm), chloride (887.8 pm), bromide (893.7 pm), hydro-hydroxy (889.3 pm) sodalite to gallosilicate nitrite (898.9 pm) chloride (893.7 pm), bromide (899.5 pm) and hydro-hydroxy (892.6 pm for $y = 0.72$) sodalites. In the hydro sodalite series the cell parameter does not change from one end member to other and remains constant at about 884.8 pm within 2σ . The interatomic distance between framework oxygen

(O(1)) and water molecule (O(2)) remains almost constant. Therefore the strength of O(1)···H···O(2) bridging bond remains constant and thereby the cell parameter. In all other described sodalites the z coordinate of framework oxygen decreases from aluminosilicate to gallosilicate framework, which is correlated with the change of cell parameter. The Al/Ga-O distances increase (between 173.0 pm to 183.0 pm from aluminosilicate to gallosilicate) with increasing gallium concentration in the framework. The Si-O distances were observed almost constant at 163.0 pm ($\sigma \sim 1.0$), 162.8 pm ($\sigma \sim 2.0$), 163.4 pm ($\sigma \sim 3.0$), 163.8 pm ($\sigma \sim 3 \sigma$) and 162.9 pm ($\sigma \sim 2.5 \sigma$) for nitrite, chloride, bromide, hydro-hydroxy and hydro sodalite series, respectively. The average tilt angle (φ) increases with increasing gallium content in the framework to release the progressive structural strain. In contrast, tetragonal tetrahedra distortion did not show any common behaviour among the investigated systems with respect to refined gallium concentration. The effective six-membered ring diameter (d_6) was tuned (within ~ 10.0 pm) with successive gallium incorporation in the framework. d_6 decreases sharply for nitrite, chloride, and bromide series from aluminosilicate to gallosilicate sodalites, while it seems to be almost constant for high gallium enriched hydro-hydroxy sodalites after an initial rapid change. The framework oxygen s-hybridisation was observed decreasing with increasing gallium content resulting either from increasing Al/Ga-O distances, tilt angles or decreasing Al/Ga-O-Si angles (γ). Therefore the T-O-T linkage stability decreases from aluminium enriched framework to gallium enriched counterpart. The Na-O(1), Na-O(2) (O(2) from NO_2^- or $(\text{OH}\cdot\text{H}_2\text{O})_x^-$), Na-Cl and Na-Br distances decrease with increasing tilt or gallium concentration, which shows a direct correlation between framework and non-framework atoms as well as a compaction phenomenon of the enclathrated templates.

The fractional coordinate of both nitrogen and oxygen of NO_2^- were observed within high deviation (max. up to third decimal). Out of these the NO_2^- was assumed to be in high disordered dynamics or in a rotational state where the nitrite ion changes the orientation of its molecular axis with respect to the crystallographic axis, and that this rotation occurs around the centre of the β -cage. In the hydro-hydroxy sodalite the template oxygen O(2) was refined with a lower local symmetry (24i) and it was impossible to distinguish between the oxygen from OH^- or H_2O in the β -cage. Therefore the guest composition was used as $\{(\text{OH}\cdot\text{H}_2\text{O})_x(\text{H}_2\text{O})_{8-4x}\}^-$.

In the ^{29}Si MAS NMR spectra single peaks (-80.0 ppm, -78.9 ppm, -80.1 ppm, -75.7 ppm for gallosilicate, -86.4 ppm, -85.0 ppm, -86.2 ppm and -83.3 ppm for aluminosilicate nitrite, chloride and hydro sodalite, respectively) were observed for the end members ($y = 0$ or 1) in all the series, which are in good agreement with the reported literature. In contrast, five distinct peaks were observed for corresponding $\text{SiO}_4(\text{Ga}_4)$, $\text{SiO}_4(\text{Ga}_3\text{Al})$, $\text{SiO}_4(\text{Ga}_2\text{Al}_2)$, $\text{SiO}_4(\text{GaAl}_3)$ and $\text{SiO}_4(\text{Al}_4)$ silicon environments for $0 < y < 1$. These five peaks were fitted and their corresponding Ga/Al ratios were accounted from the Gaussian /Lorentzian peak

area. The calculated Ga/Al ratios resulting from ^{29}Si MAS NMR are in very good agreement with XRD refined results. From the shape and shift of the intensity maxima of the five different Q_4 signals a complete statistical distribution of aluminium and gallium atoms was observed throughout the whole crystal almost in all sodalites. In contrast, a clear indication of domain formation was found in some nitrite and bromide sodalites ($\text{Na}_8[\text{Al}_{1-y}\text{Ga}_y\text{SiO}_4]_6(\text{NO}_2)_2$, $\sim 0.35 > y > 0.70$ and $\text{Na}_8[\text{Al}_{1-y}\text{Ga}_y\text{SiO}_4]_6\text{Br}_2$, $y = 0.54$) where the intensity of $\text{Si}(\text{OGa})_4$ and $\text{Si}(\text{OAl})_4$ peaks are higher than that of the other three configurations. This is a hint for a non-statistical distribution, i.e. domains formation of aluminium and gallium enriched parts in the crystals. Therefore we assume that these domains are smaller than the coherence length of the X-ray radiation but big enough to be detected by MAS NMR technique. These hints have to be proved by further investigations.

Characteristic template absorption bands were observed for the corresponding sodalite compositions in the mid infrared region. Since the chloride and bromide bands are absent within the measured range further FIR investigation would be very interesting to check whether any distinct shift of those characteristic bands are with increasing gallium concentration in the framework. The asymmetric T-O-T stretching (ν_{as} T-O-T), symmetric T-O-T stretching (ν_{s} T-O-T) and O-T-O bending (δ O-T-O) modes were observed in the mid infrared region. More than one band was observed for ν_{as} T-O-T with several maxima within a broad range of 800 cm^{-1} to 1200 cm^{-1} for $0 \leq y \leq 1$. Three bands of $\nu_{\text{s}} \text{T}^{1\text{A}}\text{-O-T}^2$ ($\text{T}^{1\text{A}} = \text{Al}$) and three to five bands of $\text{T}^{1\text{G}}\text{-O-T}^2$ ($\text{T}^{1\text{G}} = \text{Ga}$) were observed for $0 < y < 1$ in all series. We observed only a very small shift of the ν_{s} T-O-T mode from the position of one particular end member to the other for the change of cell parameter. The decreasing intensity of the ν_{s} Si-O-Al modes with increasing gallium concentration indicates that the total amount of this type of vibrations decreases. In contrast, the amount of ν_{as} Si-O-Ga vibrations increase with increasing gallium content observed in increasing intensities of these bands. Taking this behaviour as a basic observation one can derive a local origin of these vibrations separated from the neighbouring one which is then a short range order vibration involving only one T^1 , one T^2 and one oxygen atom. Two δ O-T-O bands were observed between 430 cm^{-1} and 470 cm^{-1} for $0 \leq y < 1$. The lower valued one gradually went to lower wavenumbers along with decreasing intensity with increasing gallium concentration and finally disappeared for pure gallosilicate matrix. In contrast, the second δ O-T-O band shifts to lower wavenumbers along with almost constant intensity with increasing gallium concentration. Using this linear correlation one could check the Al/Ga ratio in the framework from the regression curve.

6.2 DEUTSCH

SCHLAGWÖTER: Gallium Substitution, Sodalith, Synthese und Charakterisierung

Die Substitution des Aluminiums durch Gallium zeigt eine vollständige isomorphe Austauschbarkeit im Sodalithsystem $\text{Na}_{6+x}[\text{Al}_{1-y}\text{Ga}_y\text{SiO}_4]_6\text{Y}_x(\text{H}_2\text{O})_{8-4x}$ mit $0 < x < 2$, $0 < y < 1$ und $\text{Y} = \text{NO}_2^-$, Cl^- , Br^- oder $(\text{OH}\cdot\text{H}_2\text{O})_x^-$. Jede Zusammensetzung für $0 < y < 1$ ist isotyp zu den beiden entsprechenden Endgliedern der Reihe ($y = 0$ bzw. 1). Das Ga/Al Verhältnis wurde durch die jeweils in der Hydrothermalsynthese eingesetzten Stöchiometry bestimmt. Für die Nitrit, Chlorid und Bromid Sodalith Serie wurde NaAlO_2 und NaGaO_2 als Ausgangsverbindung für Aluminium und Gallium verwendet, wohingegen für die Darstellung der Hydro-Hydroxy-Sodalithe Al_2O_3 und Ga_2O_3 eingesetzt wurden. In allen Fällen wurde Na_2SiO_3 als Siliziumquelle genutzt. Es waren signifikante Unterschiede in der Synthese mit und ohne Templatsalze zu beobachten. $\text{Na}_8[\text{Al}_{1-y}\text{Ga}_y\text{SiO}_4]_6(\text{NO}_2)_2$ und $\text{Na}_8[\text{Al}_{1-y}\text{Ga}_y\text{SiO}_4]_6(\text{Cl}/\text{Br})_2$ Sodalithe wurden innerhalb von 48 Stunden unter Verwendung von 2M NaOH dargestellt. Im Gegensatz dazu musste bei Synthese von $\text{Na}_8[\text{Al}_{1-y}\text{Ga}_y\text{SiO}_4]_6(\text{OH}\cdot\text{H}_2\text{O})_8(\text{H}_2\text{O})_{8-4x}$ 8M NaOH bei einer Reaktionszeit von nur 6 Stunden verwendet werden. Gallosilikatische Hydro-Hydroxy Sodalith war auf diesem Weg nicht herzustellen. Dazu wurde ein gallosilikatischer Jodid-Sodalith mit Wasser hydrothermal umgesetzt. Die entsprechenden Hydro-Sodalithe der Serie $\text{Na}_6[\text{Al}_{1-y}\text{Ga}_y\text{SiO}_4]_6(\text{H}_2\text{O})_8$ wurde durch kontrollierte Säurebehandlung im pH Bereich 5.5 bis 6.5 erhalten. Bei diesem Austausch von NaOH mit H_2O wurde die Zusammensetzung des Sodalithgerüsts nicht verändert. Hinzu kommt dass diese Austauschmethode sehr schnell ist. Generell war die Galliumkonzentration im Gerüst immer geringer als die bei der Synthese eingesetzte.

Während der Strukturverfeinerung aus Röntgenpulverdaten wurden die Aluminium- und Galliumatome auf der gleichen kristallographischen Lage (6c) in der Raumgruppe P-43n gerechnet. Ihre Auslenkungsparameter und Besetzungszahlen wurden für alle Verbindungen linear gekoppelt berechnet. Silizium wurde auf der Lage 6d immer voll Besetzt gefunden. Jede Verfeinerung spiegelte den Gerüsttyp $[\text{Al}_{1-y}\text{Ga}_y\text{SiO}_4]_6$ mit $0 < y < 1$ wieder. Durch die statistische Verteilung der Aluminium- und Galliumatome auf der T^1 -Position spiegelt der T^1 -O Abstand die mittlere Al/Ga-O Bindungslänge wieder. Der Gitterparameter steigt jeweils linear vom alumosilikatischen Nitrit (893.5 pm), Chlorid (887.8 pm), Bromid (893.7 pm), Hydro-Hydroxy (889.3 pm) zum gallosilikatischem Nitrit (898.9 pm) Chlorid (893.7 pm), Bromid (899.5 pm) und Hydro-Hydroxy (892.6 pm für $y = 0.72$) Sodalith an. Nur in der Hydro-Sodalith Reihe verändert sich der Gitterparameter quasi nicht und hat eine Länge von 884.8 pm innerhalb 2σ . Die interatomaren Abstände zwischen Gerüstsauerstoff (O(1)) und Wassermolekülen (O(2)) bleiben jeweils konstant. Dies führt bei konstanter Wasserstoffbrückenbindungsstärke $\text{O}(1)\cdots\text{H}\cdots\text{O}(2)$ zu einem unveränderten Gitterparameter.

In allen anderen beschriebenen Sodalithen nimmt die z Koordinate des Gerüstsauerstoffatoms ab was mit einer Vergrößerung des Gitterparameters verbunden ist. Der Al/Ga-O Abstand nimmt von 173.0 pm auf 183.0 pm vom alumosilikatischem zum gallosilikatischen Gerüst zu, wohingegen der Si-O Abstand mit 163.0 pm ($\sigma \sim 1.0$), 162.8 pm ($\sigma \sim 2.0$), 163.4 pm ($\sigma \sim 3.0$), 163.8 pm ($\sigma \sim 3 \sigma$) und 162.9 pm ($\sigma \sim 2.5 \sigma$) für die Nitrit, Chlorid, Bromid, Hydro-Hydroxy und Hydro Sodalith Serien innerhalb der angegebenen Sigma-Schranke konstant ist. Der mittlere Tiltwinkel (φ) nimmt mit zunehmenden Galliumgehalt innerhalb des Gerüsts zu und baut so zunehmende Spannungen ab. Im Gegensatz dazu zeigt die tetragonale Tetraederverzerrung keine Veränderung in Abhängigkeit zunehmender Galliumkonzentrationen innerhalb der Verbindungen. Der effektive Sechsringfensterdurchmesser des Gerüsts kann in Abhängigkeit vom Galliumgehalt variiert werden. Er nimmt beim Nitrit und den Halogenid Sodalithen deutlich ab. Lediglich bei den Hydro-Hydrox Sodalithen scheint der Fensterdurchmesser nach einer deutlichen Veränderung bei hohen Galliumkonzentrationen konstant zu sein. Die Gerüstsauerstoff s-Hybridisierung nimmt mit zunehmendem Galliumgehalt als Folge der zunehmenden Al/Ga-O Abstände, Tiltwinkel oder abnehmender Al/Ga-O-Si Winkel (γ) ab. Deshalb nimmt auch die T-O-T Verknüpfungsstabilität von der aluminium- zur galliumreichen Seite des Gerüsts ab. Die Na-O(1), Na-O(2) (O(2) von NO_2^- oder $(\text{OH}\cdot\text{H}_2\text{O})_x^-$), Na-Cl und Na-Br Abstände verkürzen sich mit zunehmendem Tilt bzw. zunehmender Galliumkonzentration. Dies zeigt eine direkte Korrelation zwischen Gerüst- und Nicht-Gerüstatomen und ein Kompaktierungsphänomen des eingebauten Templates.

Die Stickstoff- und Sauerstoffpositionen des NO_2^- konnten nur mit großen Standardabweichungen bestimmt und dadurch die Position dieser Atome nicht exakt bestimmt werden. Deshalb wird eine hohe Fehlordnungsdynamik bzw. ein Rotationszustand angenommen in dem das Molekül seine Orientierung in Bezug auf das kristallographischen Achssystem ständig im Zentrum des β -Käfigs ändert. Im Hydro-Hydroxy Sodalith wurde der Templatsauerstoff O(2) mit niedriger lokaler Symmetrie (24i) verfeinert wodurch es unmöglich ist zwischen dem Sauerstoff der OH bzw. der H_2O Moleküle im β -Käfig zu unterscheiden. Deshalb werden diese Gastkomponenten als $\{(\text{OH}\cdot\text{H}_2\text{O})_x(\text{H}_2\text{O})_{8-4x}\}^-$ beschrieben.

In ^{29}Si MAS NMR Spektren wurden einzelne Peaks (-80.0 ppm, -78.9 ppm, -80.1 ppm, -75.7 ppm für gallosilikatische, -86.4 ppm, -85.0 ppm, -86.2 ppm und -83.3 ppm für alumosilikatische Nitrit, Chlorid und Hydro Sodalithe) für die entsprechenden Endglieder ($y = 0$ or 1) der einzelnen Serien beobachtet, welche mit Literaturwerten übereinstimmen. Im Gegensatz dazu wurden jeweils fünf Signale entsprechend der Siliziumumgebung $\text{SiO}_4(\text{Ga}_4)$, $\text{SiO}_4(\text{Ga}_3\text{Al})$, $\text{SiO}_4(\text{Ga}_2\text{Al}_2)$, $\text{SiO}_4(\text{GaAl}_3)$ und $\text{SiO}_4(\text{Al}_4)$ für $0 < y < 1$ beobachtet. Bei einer vollständigen statistischen Verteilung der Aluminium- und Galliumatome innerhalb der Kristalle erwartet man eine Verschiebung des Intensitätsmaximums der Signalsumme der fünf

unterschiedlichen Q_4 Signale von einem Endglied zum anderen, wie es in fast allen Proben der Serien beobachtet wurde. Eine Abweichung und damit ein Hinweis auf Domänenbildung wurde lediglich in wenigen Verbindungen der Nitrit und Bromid Serie ($\text{Na}_8[\text{Al}_{1-y}\text{Ga}_y\text{SiO}_4]_6(\text{NO}_2)_2$, $\sim 0.35 > y > 0.70$ und $\text{Na}_8[\text{Al}_{1-y}\text{Ga}_y\text{SiO}_4]_6\text{Br}_2$, $y = 0.54$) gefunden, bei denen die Intensität der $\text{Si}(\text{OGa})_4$ und $\text{Si}(\text{OAl})_4$ Peaks höher ist als die der drei anderen Konfigurationen. Da in den Röntgenuntersuchungen kein Hinweis gefunden wurde, muss man annehmen das die Größe möglicher Domänen kleiner ist als die Kohärenzlänge der Röntgenstrahlung aber groß genug um mit der MAS NMR gesehen zu werden. Dies muss allerdings in späteren Untersuchungen noch genauer geprüft werden. Nicht desto trotz läßt sich aus den 5 Signalen das Ga/Al-Verhältnis bestimmen, welches mit den röntgenographischen Ergebnissen gut übereinstimmt.

Charakteristische Absorptionsbanden der Template korrespondierender Sodalithe wurden im mittleren Infrarot beobachtet. Allerdings liegen die Banden für Chlorid und Bromid im fernen Infrarot, welches hier nicht gemessen wurde, so dass eine mögliche systematische Veränderung dieser Banden in späteren Untersuchungen zu klären ist. Die asymmetrische T-O-T Streck- (ν_{as} T-O-T), symmetrische T-O-T Streck- (ν_{s} T-O-T) und O-T-O Biege- (δ O-T-O) Schwingung liegen im MIR. Für ν_{as} T-O-T wurde mehr als eine Bande im Bereich zwischen 800 cm^{-1} und 1200 cm^{-1} für $0 \leq y \leq 1$ gefunden. Drei ν_{s} $\text{T}^{1\text{A}}$ -O-T² ($\text{T}^{1\text{A}} = \text{Al}$) und fünf $\text{T}^{1\text{G}}$ -O-T² ($\text{T}^{1\text{G}} = \text{Ga}$) Banden wurden für $0 < y < 1$ in allen Serien beobachtet, wobei nur eine sehr kleine Verschiebung für ν_{s} T-O-T von einem Endglied zum anderen zu bestimmen war. Die abnehmende Intensität der ν_{s} Si-O-Al Banden mit zunehmenden Galliumgehalt zeigt, dass dabei die Gesamtmenge dieser Schwingung abnimmt. Im gleichen Zuge nimmt die Intensität der ν_{as} Si-O-Ga Vibrationen zu. Nimmt man dies als grundlegende Beobachtung folgt daraus, das dieser Schwingungstyp lokalen Ursprungs und somit von der näheren Umgebung separiert ist. Damit handelt es sich um eine kurzreichweitige Schwingung an der nur ein T^1 -, ein T^2 - und ein Sauerstoffatom beteiligt ist. Zwei δ O-T-O Banden wurden zwischen $\sim 430 \text{ cm}^{-1}$ und 470 cm^{-1} für $0 \leq y < 1$ gemessen. Diejenige mit der niedrigeren Wellenzahl verschiebt sich zu kleineren Werten in Verbindung mit abnehmender Intensität bei zunehmender Galliumkonzentration um schließlich bei der reinen gallosilikatischen Verbindung zu verschwinden. Im Gegensatz dazu verschiebt sich die zweite Biegeschwingung δ O-T-O bei nahezu konstanter Intensität zu kleineren Wellenzahlen. Die lineare Korrelation zwischen Galliumgehalt und Wellenzahlverschiebung dieser Bande kann man nutzen um das Ga/Al-Verhältnis des Gerüsts zu überprüfen.

7 LITERATURE

- [1] Deer, W. A.; Howie, R. A.; Zussman, J.: An introduction to the rock forming minerals (2nd edition), John Wiley, New York, 1992.
- [2] Rabo, J. A.: Zeolite chemistry and Catalysis. American Chem. Soc., Washington DC, 1976.
- [3] Strunz, H.; Nickel, E. H.: Strunz Mineralogical Tables. Chemical-Structural Mineral Classification System. 9th Edition, Schweizerbart, Stuttgart, 2001.
- [4] Hassan, I.; Grundy, H. D.: The crystal structures of helvite group minerals, (Mn, Fe, Zn)₈(Be₆Si₆O₂₄)S₂. *Am. Min.* **70** (1985) 186-192.
- [5] Komada, N.; Westrum, Jr. E. F.; Hemingway, B. S.; Zolotov, M. Y.; Semenov, Y. V.; Khodakovsky, I. L.; Anovitz, L. M.: Thermodynamic properties of sodalite at temperatures from 15 K to 1000 K. *J. Chem. Thermodynamics* **27** (1995) 1119-1132.
- [6] Deer, W. A.; Howie, R. A.; Zussman, J.: Rock forming minerals (framework silicates), Vol. 4, Longman, London, 1963.
- [7] Hassan, I.: Feldspathoids and their relationships to zeolites. *Kuwait J. Sc. Eng.* **24(1)** (1997) 163-182.
- [8] Johnson, J. M.; Mead, P. J.; Weller, M.T.: Synthesis of a range of anion-containing gallium and germanium sodalites. *Micro. Meso. Mater.* **38** (2000) 445-460.
- [9] Buhl, J. -Ch.; Gesing, T. M.; Gurriss, C.: Synthesis and crystal structure of rhodanide enclathrated sodalite Na₈[AlSiO₄]₆(SCN)₂. *Micro. and Meso. Mater.* **50** (2001) 25-32.
- [10] Brenchley, M. E.; Weller, M. T.: Synthesis and structures of M₈[AlSiO₄]₆(XO₄)₂, M= Na, Li, K; X= Cl, Mn sodalites. *Zeolites* **14** (1994) 682-686.
- [11] van Smaalen, S.; Dinnebier, R. E.; Katzke, H.; Depmeier, W.: Structural characterisation of the high-temperature phase transitions in Ca₈[Al₁₂O₂₄](MoO₄)₂ aluminate sodalite using X-ray powder diffraction. *J. Solid State Chem.* **129** (1997) 130-143.
- [12] Depmeier, W.: Structure of cubic aluminate sodalite Ca₈[Al₁₂O₂₄](WO₄)₂ in comparison with its orthorhombic phase and with cubic Sr₈[Al₁₂O₂₄](CrO₄)₂. *Acta Crystallogr.* **B44** (1988) 201-207.
- [13] Gesing, T. M.; Buhl, J.-Ch.: Kristallstrukturverfeinerung von Na₈[AlSiO₄]₆(B(OH)₄)₂ bei 350 K. *Z. Kristallogr. Supp.* **11** (1996) 81.
- [14] Wiebecke, M.; Engelhardt, G.; Felsche, J.; Kempa, P. B.; Sieger, P.; Schefer, J.; Fischer, P.: Orientational disorder of the hydrogen dihydroxide anion, O₂H₃⁻, in sodium hydroxosodalite dihydrate, Na₈[AlSiO₄]₆(OH)₂·2H₂O: Single crystal x-ray and powder neutron diffraction and MAS NMR and FT IR spectroscopy. *J. Phys. Chem.* **96** (1992) 392-397.

- [15] Buhl, J. –Ch.; Gesing, T. M.; Rüscher, C. H.: Hydrothermal synthesis and characterisation of tetrahydroborate sodalite $\text{Na}_8[\text{AlSiO}_4]_6(\text{BH}_4)_2$. *Beih. E. J. Min.* **16** (2004) 24.
- [16] Bibby, D. M.; Dale, M. P.: Synthesis of silica sodalite from non-aqueous systems. *Nature*, **317** (1985) 157-158.
- [17] Fuetterer, K.; Depmeier, W.; Altdorfer, F.; Behrens, P.; Felsche, J.: Compression mechanism in trioxane silica sodalite, $[\text{Si}_{12}\text{O}_{24}] \cdot 2\text{C}_3\text{H}_6\text{O}_3$. *Z. Kristallogr.* **209** (1994) 517-523.
- [18] Taylor, D.: Cell parameter correlations in aluminosilicate-sodalites. *Contrib. Mineral. Petrol.* **51(1)** (1975) 39-47.
- [19] Weller, M. T.; Wong, G.: Characterisation of novel sodalites by neutron diffraction and solid state NMR. *Solid State Ionics* **32** (1989) 430-435.
- [20] Toebbens, D. M.; Depmeier, W.: Intermediate phases in the Ca-rich part of the system $(\text{Ca}_{1-x}\text{Sr}_x)_8(\text{Al}_{12}\text{O}_{24})(\text{WO}_4)_2$. *Z. Kristallogr.* **213** (1998) 522-531.
- [21] Weller, M. T.; Wong, G.: Mixed halide sodalites. *Eur. J. Solid State Inorg. Chem.* **26** (1989) 619-633.
- [22] Buhl, J. –Ch.; Löns, J.: Orientational disorder and heterogeneous reaction behaviour of NO_2^- and NO_3^- anions inside a sodalite matrix. *J. Solid State Chem.* **112** (1994) 243-250.
- [23] Lattner, S. E.; Sachleben, J.; Iversen, B. B.; Hanson, J. C.; Stucky, G. D.: Covalent guest-framework interactions in heavy metal sodalites: structure and properties of thallium and silver sodalite. *J. Phys. Chem.* **B103** (1999) 7135-7144.
- [24] Eiden-Assmann, S.; Schneider, A. M.; Behrens, P.; Wiebcke, M.; Engelhardt, G.; Felsche, J.: Lead hydro sodalite $(\text{Pb}_2(\text{OH})(\text{H}_2\text{O})_3)_2[\text{Al}_3\text{Si}_3\text{O}_{12}]_2$: synthesis and structure determination by combining X-ray Rietveld refinement, ^1H MAS NMR, FTIR and XANES spectroscopy. *Chemistry - A European Journal* **6(2)** (2000) 292-297.
- [25] Eiden-Assmann, S.; Schneider, A. M.; Behrens, P.; Engelhardt, G.; Mandar, H.; Felsche, J.: Silver hydrosodalite $(\text{Ag}_3(\text{H}_2\text{O})_4)_2[\text{Al}_3\text{Si}_3\text{O}_{12}]_2$: synthesis and structure determination by combination of X-ray refinement, thermogravimetry, FT-IR and ^1H -MAS NMR spectroscopy. *Eur. J. Inorg. Chem.* **6** (2001) 1527-1534.
- [26] Pauling, L.: The structure of sodalite and helvite. *Z. Kristallogr.* **74** (1930) 213-225.
- [27] Löns, J.; Schulz, H.: Strukturverfeinerung von Sodalith, $\text{Na}_8\text{Si}_6\text{Al}_6\text{O}_{24}\text{Cl}_2$. *Acta Crystallogr.* **23** (1967) 434-436.
- [28] Hassan, I.; Grundy, H. D.: The crystal structures of sodalite group minerals. *Acta Crystallogr.* **B40** (1984) 6-13.
- [29] Depmeier, W.: Tetragonal tetrahedra distortion in cubic sodalite frameworks. *Acta Crystallogr.* **B40** (1984) 185-191.
- [30] Depmeier, W.: Remarks on symmetry occurring in the sodalite family. *Z. Kristallogr.* **199** (1992) 75-89.

- [31] Depmeier, W.; Bührer, W.: Aluminate sodalite: $\text{Sr}_8[\text{Al}_{12}\text{O}_{24}](\text{MoO}_4)_2$ (SAM) at 293, 423, 523, 623 and 723 K and $\text{Sr}_8[\text{Al}_{12}\text{O}_{24}](\text{WO}_4)_2$ (SAW) at 293 K. *Acta Crystallogr.* **B47** (1991) 197-206.
- [32] Depmeier, W.; Schmid, H.; Setter, M.; Werk, M.: Structure of cubic aluminate sodalite $\text{Sr}_8[\text{Al}_{12}\text{O}_{24}](\text{CrO}_4)_2$. *Acta Cryst.* **C43** (1987) 2251-2255.
- [33] Rüscher, C. H.; Gesing, Th. M.; Buhl, J. –Ch.: Anomalous thermal expansion behaviour of $\text{Na}_8[\text{AlSiO}_4]_6(\text{NO}_3)_2$. *Z. Kristallogr.* **218** (2003) 332-344.
- [34] Taylor, D.: The thermal expansion behaviour of the framework silicates. *Mineral. Mag.* **38** (1972) 593-604.
- [35] Sahl, K.: Refinement of the crystal structure of bicchulite, $\text{Ca}_2[\text{Al}_2\text{SiO}_6](\text{OH})_2$. *Z. Kristallogr.* **152** (1980) 13-21.
- [36] Belekoneva, E. L.; Dem'yanets, L. N.; Uvarova, T. G.; Belov, N. V.: Crystal structure of Ge sodalite $\text{Na}_8[\text{AlGeO}_4]_6(\text{OH})_2$. *Soviet Physics and Crystallography* **129** (1982) 597-598.
- [37] Loewenstein, W.: The distribution of aluminium in the tetrahedra of silicates and aluminates. *Am. Mineral.* **39** (1954) 92-96.
- [38] Breck, D. W.: *Zeolite Molecular Sieves*: Krieger Publishing Co. Malabar, FL. 1984.
- [39] Mead, P. J.; Weller, M. T.: Synthesis, structure, and characterisation of halate sodalites: $\text{M}_8[\text{AlSiO}_4]_6(\text{XO}_3)_x(\text{OH})_{2-x}$; M = Na, Li, or K; X = Cl, Br, or I. *Zeolites* **15** (1995) 561-568.
- [40] Nenoff, T. M.; Harrison, W. T. A.; I.; Stucky, G. D.; Nicol, J. M.; Newsam, J. M.: The crystal structure of a new sodalium zinc arsenate phase solvated by simulated annealing. *Zeolites* **13(7)** (1993) 506- 510.
- [41] Felche, J.; Luger, S.; Baerlocher, Ch.: Crystal structures of the hydro-sodalite $\text{Na}_6[\text{AlSiO}_4]_6 \cdot 8(\text{H}_2\text{O})$ and of the anhydrous sodalite $\text{Na}_6[\text{AlSiO}_4]_6$. *Zeolites* **6** (1986) 367-372.
- [42] Buhl, J. –Ch.; Engelhardt, G.; Felsche, J.; Luger, S.: ^{23}Na MAS-NMR and ^1H MAS-NMR studies in the hydro-sodalite system. *Ber. Bunsenges. Phys. Chem.* **92** (1988) 176-181.
- [43] Engelhardt, G.; Felsche, J.; Sieger, P. J.: The hydrosodalite system $\text{Na}_{6+x}[\text{AlSiO}_4]_6(\text{OH})_x \cdot n\text{H}_2\text{O}$: formation, phase composition, and de- and rehydration studied by ^1H , ^{23}Na , and ^{29}Si MAS-NMR spectroscopy in tandem with thermal analysis, X-ray diffraction, and IR spectroscopy. *J. Am. Chem. Soc.* **114** (1992) 1173-1182.
- [44] Wang, Y.; Herron, N.: Photoluminescence and relaxation dynamics of CdS superclusters in zeolites. *J. Phys. Chem.* **92(17)** (1988) 4988-4994.
- [45] Moller, K.; Eddy, M.; Stucky, G. D.; Herron, N.; Bein, T.: Stabilisation of cadmium selenide molecular clusters in zeolite-Y – EXAFS and X-ray diffraction studies. *J. Am. Chem. Soc.* **111 (7)** (1989) 2564-2571.

-
- [46] Ozin, G. A.; Kupperman, A.; Stein, A.: Advanced zeolite materials science. *Angew. Chem. Int. Ed. Engl.* **28** (1989) 359-376.
- [47] Moran, K. L.; Harrison, W. T.A.; Kamber, I.; Gier, T. E.; Bu, X.; Herren, D.; Behrens, P.; Eckert, H; Stucky, G. D.: Synthesis, characterisation and tunable electronic/optical properties of II-VI semiconductor species included in the sodalite structure. *Chem. Mater.* **8** (1996) 1930-1943.
- [48] Van Doorn, C. Z.; Schipper, D. J.; Bolwijn, P. T.: Optical investigation of cathodochromic sodalite. *J. Electrochem. Soc.* **119(1)** (1972) 85-92.
- [49] Kasai, P.H.: Electron spin resonance studies of gamma- and x-ray irradiated zeolites. *J. Chem. Phys.* **43** (1965) 3322.
- [50] Srdanov, V. I; Haug, K.; Metiu, H.; Stucky, G. D.: Na₄³⁺ clusters in sodium sodalite. *J. Phys. Chem.* **96** (1992) 9039-9043.
- [51] Medved, D. V.: Hackmanite and its tenebrescent properties. *Am. Mineral.* **39** (1954) 615-629.
- [52] Kirk, R. D.: Role of sulphur in the luminescence and colouration of sodalite aluminosilicates. *J. Electrochem. Soc.* **101** (1954) 661-665.
- [53] Bershov, L. V.; Matriosya, V. O.; Platon, A. N.; Tarschan, A. N.: Neogarnish Mater. **5** (1969) 1780.
- [54] Williams, E. F.; Hodgson, W. G.; Brinnen, J. S.: Synthetic photochromic sodalite. *J. Am. Ceramic Soc.* **52(3)** (1969) 139-145.
- [55] Hodgson, W. G.; Brinnen, J. S.; Williams, E. F.: Electron spin resonance investigation of photochromic sodalites. *J. Chem. Phys.* **47** (1967) 3719.
- [56] Schipper, D. J; van Doorn, C. Z.; Bolwijn, P. T.: Preparation of cathodochromic sodalites. *J. Am. Ceram. Soc.* **55(5)** (1972) 256 &.
- [57] Bolwijn, P. T.; Schipper, D. J.; van Doorn, C. Z.: Cathodochromic properties of sodalites. *J. Appl. Phys.* **43(1)** (1972) 132-137.
- [58] Phillips, W.: Properties of cathodochromic sodalite. *J. Electrochem. Soc.* **117(12)** (1970) 1557-1561.
- [59] Taylor, M. J.; Marshall, D. J.; Forrester, P. A.; MacLaughlan.: Colour centre in sodalites and their use in storage displays. *Radio Electron. Eng.* **40(1)** (1970) 17.
- [60] Faughnan, B. W.; Shidlovsky, I.: High contrast, high sensitivity cathodochromic sodalite for storage and display applications. *RCA Review* **33(1)** (1972) 273-295.
- [61] Faughnan, B. W.; Gorog, I.; Heyman, P. M.; Shidlovsky, I.: Cathodochromic materials and applications. *IEEE* **61(7)** (1973) 927-941.
- [62] Chang, I. F.: Synthesis of photochromic and cathodochromic sodalite. *J. Electrochem. Soc.* **121(6)** (1974) 815-820.
- [63] Tranjan, F. M.; Todd, L. T.: Effect of various chemical substitution on the physical properties of cathodochromic sodalite. *J. Electrochem. Soc.* **135(9)** (1988) 2288-2291.

- [64] Bhalla, R. J. R. S.: Electron-beam damage in chathochromic sodalite. *J. App. Phys.* **45(9)** (1974) 3703-3709.
- [65] Hassib, A.; Beckman, O.; Annersten, H.: Photochromic properties of natural sodalite. *J. Phys.D-App. Phys.* **10(5)** (1977) 771-777.
- [66] Buhl, J. –Ch.: The properties of salt filled sodalites. Part 3. Synthesis and thermal behaviour of basic and non-basic carbonate enclathrated sodalites. *Thermochimica Acta* **219** (1993) 205-214.
- [67] Weller, M. T.; Wong, G.; Adamson, C. L.; Dodd, S. M.; James, J.; Roe, B.: Intracage reactions in sodalites. *J. Chem. Soc. Dalton Trans.* **2** (1990) 593-597.
- [68] Felsche, J.; Luger, S.: Phases and thermal decomposition characteristics of hydro-sodalites $\text{Na}_{6+x}[\text{AlSiO}_4]_6(\text{OH})_x \cdot n\text{H}_2\text{O}$. *Thermochimica Acta* **118** (1987) 35-55.
- [69] Nenoff, T. M.; Harrison, W. T. A.; Gier, T. E.; Stucky, G. D.: Room temperature synthesis and characterisation of new ZnPO and ZnAsO sodalite open framework. *J. Am. Chem. Soc.* **113** (1991) 378-379.
- [70] Gesing, Th. M.: Structure and properties of tecto-gallosilicates. I. Hydrosodalites and their phase transitions. *Z. Kristallogr.* **215** (2000) 510-517.
- [71] Weller, M. T.; Dodd, S. M.; Jiang, M. R. M.: Synthesis, structure and ionic conductivity in nitrite sodalites. *J. Mater Chem.* **1(1)** (1991) 11-15.
- [72] Demidenco, V. A.; Astakhova, V. V.; Volynets, F. K.: The structural transitions of sodalite. *Sov. Phys. Crystallogr.* **28(3)** (1983) 350-351.
- [73] Depmeier, W.: Aluminate sodalite, thoughts on a new type of structural family and its ferric properties. *Z. Krystallogr.* **174** (1986) 41-42.
- [74] Depmeier, W.: Aluminate sodalite $\text{Ca}_8[\text{Al}_{12}\text{O}_{24}](\text{WO}_4)_2$ at room temperature. *Acta Cryst.* **C40** (1984) 226-231.
- [75] Depmeier, W.: Revised crystal data for the aluminate sodalite $\text{Ca}_8[\text{Al}_{12}\text{O}_{24}](\text{WO}_4)_2$. *J. Appl. Cryst.* **12** (1979) 623-626.
- [76] Taylor, D.: The thermal expansion of sodalite group of minerals. *Min. Mag.* **36** (1968) 761-769.
- [77] Henderson, C. M. B.; Taylor, D.: The thermal expansion of synthetic aluminate-sodalites. *Phys. Chem. Miner.* **2** (1978) 337-347.
- [78] McMullan, R. K.; Ghose, S.; Haga, N.; Schomaker, V.: Sodalite, $\text{Na}_3\text{Si}_3\text{Al}_3\text{O}_{12}\text{Cl}$: structure and ionic mobility at high temperatures by neutron diffraction. *Acta Cryst.* **B52** (1996) 616-627.
- [79] Fechtelkord, M.: Influence of sodium ion dynamics on the ^{23}Na quadrupolar interaction in sodalite: a high-temperature NMR study. *Solid State NMR.* **18** (2000) 70-88.
- [80] Antao, S. M.; Hassan, I.: Thermal analyses of sodalite, tugtupite, danalite and helvite. *Can. Min.* **40** (2002) 163-172.

- [81] Hassan, I.; Antao, S. M.; Parise, J. B.: Sodalite: high temperature structures from synchrotron radiation and Rietveld refinement. *Am. Min.* **89** (2004) 359-364.
- [82] Hazen, R. M.; Sharp, Z. D.: Compressibility of sodalite and scapolite. *Am. Min.* **73** (1988) 1120-1122.
- [83] Mezler, R.; Depmeier, W.; Vogt, T.; Gering, E.: Neutron and synchrotron radiation high pressure experiments on aluminate sodalite $\text{Sr}_8[\text{Al}_{12}\text{O}_{24}](\text{CrO}_4)_2$. *Cryst. Res. Technol.* **30(6)** (1995) 767-773.
- [84] Werner, S.; Barth, S.; Jordan, R.; Schulz, H.: Single crystal study of sodalite at high pressure. *Z. Kristallogr.* **211** (1996) 158-162.
- [85] Thomas, J. M.; Liu, X. S.: Gallozeolite catalysts: preparation, characterisation, and performance. *J. Phys. Chem.* **90** (1986) 4843-4847.
- [86] McCusker, L. B.; Meier, W. M.; Suzuki, K.; Shin, S.: The crystal structure of a sodium gallosilicate sodalite. *Zeolites* **6** (1986) 388-391.
- [87] Newsam, J. M.; Jorgensen, J. D.: Gallosilicate sodalite-further syntheses and structural details. *Zeolites* **7** (1987) 569-573.
- [88] Bachmann, S.; Buhl, J. –Ch.: Crystallisation, characterisation and structure of nitrite aluminogermanate sodalite $\text{Na}_8[\text{AlGeO}_4]_6(\text{NO}_2)_2$. *Micro. Meso. Mater.* **28** (1999) 35-47.
- [89] Tielen, M.; Geelen, M.; Jacobs, P. A.: Isomorphic substitution in zeolite: its potential catalytic implication. *Acta physica et chemica* **0** (1985) 1-18.
- [90] Perlmutter, M. S.; Todd, L. T.; Farrell, E. F.: Lattice parameters and chemical analysis of germanium substituted sodalite. *Mat. Res. Bull.* **9(1)** (1974) 65-70.
- [91] Cynthia T-W, C.; Chang, C. D.: Isomorphous substitution in zeolite frameworks. 1. Acidity of surface hydroxyls in [B]-, [Fe]-, [Ga]-, and [Al]-ZSM-5. *J. Phys. Chem.* **89** (1985) 1569-1571.
- [92] Izumi, F.: In *The Rietveld Method* (Ed. R. A. Young), Oxford University Press 1993, p 236-253.
- [93] Massiot D.; Fayon F.; Capron, M.; King, I.; Le Calve, S.; Alonso, B.; Durand, J.; Bujoli, B.; Gan, Z.; Hoatson, G.: Modelling one- and two-dimensional solid-state NMR spectra. *Mag. Res. Chem.* **40** (2002) 70-76.
- [94] Taylor, J. M.; Marshall, D. J.; Evans, H. J.: Infra-red spectra of photochromic sodalites. *J. Phys. Chem. Solids* **32** (1971) 2021.
- [95] Nenoff, T. M.; Harrison, W. T. A.; Gier, T. E.; Keder, N. I.; Zaremba, C. M.; Srdanov, V. I.; Nicol, J. M.; Stucky, G. D.: Structures and chemical investigations of $\text{Na}_3(\text{ABO}_4)\cdot 4\text{H}_2\text{O}$ -type sodalite phases. *Inorg. Chem.* **33** (1994) 2472-2480.
- [96] Murshed, M. M.; Gesing, Th. M.: Partial T-atom substitution in the sodalite framework. *Z. Kristallogr., Suppl.* **20** (2003) 145.
- [97] Meriaudeau, P.; Sapaly, G.; Wicker, G.; Naccache, C.: Revisiting $\text{Ga}_2\text{O}_3/\text{H-ZSM-5}$ propane aromatisation catalysts. *Catalysis Letter* **27** (1994) 143-148.

- [98] Jiang, M. R. M.; Weller, M. T.: A nitrite sodalite-based NO₂ gas sensor. *Sensors and Actuators* **B30** (1996) 3-6.
- [99] Fois, E.; Gamba, A.; Maric, D.: Structure and dynamics of nitrite sodalite. An ab initio study. *Nuovo Cemento Soc. Italiana*. **19(11)** (1997) 1679-1685.
- [100] Buhl, J. –Ch.: Basic nitrite sodalite–Na₈[AlGaSiO₄]₆(OH·H₂O)(NO₂)–A suitable material for the uptake of carbon dioxide. *J. Solid State Chem.* **94** (1991) 19-26.
- [101] Buhl, J. –Ch.: Hydrothermal synthesis and characterisation of nitrite sodalite single crystals. *J. Crystal Growth* **108** (1991) 143-149.
- [102] Sieger, P.; Wiebcke, M.; Felsche, J.; Buhl, J.-C.: Orientational disorder of the nitrite anion in the sodalite Na₈[AlSiO₄]₆(NO₂)₂. *Acta Cryst.* **C47** (1991) 498-501.
- [103] Beagley, B.; Henderson, C. M. B.; Taylor, D.: The crystal structures of aluminosilicate-sodalites: X-ray diffraction studies and computer modelling. *Mineral. Mag.* **46** (1982) 459-464.
- [104] Hinze, J.: Elektronegativität der Valenzzustände. *Fort. Chem. Forsch.* **9** (1968) 448-485.
- [105] Megaw, H. D.: *Crystal Structure: A working approach*. Philadelphia, London, Toronto: (W. B. Saunders) 1973.
- [106] Johnson, G. M.; Mead, P. J.; Dann, S. E.; Weller, M. T.: Multinuclear MAS NMR studies of sodalite framework materials. *J. Phys. Chem.* **B104** (2000) 1454-1463.
- [107] Gesing, Th. M.; Buhl, J. –Ch.: Crystal structure of carbonate nosean, Na₈[AlSiO₄]₆CO₃. *Eur. J. Mineral.* **10** (1997) 71-77.
- [108] Shannon, R. D.: Revised effective ionic radii and systematic studies of interatomic distances in Halides and Chalcogenides. *Acta Cryst.* **A32** (1976) 751-767.
- [109] Henderson, C. M. B.; Taylor, D.: Infrared spectra of aluminogermanate and aluminate-sodalites and a re-examination of the relationship between T-O bond length, T-O-T angle and the position of the main i.r. absorption band for compounds with framework structures. *Spectrochimica Acta* **35A** (1979) 929-935.
- [110] Engelhardt, G.; Sieger, P.; Felsche, J.: Multinuclear solid state NMR of host-guest systems with TO₂ (T = Si, Al) host-frameworks. A case study on sodalites. *Analytica Chimica Acta* **283** (1993) 967-985.
- [111] Weller, M. T.; Wong, G.: New limits of Si-29 solid state NMR chemical shifts. *J. Chem. Soc.-Chem. Comm.* **16** (1988) 1103-1104.
- [112] Murshed, M. M.; Gesing, Th. M.: ²⁹Si NMR study of partial T-atom substituted sodalites. *Z. Kristallogr. Suppl.* **21** (2004) 148.
- [113] Nielsen, N. C.; Bildsoe, H.; Jakobsen, H. J.; Norby, P.: ⁷Li, ²³Na and ²⁷Al quadrupolar interactions in some aluminosilicate sodalites from MAS NMR-spectra of satellite transitions. *Zeolites* **11** (1991) 622-632.
- [114] Johnson, G. M.; Mead, P. J.; Weller, M. T.: Structural trends in the sodalite family. *Phys. Chem. Chem. Phys.* **1** (1999) 3709-3714.

-
- [115] Fleet, M. E.: Structures of sodium alumino-germanate sodalites. *Acta Crystallogr.* **C45** (1989) 843-847.
- [116] Iiishi, K.; Tomisaka, T.; Kato, T.; Umegaki, Y.: Isomorphous substitution and infrared and far infrared spectra of the feldspar group. *Neues Mineral. Abh.* **115** (1971) 98-119.
- [117] Godber, J.; Ozin, G. A.: Fourier transform far-infrared spectroscopic study of cation and anion dynamics in M,X-sodalites, where M = Li⁺, Na⁺, K⁺, Rb⁺, Ca²⁺; X = Cl⁻, Br⁻, I⁻, ClO₄⁻, OH⁻. *J. Phys. Chem.* **92** (1988) 4980-4989.
- [118] Henderson, C. M. B.; Taylor, D.: Infrared spectra of anhydrous members of the sodalite family. *Spectrochimica Acta* **33A** (1977) 283-290.
- [119] Creighton, J. A.; Deckman, H. W.; Newsam, J. M.: Computer simulation and interpretation of the infrared and raman spectra of sodalite frameworks. *J. Phys. Chem.* **98** (1994) 448-459.
- [120] Felsche, J.; Luger, S.: Structural collapse or expansion of the hydro-sodalite series Na₈[AlSiO₄]₆(OH)₂·n(H₂O) and Na₆[AlSiO₄]₆·nH₂O upon dehydration. *Ber. Bunsenges. Phys. Chem.* **90** (1986) 731-736.
- [121] M. M. Murshed and Th. M. Gesing: Systematic T-site substitution in aluminosilicate nitrite sodalites. Submitted.
- [122] Hackbarth, K.; Gesing, T. M.; Fechtelkord, M.; Stief, F.; Buhl, J. –Ch. Synthesis and crystal structure of carbonate cancrinite Na₈[AlSiO₄]₆CO₃(H₂O)_{3,4}, grown under low-temperature hydrothermal conditions. *Micro. Meso. Mater.* **30** (1999) 347-358.
- [123] Homayer, J.: Ph.D. thesis, Universität Hannover. 2001.
- [124] Hassan, I.; Grundy, H. D.: Structure of basic sodalite, Na₈Al₆Si₆O₂₄(OH)₂·2H₂O. *Acta Crystallogr.* **C39** (1983) 3-5.
- [125] Emsley, J.: Very strong hydrogen bonding. *Chem. Soc. Rev.* **9(1)** (1980) 91-124.
- [126] Mushed, M. M.; Gesing, T. M.: Unpublished data.
- [127] Fyfe, W. S.: The problem of bond type. *Am. Mineral.* **39** (1954) 991-1004.

8 ATTACHMENT

Table 3.2: Results of the XRD powder diffraction structure refinement of the sodalite systems in the space group P-43n

Atom	Site	Occupancy	x	y	z	B[pm ² 10 ⁴]
Na ₈ [AlSiO ₄] ₆ (NO ₂) ₂ ; a = 893.54(2) pm; R _{wp} = 0.064; R _p = 0.050; R _i = 0.009; R _F = 0.005,						
Na1	8e	1 ^c	0.1875(2)	0.1875	0.1875	3.05(9) ^a
Al1	6c	1	¼	½	0	1.3(1)
Si1	6d	1	¼	0	½	1.5(1)
O1	24i	1	0.1508(3)	0.1412(3)	0.4422(2)	0.99(6)
N1	8e	0.25 ^c	0.028(1)	0.028	0.028	3.05(9) ^a
O2	24i	0.1667 ^c	0.394(2)	0.452(6)	0.441(7)	3.05(9) ^a
Na ₈ [Al _{0.83(1)} Ga _{0.17(1)} SiO ₄] ₆ (NO ₂) ₂ ; a = 894.48(2) pm; R _{wp} = 0.085; R _p = 0.063; R _i = 0.011; R _F = 0.006						
Na1	8e	1 ^c	0.1851(2)	0.1851	0.1851	3.2(1) ^a
Al1/Ga1	6c	0.83/0.17(1)	¼	½	0	1.0(1)
Si1	6d	1	¼	0	½	1.1(1)
O1	24i	1	0.1507(6)	0.1407(7)	0.4399(3)	1.4(1)
N1	8e	0.25 ^c	0.029(1)	0.029	0.029	3.2(1) ^a
O2	24i	0.1667 ^c	0.388(2)	0.465(5)	0.442(5)	3.2(1) ^a
Na ₈ [Al _{0.80(1)} Ga _{0.20(1)} SiO ₄] ₆ (NO ₂) ₂ ; a = 894.67(1) pm; R _{wp} = 0.042; R _p = 0.030; R _i = 0.006; R _F = 0.004						
Na1	8e	1 ^c	0.1861(2)	0.1861	0.1861	2.25(8) ^a
Al1/Ga1	6c	0.80/0.20(1)	¼	½	0	1.22(5) ^b
Si1	6d	1	¼	0	½	1.22(5) ^b
O1	24i	1	0.1503(2)	0.1415(2)	0.4400(2)	0.65(7)
N1	8e	0.25 ^c	0.031(1)	0.031	0.031	2.25(8) ^a
O2	24i	0.1667 ^c	0.399(2)	0.461(2)	0.434(4)	2.25(8) ^a
Na ₈ [Al _{0.78(1)} Ga _{0.22(1)} SiO ₄] ₆ (NO ₂) ₂ ; a = 893.82(1) pm; R _{wp} = 0.095; R _p = 0.072; R _i = 0.020; R _F = 0.010						
Na1	8e	1 ^c	0.1862(2)	0.1862	0.1862	3.5(1) ^a
Al1/Ga1	6c	0.78/0.22(1)	¼	½	0	2.53(5) ^b
Si1	6d	1	¼	0	½	2.53(5) ^b
O1	24i	1	0.1512(2)	0.1409(3)	0.4416(2)	1.25(7)
N1	8e	0.25 ^c	0.031(1)	0.031	0.031	3.5(1) ^a
O2	24i	0.1667 ^c	0.411(4)	0.441(47)	0.442(48)	3.5(1) ^a
Na ₈ [Al _{0.70(1)} Ga _{0.30(1)} SiO ₄] ₆ (NO ₂) ₂ ; a = 894.45(1) pm; R _{wp} = 0.076; R _p = 0.059; R _i = 0.010; R _F = 0.006						
Na1	8e	1 ^c	0.1860(2)	0.1860	0.1860	2.5(1) ^a
Al1/Ga1	6c	0.70/0.30(1)	¼	½	0	1.8(1) ^b
Si1	6d	1	¼	0	½	1.3(1) ^b
O1	24i	1	0.1509(4)	0.1417(3)	0.4397(2)	0.9(1)
N1	8e	0.25 ^c	0.029(1)	0.029	0.029	2.5(1) ^a
O2	24i	0.1667 ^c	0.405(3)	0.442(11)	0.440(13)	2.5(1) ^a
Na ₈ [Al _{0.64(1)} Ga _{0.36(1)} SiO ₄] ₆ (NO ₂) ₂ ; a = 895.24(1) pm; R _{wp} = 0.085; R _p = 0.065; R _i = 0.013; R _F = 0.006						
Na1	8e	1 ^c	0.1855(2)	0.1855	0.1855	3.6(1) ^a
Al1/Ga1	6c	0.64/0.36(1)	¼	½	0	2.76(6) ^b
Si1	6d	1	¼	0	½	2.76(6) ^b
O1	24i	1	0.1511(2)	0.1406(2)	0.4387(2)	1.38(8)
N1	8e	0.25 ^c	0.029(1)	0.029	0.029	3.6(1) ^a
O2	24i	0.1667 ^c	0.448(37)	0.408(3)	0.436(36)	3.6(1) ^a
Na ₈ [Al _{0.53(1)} Ga _{0.47(1)} SiO ₄] ₆ (NO ₂) ₂ ; a = 895.89(3) pm; R _{wp} = 0.074; R _p = 0.056; R _i = 0.012; R _F = 0.005						
Na1	8e	1 ^c	0.1848(2)	0.1848	0.1848	3.5(1) ^a
Al1/Ga1	6c	0.53/0.47(1)	¼	½	0	2.70(7)
Si1	6d	1	¼	0	½	1.87(3)
O1	24i	1	0.1506(2)	0.1411(2)	0.4387(3)	1.52(8)
N1	8e	0.25 ^c	0.027(1)	0.027	0.027	3.5(1) ^a
O2	24i	0.1667 ^c	0.413(10)	0.450(6)	0.426(15)	3.5(1) ^a
Na ₈ [Al _{0.44(1)} Ga _{0.56(1)} SiO ₄] ₆ (NO ₂) ₂ ; a = 895.99(3) pm; R _{wp} = 0.066; R _p = 0.051; R _i = 0.009; R _F = 0.004						
Na1	8e	1 ^c	0.1844(2)	0.1844	0.1844	2.9(1) ^a
Al1/Ga1	6c	0.44/0.56(1)	¼	½	0	2.2(1)
Si1	6d	1	¼	0	½	0.90(2)
O1	24i	1	0.1524(3)	0.1402(2)	0.4382(2)	0.97(2)
N1	8e	0.25 ^c	0.025(1)	0.025	0.025	2.9(1) ^a
O2	24i	0.1667 ^c	0.406(4)	0.452(5)	0.431(8)	2.9(1) ^a

continued

Atom	Site	Occupancy	x	y	z	B[pm*10 ⁴]
Na ₈ [Al _{0.40(1)} Ga _{0.60(1)} SiO ₄] ₆ (NO ₂) ₂ ; a = 896.51(2) pm; R _{wp} = 0.069; R _p = 0.054; R _i = 0.010; R _F = 0.004						
Na1	8e	1 ^c	0.1833(2)	0.1833	0.1833	3.6(1) ^a
Al1/Ga1	6c	0.40/0.60(1)	¼	½	0	2.06(5) ^b
Si1	6d	1	¼	0	½	2.06(5) ^b
O1	24i	1	0.1509(2)	0.1393(2)	0.4368(2)	1.44(8)
N1	8e	0.25 ^c	0.026(1)	0.026	0.026	3.6(1) ^a
O2	24i	0.1667 ^c	0.403(3)	0.450(7)	0.438(9)	3.6(1) ^a
Na ₈ [Al _{0.37(1)} Ga _{0.63(1)} SiO ₄] ₆ (NO ₂) ₂ ; a = 897.06(1) pm; R _{wp} = 0.093; R _p = 0.068; R _i = 0.012; R _F = 0.005						
Na1	8e	1 ^c	0.1822(2)	0.1822	0.1822	3.4(1) ^a
Al1/Ga1	6c	0.37/0.63(1)	¼	½	0	1.62(6)
Si1	6d	1	¼	0	½	2.01(8)
O1	24i	1	0.1505(3)	0.1392(3)	0.4356(3)	1.8(1)
N1	8e	0.25 ^c	0.025(1)	0.025	0.025	3.4(1) ^a
O2	24i	0.1667 ^c	0.399(2)	0.447(7)	0.450(6)	3.4(1) ^a
Na ₈ [Al _{0.30(1)} Ga _{0.70(1)} SiO ₄] ₆ (NO ₂) ₂ ; a = 897.47(2) pm; R _{wp} = 0.112; R _p = 0.082; R _i = 0.021; R _F = 0.009						
Na1	8e	1 ^c	0.1815(2)	0.1815	0.1815	3.4(1) ^a
Al1/Ga1	6c	0.30/0.70(1)	¼	½	0	1.74(8)
Si1	6d	1	¼	0	½	2.1(1)
O1	24i	1	0.1510(4)	0.1385(3)	0.4344(4)	1.9(1)
N1	8e	0.25 ^c	0.026(1)	0.026	0.026	3.4(1) ^a
O2	24i	0.1667 ^c	0.402(3)	0.441(16)	0.447(16)	3.4(1) ^a
Na ₈ [Al _{0.15(1)} Ga _{0.85(1)} SiO ₄] ₆ (NO ₂) ₂ ; a = 898.43(1) pm; R _{wp} = 0.078; R _p = 0.055; R _i = 0.011; R _F = 0.006						
Na1	8e	1 ^c	0.1806(2)	0.1806	0.1806	3.24(9) ^a
Al1/Ga1	6c	0.15/0.85(1)	¼	½	0	1.58(4)
Si1	6d	1	¼	0	½	1.67(6)
O1	24i	1	0.1512(3)	0.1369(2)	0.4335(2)	1.71(9)
N1	8e	0.25 ^c	0.024(1)	0.024	0.024	3.24(9) ^a
O2	24i	0.1667 ^c	0.395(1)	0.446(7)	0.451(7)	3.24(9) ^a
Na ₈ [Al _{0.10(1)} Ga _{0.90(1)} SiO ₄] ₆ (NO ₂) ₂ ; a = 898.63(1) pm; R _{wp} = 0.093; R _p = 0.064; R _i = 0.019; R _F = 0.010						
Na1	8e	1 ^c	0.1806(2)	0.1806	0.1806	3.2(1) ^a
Al1/Ga1	6c	0.10/0.90(1)	¼	½	0	1.76(4)
Si1	6d	1	¼	0	½	1.63(7)
O1	24i	1	0.1521(2)	0.1362(2)	0.4330(3)	1.61(9)
N1	8e	0.25 ^c	0.024(1)	0.024	0.024	3.2(1) ^a
O2	24i	0.167 ^c	0.397(2)	0.450(8)	0.450(8)	3.2(1) ^a
Na ₈ [GaSiO ₄] ₆ (NO ₂) ₂ ; a = 898.86(1) pm; R _{wp} = 0.120; R _p = 0.079; R _i = 0.028; R _F = 0.012						
Na1	8e	1 ^c	0.1797(2)	0.1797	0.1797	2.8(1) ^a
Ga1	6c	1	¼	½	0	1.75(4)
Si1	6d	1	¼	0	½	1.09(7)
O1	24i	1	0.1534(3)	0.1352(3)	0.4322(4)	1.5(1)
N1	8e	0.25 ^c	0.022(2)	0.022	0.022	2.8(1) ^a
O2	24i	0.1667 ^c	0.447(7)	0.452(7)	0.397(2)	2.8(1) ^a

^a, ^b, ^clinear constraints were used for these parameters within the same composition

Table 4.2: Results of the XRD powder diffraction structure refinement of the sodalite systems in the space group P-43n

Atom	Site	Occupancy	x	y	z	B[pm ² *10 ⁴]
Na ₈ [AlSiO ₄] ₆ Cl ₂ ; a = 887.85(0) pm; R _{wp} = 0.040; R _p = 0.031; R _i = 0.009; R _F = 0.004						
Na1	8e	1	0.1782(1)	0.1782	0.1782	1.82(4)
Al1	6c	1	¼	½	0	1.19(9)
Si1	6d	1	¼	0	½	1.05(8)
O1	24i	1	0.1498(2)	0.1392(2)	0.4378(1)	0.90(4)
Cl1	2a	1	0	0	0	3.06(5)
Na ₈ [Al _{0.95(1)} Ga _{0.05(1)} SiO ₄] ₆ Cl ₂ ; a = 888.22(1) pm; R _{wp} = 0.067; R _p = 0.046; R _i = 0.011; R _F = 0.007						
Na1	8e	1	0.1780(2)	0.1780	0.1780	2.70(8)
Al1/Ga1	6c	0.95/0.05(1)	¼	½	0	0.4(1)
Si1	6d	1	¼	0	½	2.1(1)
O1	24i	1	0.1489(4)	0.1380(3)	0.4366(2)	1.84(9)
Cl1	2a	1	0	0	0	3.6(1)
Na ₈ [Al _{0.90(1)} Ga _{0.10(1)} SiO ₄] ₆ Cl ₂ ; a = 888.14(1) pm; R _{wp} = 0.076; R _p = 0.053; R _i = 0.013; R _F = 0.009						
Na1	8e	1	0.1780(2)	0.1780	0.1780	2.50(8)
Al1/Ga1	6c	0.90/0.10(1)	¼	½	0	0.7(1)
Si1	6d	1	¼	0	½	2.0(1)
O1	24i	1	0.1490(5)	0.1394(5)	0.4364(2)	1.73(8)
Cl1	2a	1	0	0	0	3.4(1)
Na ₈ [Al _{0.85(1)} Ga _{0.15(1)} SiO ₄] ₆ Cl ₂ ; a = 888.38(1) pm; R _{wp} = 0.068; R _p = 0.047; R _i = 0.010; R _F = 0.006						
Na1	8e	1	0.1773(2)	0.1773	0.1773	2.52(8)
Al1/Ga1	6c	0.85/0.15(1)	¼	½	0	0.8(1)
Si1	6d	1	¼	0	½	1.8(1)
O1	24i	1	0.1495(4)	0.1383(4)	0.4360(2)	1.72(9)
Cl1	2a	1	0	0	0	3.2(1)
Na ₈ [Al _{0.77(1)} Ga _{0.23(1)} SiO ₄] ₆ Cl ₂ ; a = 888.55(1) pm; R _{wp} = 0.072; R _p = 0.051; R _i = 0.011; R _F = 0.007						
Na1	8e	1	0.1770(2)	0.1770	0.1770	1.86(7)
Al1/Ga1	6c	0.77/0.23(1)	¼	½	0	0.6(1)
Si1	6d	1	¼	0	½	1.34(9)
O1	24i	1	0.1493(4)	0.1391(3)	0.4352(2)	1.11(8)
Cl1	2a	1	0	0	0	2.60(9)
Na ₈ [Al _{0.75(1)} Ga _{0.25(1)} SiO ₄] ₆ Cl ₂ ; a = 890.19(1) pm; R _{wp} = 0.074; R _p = 0.052; R _i = 0.015; R _F = 0.007						
Na1	8e	1	0.1777(3)	0.1777	0.1777	1.47(4)
Al1/Ga1	6c	0.75/0.25(1)	¼	½	0	0.67(1)
Si1	6d	1	¼	0	½	1.65(9)
O1	24i	1	0.1487(3)	0.1382(4)	0.4351(7)	0.66(4)
Cl1	2a	1	0	0	0	2.72(5)
Na ₈ [Al _{0.70(1)} Ga _{0.30(1)} SiO ₄] ₆ Cl ₂ ; a = 890.46(1) pm; R _{wp} = 0.045; R _p = 0.031; R _i = 0.013; R _F = 0.007						
Na1	8e	1	0.1778(2)	0.1778	0.1778	1.75(8)
Al1/Ga1	6c	0.70/0.30(1)	¼	½	0	1.3(1)
Si1	6d	1	¼	0	½	1.67(8)
O1	24i	1	0.1504(2)	0.1389(2)	0.4358(2)	0.51(7)
Cl1	2a	1	0	0	0	2.76(9)
Na ₈ [Al _{0.64(1)} Ga _{0.36(1)} SiO ₄] ₆ Cl ₂ ; a = 890.70(1) pm; R _{wp} = 0.078; R _p = 0.054; R _i = 0.018; R _F = 0.009						
Na1	8e	1	0.1772(4)	0.1772	0.1772	2.0(5)
Al1/Ga1	6c	0.64/0.36(1)	¼	½	0	1.5(6)
Si1	6d	1	¼	0	½	2.1(6)
O1	24i	1	0.1486(5)	0.1382(7)	0.4342(9)	1.1(5)
Cl1	2a	1	0	0	0	3.0(6)
Na ₈ [Al _{0.62(1)} Ga _{0.38(1)} SiO ₄] ₆ Cl ₂ ; a = 891.18(1) pm; R _{wp} = 0.065; R _p = 0.048; R _i = 0.011; R _F = 0.006						
Na1	8e	1	0.1772(2)	0.1772	0.1772	1.79(8)
Al1/Ga1	6c	0.62/0.38(1)	¼	½	0	1.24(8)
Si1	6d	1	¼	0	½	1.47(8)
O1	24i	1	0.1497(3)	0.1389(2)	0.4352(2)	0.66(8)
Cl1	2a	1	0	0	0	2.6(1)

continued

Atom	Site	Occupancy	x	y	z	B[pm ² 10 ⁴]
Na ₈ [Al _{0.51(1)} Ga _{0.49(1)} SiO ₄] ₆ Cl ₂ ; a = 891.63(2) pm; R _{wp} = 0.046; R _p = 0.034; R _I = 0.010 R _F = 0.005						
Na1	8e	1	0.1767(2)	0.1767	0.1767	2.02(9)
Al1/Ga1	6c	0.51/0.49(1)	¼	½	0	1.3(1)
Si1	6d	1	¼	0	½	1.3(1)
O1	24i	1	0.1498(5)	0.1389(4)	0.4340(2)	1.0(1)
Cl1	2a	1	0	0	0	3.2(1)
Na ₈ [Al _{0.49(1)} Ga _{0.51(1)} SiO ₄] ₆ Cl ₂ ; a = 891.94(2) pm; R _{wp} = 0.055; R _p = 0.041; R _I = 0.007; R _F = 0.004						
Na1	8e	1	0.1763(1)	0.1763	0.1763	1.94(8)
Al1/Ga1	6c	0.49/0.51(1)	¼	½	0	1.21(7)
Si1	6d	1	¼	0	½	1.21(8)
O1	24i	1	0.1499(3)	0.1385(2)	0.4340(2)	0.77(8)
Cl1	2a	1	0	0	0	2.82(8)
Na ₈ [Al _{0.44(1)} Ga _{0.56(1)} SiO ₄] ₆ Cl ₂ ; a = 891.19(1) pm; R _{wp} = 0.041; R _p = 0.032; R _I = 0.004; R _F = 0.002						
Na1	8e	1	0.1761(1)	0.1761	0.1761	1.93(6)
Al1/Ga1	6c	0.44/0.56(1)	¼	½	0	1.06(5)
Si1	6d	1	¼	0	½	1.26(6)
O1	24i	1	0.1499(2)	0.1377(2)	0.4329(2)	0.93(6)
Cl1	2a	1	0	0	0	3.00(7)
Na ₈ [Al _{0.28(1)} Ga _{0.72(1)} SiO ₄] ₆ Cl ₂ ; a = 892.35(1) pm; R _{wp} = 0.051; R _p = 0.037; R _I = 0.008; R _F = 0.004						
Na1	8e	1	0.1751(2)	0.1751	0.1751	2.02(8)
Al1/Ga1	6c	0.28/0.72(1)	¼	½	0	1.06(6)
Si1	6d	1	¼	0	½	1.40(8)
O1	24i	1	0.1495(3)	0.1368(2)	0.4313(2)	1.06(9)
Cl1	2a	1	0	0	0	2.8(1)
Na ₈ [Al _{0.23(1)} Ga _{0.77(1)} SiO ₄] ₆ Cl ₂ ; a = 892.67(2) pm; R _{wp} = 0.071; R _p = 0.049; R _I = 0.016; R _F = 0.010						
Na1	8e	1	0.1749(3)	0.1749	0.1749	2.7(1)
Al1/Ga1	6c	0.23/0.77(1)	¼	½	0	1.80(9)
Si1	6d	1	¼	0	½	1.8(1)
O1	24i	1	0.1502(2)	0.1365(2)	0.4316(2)	1.4(1)
Cl1	2a	1	0	0	0	3.0(1)
Na ₈ [Al _{0.16(1)} Ga _{0.84(1)} SiO ₄] ₆ Cl ₂ ; a = 893.02(1) pm; R _{wp} = 0.065; R _p = 0.047; R _I = 0.017; R _F = 0.010						
Na1	8e	1	0.1748(2)	0.1748	0.1748	2.3(1)
Al1/Ga1	6c	0.16/0.84(1)	¼	½	0	1.45(7)
Si1	6d	1	¼	0	½	1.26(9)
O1	24i	1	0.1506(4)	0.1358(3)	0.4310(3)	1.0(1)
Cl1	2a	1	0	0	0	2.8(1)
Na ₈ [Al _{0.15(1)} Ga _{0.85(1)} SiO ₄] ₆ Cl ₂ ; a = 893.45(1) pm; R _{wp} = 0.073; R _p = 0.051; R _I = 0.012; R _F = 0.007						
Na1	8e	1	0.1739(2)	0.1739	0.1739	2.0(1)
Al1/Ga1	6c	0.15/0.85(1)	¼	½	0	0.94(6)
Si1	6d	1	¼	0	½	0.96(8)
O1	24i	1	0.1508(3)	0.1355(3)	0.4300(3)	1.1(1)
Cl1	2a	1	0	0	0	2.9(1)
Na ₈ [GaSiO ₄] ₆ Cl ₂ ; a = 893.70(1) pm; R _{wp} = 0.086; R _p = 0.057; R _I = 0.016; R _F = 0.007						
Na1	8e	1	0.1734(3)	0.1734	0.1734	1.8(1)
Ga1	6c	1	¼	½	0	0.99(6)
Si1	6d	1	¼	0	½	0.63(9)
O1	24i	1	0.1521(3)	0.1342(3)	0.4279(4)	0.4(1)
Cl1	2a	1	0	0	0	2.7(1)

Na ₈ [AlSiO ₄] ₆ Br ₂ ; a = 893.72(1) pm; R _{wp} = 0.045; R _p = 0.034; R _I = 0.013; R _F = 0.007						
Na1	8e	1	0.1863(1)	0.1863	0.1863	1.81(6)
Al1	6c	1	¼	½	0	0.93(4)
Si1	6d	1	¼	0	½	0.93(4)
O1	24i	1	0.1508(3)	0.1408(3)	0.4425(2)	0.44(5)
Br1	2a	1	0	0	0	2.50(5)

continued

Atom	Site	Occupancy	x	y	z	B[pm*10 ⁴]
Na ₈ [Al _{0.76(1)} Ga _{0.24(1)} SiO ₄] ₆ Br ₂ ; a = 895.30(1) pm; R _{wp} = 0.041; R _p = 0.028; R _i = 0.014; R _F = 0.008						
Na1	8e	1	0.1864(1)	0.1864	0.1864	2.16(7)
Al1/Ga1	6c	0.76/0.24(1)	¼	½	0	1.5(1)
Si1	6d	1	¼	0	½	1.66(9)
O1	24i	1	0.1506(3)	0.1409(3)	0.4411(2)	0.54(6)
Br1	2a	1	0	0	0	3.69(5)
Na ₈ [Al _{0.66(1)} Ga _{0.34(1)} SiO ₄] ₆ Br ₂ ; a = 895.16(2) pm; R _{wp} = 0.037; R _p = 0.028; R _i = 0.005; R _F = 0.003						
Na1	8e	1	0.1846(2)	0.1846	0.1846	1.63(7)
Al1/Ga1	6c	0.66/0.34(1)	¼	½	0	1.23(2)
Si1	6d	1	¼	0	½	1.23(5)
O1	24i	1	0.1500(3)	0.1412(3)	0.4392(2)	0.40(7)
Br1	2a	1	0	0	0	2.43(5)
Na ₈ [Al _{0.63(1)} Ga _{0.37(1)} SiO ₄] ₆ Br ₂ ; a = 895.93(2) pm; R _{wp} = 0.057; R _p = 0.041; R _i = 0.010; R _F = 0.005						
Na1	8e	1	0.1847(2)	0.1847	0.1847	2.30(9)
Al1/Ga1	6c	0.63/0.37(1)	¼	½	0	0.65(6)
Si1	6d	1	¼	0	½	1.94(9)
O1	24i	1	0.1505(4)	0.1408(3)	0.4388(3)	0.83(7)
Br1	2a	1	0	0	0	3.37(6)
Na ₈ [Al _{0.53(1)} Ga _{0.47(1)} SiO ₄] ₆ Br ₂ ; a = 896.04(1) pm; R _{wp} = 0.044; R _p = 0.033; R _i = 0.008; R _F = 0.004						
Na1	8e	1	0.1856(2)	0.1856	0.1856	1.57(7)
Al1/Ga1	6c	0.53/0.47(1)	¼	½	0	1.76(5)
Si1	6d	1	¼	0	½	1.56(7)
O1	24i	1	0.1510(3)	0.1410(3)	0.4389(2)	1.15(6)
Br	2a	1	0	0	0	3.17(5)
Na ₈ [Al _{0.53(1)} Ga _{0.47(1)} SiO ₄] ₆ Br ₂ ; a = 895.87(2) pm; R _{wp} = 0.059; R _p = 0.043; R _i = 0.013; R _F = 0.007						
Na1	8e	1	0.1848(2)	0.1848	0.1848	2.20(9)
Al1/Ga1	6c	0.53/0.47(1)	¼	½	0	2.1(1)
Si1	6d	1	¼	0	½	1.3(1)
O1	24i	1	0.1508(4)	0.1406(3)	0.4389(3)	0.87(9)
Br	2a	1	0	0	0	3.40(7)
Na ₈ [Al _{0.45(1)} Ga _{0.55(1)} SiO ₄] ₆ Br ₂ ; a = 896.68(2) pm; R _{wp} = 0.037; R _p = 0.028; R _i = 0.006; R _F = 0.002						
Na1	8e	1	0.1832(2)	0.1832	0.1832	2.33(8)
Al1/Ga1	6c	0.45/0.55(1)	¼	½	0	1.05(6)
Si1	6d	1	¼	0	½	1.52(8)
O1	24i	1	0.1491(3)	0.1403(2)	0.4370(2)	1.15(8)
Br	2a	1	0	0	0	3.10(5)
Na ₈ [Al _{0.45(1)} Ga _{0.55(1)} SiO ₄] ₆ Br ₂ ; a = 896.72(2) pm; R _{wp} = 0.054; R _p = 0.038; R _i = 0.011; R _F = 0.005						
Na1	8e	1	0.1842(2)	0.1842	0.1842	2.45(9)
Al1/Ga1	6c	0.45/0.55(1)	¼	½	0	1.92(5)
Si1	6d	1	¼	0	½	1.92(5)
O1	24i	1	0.1501(3)	0.1404(3)	0.4347(2)	1.25(8)
Br	2a	1	0	0	0	3.24(6)
Na ₈ [Al _{0.39(1)} Ga _{0.61(1)} SiO ₄] ₆ Br ₂ ; a = 896.95(1) pm; R _{wp} = 0.038; R _p = 0.028; R _i = 0.005; R _F = 0.002						
Na1	8e	1	0.1825(1)	0.1825	0.1825	2.30(7)
Al1/Ga1	6c	0.39/0.61(1)	¼	½	0	0.98(5)
Si1	6d	1	¼	0	½	1.52(7)
O1	24i	1	0.1498(3)	0.1392(2)	0.4359(2)	1.23(7)
Br	2a	1	0	0	0	2.99(4)
Na ₈ [Al _{0.29(1)} Ga _{0.71(1)} SiO ₄] ₆ Br ₂ ; a = 897.59(2) pm; R _{wp} = 0.050; R _p = 0.037; R _i = 0.005; R _F = 0.003						
Na1	8e	1	0.1824(2)	0.1824	0.1824	2.2(1)
Al1/Ga1	6c	0.29/0.71(1)	¼	½	0	1.03(6)
Si1	6d	1	¼	0	½	1.39(9)
O1	24i	1	0.1502(3)	0.1380(3)	0.4352(2)	1.2(1)
Br	2a	1	0	0	0	2.95(6)
Na ₈ [Al _{0.22(1)} Ga _{0.78(1)} SiO ₄] ₆ Br ₂ ; a = 898.21(2) pm; R _{wp} = 0.057; R _p = 0.042; R _i = 0.008; R _F = 0.004						
Na1	8e	1	0.1824(2)	0.1824	0.1824	2.15(9)
Al1/Ga1	6c	0.22/0.78(1)	¼	½	0	1.01(6)
Si1	6d	1	¼	0	½	1.05(9)
O1	24i	1	0.1510(3)	0.1373(3)	0.4343(3)	1.1(1)
Br	2a	1	0	0	0	2.99(6)

continued

Atom	Site	Occupancy	x	y	z	B[pm*10 ⁴]
Na ₈ [Al _{0.12(1)} Ga _{0.88(1)} SiO ₄] ₆ Br ₂ ; a = 899.23(1) pm; R _{wp} = 0.057; R _p = 0.041; R _i = 0.008; R _F = 0.005						
Na1	8e	1	0.1820(2)	0.1820	0.1820	2.04(8)
Al1/Ga1	6c	0.12/0.88(1)	¼	½	0	0.78(4)
Si1	6d	1	¼	0	½	0.74(6)
O1	24i	1	0.1516(2)	0.1363(3)	0.4332(2)	0.92(8)
Cl1	2a	1	0	0	0	2.74(5)
Na ₈ [GaSiO ₄] ₆ Br ₂ ; a = 899.48(1) pm; R _{wp} = 0.075; R _p = 0.052; R _i = 0.013; R _F = 0.007						
Na1	8e	1	0.1818(2)	0.1818	0.1818	1.64(8)
Al1/Ga1	6c	1	¼	½	0	1.11(4)
Si1	6d	1	¼	0	½	0.16(6)
O1	24i	1	0.1534(3)	0.1347(2)	0.4335(3)	0.56(8)
Br	2a	1	0	0	0	2.53(6)

Table 5.2: Results of the XRD powder diffraction structure refinement of the sodalite systems in the space group P-43n.

Atom	Site	Occupancy	x	y	z	B[$\text{pm}^2 \cdot 10^4$]
Na_{7.7(1)}[Al_{0.28(1)}Ga_{0.72(1)}SiO₄]₆(OH·H₂O)_{1.7(1)}(H₂O)_{1.1(1)}; a = 892.59(1) pm; R_{wp} = 0.058; R_p = 0.041; R_i = 0.011; R_F = 0.007						
Na1	8e	0.96(1)	0.1700(2)	0.1700	0.1700	2.4(1)
Al1/Ga1	6c	0.28/0.72(1)	¼	½	0	1.34(4) ^a
Si1	6d	1	¼	0	½	1.34(4) ^a
O1	24i	1	0.1505(2)	0.1368(2)	0.4299(3)	1.79(9) ^b
O2	24i	0.186(2)	0.061(3)	0.088(6)	0.891(4)	1.79(9) ^b
Na_{7.7(1)}[Al_{0.41(1)}Ga_{0.59(1)}SiO₄]₆(OH·H₂O)_{1.7(1)}(H₂O)_{1.4(1)}; a = 892.44(2) pm; R_{wp} = 0.095; R_p = 0.070; R_i = 0.020; R_F = 0.010						
Na1	8e	0.97(1)	0.1748(1)	0.1748	0.1748	1.9(1)
Al1/Ga1	6c	0.41/0.59(1)	¼	½	0	1.04(6) ^a
Si1	6d	1	¼	0	½	1.04(6) ^a
O1	24i	1	0.1506(2)	0.1381(2)	0.4301(1)	1.1(1) ^b
O2	24i	0.200(3)	0.054(2)	0.099(10)	0.900(10)	1.1(1) ^b
Na_{7.7(1)}[Al_{0.43(1)}Ga_{0.57(1)}SiO₄]₆(OH·H₂O)_{1.7(1)}(H₂O)_{1.2(1)}; a = 891.83(1) pm; R_{wp} = 0.056; R_p = 0.041; R_i = 0.007; R_F = 0.004						
Na1	8e	0.96(1)	0.1728(2)	0.1728	0.1728	2.2(1)
Al1/Ga1	6c	0.43/0.57(1)	¼	½	0	1.24(4) ^a
Si1	6d	1	¼	0	½	1.24(4) ^a
O1	24i	1	0.1511(2)	0.1384(2)	0.4311(3)	1.38(9) ^b
O2	24i	0.189(2)	0.054(2)	0.091(5)	0.893(4)	1.38(9) ^b
Na_{7.7(1)}[Al_{0.50(1)}Ga_{0.50(1)}SiO₄]₆(OH·H₂O)_{1.7(1)}(H₂O)_{1.3(1)}; a = 891.94(2) pm; R_{wp} = 0.084; R_p = 0.065; R_i = 0.016; R_F = 0.009						
Na1	8e	0.96(1)	0.1750(3)	0.1750	0.1750	1.7(1)
Al1/Ga1	6c	0.50/0.50(1)	¼	½	0	1.16(6) ^a
Si1	6d	1	¼	0	½	1.16(6) ^a
O1	24i	1	0.1507(4)	0.1399(3)	0.4311(4)	1.1(1) ^b
O2	24i	0.197(3)	0.050(2)	0.093(9)	0.896(8)	1.1(1) ^b
Na_{7.7(1)}[Al_{0.58(1)}Ga_{0.42(1)}SiO₄]₆(OH·H₂O)_{1.7(1)}(H₂O)_{1.3(1)}; a = 891.62(1) pm; R_{wp} = 0.086; R_p = 0.064; R_i = 0.016; R_F = 0.009						
Na1	8e	0.97(1)	0.1739(2)	0.1739	0.1739	2.1(1)
Al1/Ga1	6c	0.58/0.42(1)	¼	½	0	1.14(6) ^a
Si1	6d	1	¼	0	½	1.14(6) ^a
O1	24i	1	0.1503(3)	0.1398(3)	0.4325(3)	1.2(1) ^b
O2	24i	0.198(2)	0.048(2)	0.092(5)	0.892(4)	1.2(1) ^b
Na_{7.9(1)}[Al_{0.65(1)}Ga_{0.35(1)}SiO₄]₆(OH·H₂O)_{1.9(1)}(H₂O)_{1.1(1)}; a = 891.20(1) pm; R_{wp} = 0.099; R_p = 0.070; R_i = 0.032; R_F = 0.017						
Na1	8e	0.99(1)	0.1767(2)	0.1767	0.1767	1.8(1)
Al1/Ga1	6c	0.65/0.35(1)	¼	½	0	0.58(6) ^a
Si1	6d	1	¼	0	½	0.58(6) ^a
O1	24i	1	0.1496(4)	0.1400(4)	0.4333(3)	0.2(1) ^b
O2	24i	0.201(2)	0.056(2)	0.102(10)	0.901(11)	0.2(1) ^b
Na_{7.7(1)}[Al_{0.74(1)}Ga_{0.26(1)}SiO₄]₆(OH·H₂O)_{1.7(1)}(H₂O)_{1.4(1)}; a = 889.78(2) pm; R_{wp} = 0.051; R_p = 0.036; R_i = 0.014; R_F = 0.008						
Na1	8e	0.96(1)	0.1763(3)	0.1763	0.1763	1.8(1)
Al1/Ga1	6c	0.74/0.26(1)	¼	½	0	1.04(7) ^a
Si1	6d	1	¼	0	½	1.04(7) ^a
O1	24i	1	0.1504(4)	0.1416(4)	0.4344(3)	0.6(1) ^b
O2	24i	0.203(2)	0.049(1)	0.103(10)	0.893(10)	0.6(1) ^b
Na_{7.7(1)}[Al_{0.80(1)}Ga_{0.20(1)}SiO₄]₆(OH·H₂O)_{1.7(1)}(H₂O)_{1.3(1)}; a = 889.84(1) pm; R_{wp} = 0.050; R_p = 0.035; R_i = 0.011; R_F = 0.006						
Na1	8e	0.96(1)	0.1778(2)	0.1778	0.1778	1.8(1)
Al1/Ga1	6c	0.80/0.20(1)	¼	½	0	1.17(6) ^a
Si1	6d	1	¼	0	½	1.17(6) ^a
O1	24i	1	0.1501(2)	0.1403(2)	0.4372(2)	1.1(1) ^b
O2	24i	0.193(1)	0.042(1)	0.086(4)	0.892(3)	1.1(1) ^b

continued

Atom	Site	Occupancy	x	y	z	B[pm*10 ⁴]
Na _{7.1(1)} [AlSiO ₄] ₆ (OH·H ₂ O) _{1.1(1)} (H ₂ O) _{3.5(1)} ; a = 889.30(3) pm; R _{wp} = 0.086; R _p = 0.064; R _i = 0.019; R _F = 0.009						
Na1	8e	0.88(1)	0.1746(3)	0.1746	0.1746	4.9(2)
Al	6c	1	¼	½	0	1.93(8) ^a
Si1	6d	1	¼	0	½	1.93(8) ^a
O1	24i	1	0.1511(3)	0.1406(3)	0.4411(3)	2.8(1) ^b
O2	24i	0.236(3)	0.062(1)	0.102(3)	0.865(3)	2.8(1) ^b

Na ₆ [GaSiO ₄] ₆ (H ₂ O) ₈ ; a = 885.45(0) pm; R _{wp} = 0.080; R _p = 0.060; R _i = 0.017; R _F = 0.010						
Na1	8e	0.75	0.1478(4)	0.1478	0.1478	5.2(1)
Ga1	6c	1	¼	½	0	2.37(3)
Si1	6d	1	¼	0	½	1.33(5)
O1	24i	1	0.1500(2)	0.1303(2)	0.4234(3)	1.85(8)
O2	8e	1	0.3730(3)	0.3730	0.3730	1.6(1)
Na ₆ [Al _{0.25(1)} Ga _{0.75(1)} SiO ₄] ₆ (H ₂ O) ₈ ; a = 885.67(1) pm; R _{wp} = 0.078; R _p = 0.054; R _i = 0.016; R _F = 0.008						
Na1	8e	0.75	0.1558(4)	0.1558	0.1558	3.5(1)
Al1/Ga1	6c	0.25/0.75(1)	¼	½	0	0.68(5)
Si1	6d	1	¼	0	½	0.55(8)
O1	24i	1	0.1495(2)	0.1336(2)	0.4233(3)	1.0(1)
O2	8e	1	0.3792(3)	0.3792	0.3792	5.6(3)
Na ₆ [Al _{0.43(1)} Ga _{0.57(1)} SiO ₄] ₆ (H ₂ O) ₈ ; a = 884.38(2) pm; R _{wp} = 0.088; R _p = 0.060; R _i = 0.021; R _F = 0.012						
Na1	8e	0.75	0.1562(5)	0.1562	0.1562	3.5(2)
Al1/Ga1	6c	0.43/0.57(1)	¼	½	0	1.11(1)
Si1	6d	1	¼	0	½	0.5(1)
O1	24i	1	0.1502(2)	0.1357(3)	0.4271(4)	0.7(1)
O2	8e	1	0.3791(4)	0.3791	0.3791	3.0(3)
Na ₆ [Al _{0.44(1)} Ga _{0.56(1)} SiO ₄] ₆ (H ₂ O) ₈ ; a = 885.91(1) pm; R _{wp} = 0.077; R _p = 0.056; R _i = 0.016; R _F = 0.008						
Na1	8e	0.75	0.1497(4)	0.1497	0.1497	2.8(1)
Al1/Ga1	6c	0.44/0.56(1)	¼	½	0	0.25(7)
Si1	6d	1	¼	0	½	0.5(1)
O1	24i	1	0.1480(4)	0.1359(3)	0.4249(3)	1.0(1)
O2	8e	1	0.3780(3)	0.3780	0.3780	2.0(2)
Na ₆ [Al _{0.55(1)} Ga _{0.45(1)} SiO ₄] ₆ (H ₂ O) ₈ ; a = 884.45(1) pm; R _{wp} = 0.049; R _p = 0.035; R _i = 0.017; R _F = 0.008						
Na1	8e	0.75	0.1503(3)	0.1503	0.1503	3.0(1)
Al1/Ga1	6c	0.55/0.45(1)	¼	½	0	0.7(1)
Si1	6d	1	¼	0	½	0.5(1)
O1	24i	1	0.1491(3)	0.1366(3)	0.4277(3)	0.9(1)
O2	8e	1	0.3783(3)	0.3783	0.3783	1.3(2)
Na ₆ [Al _{0.58(1)} Ga _{0.42(1)} SiO ₄] ₆ (H ₂ O) ₈ ; a = 885.25(1) pm; R _{wp} = 0.083; R _p = 0.061; R _i = 0.023; R _F = 0.014						
Na1	8e	0.75	0.1572(4)	0.1572	0.1572	4.0(3)
Al1/Ga1	6c	0.58/0.42(1)	¼	½	0	1.6(1)
Si1	6d	1	¼	0	½	0.9(1)
O1	24i	1	0.1492(2)	0.1364(2)	0.4282(2)	1.4(1)
O2	8e	1	0.3817(4)	0.3817	0.3817	2.1(4)
Na ₆ [Al _{0.64(1)} Ga _{0.36(1)} SiO ₄] ₆ (H ₂ O) ₈ ; a = 884.40(1) pm; R _{wp} = 0.041; R _p = 0.030; R _i = 0.015; R _F = 0.008						
Na1	8e	0.75	0.1507(3)	0.1507	0.1507	3.2(1)
Al1/Ga1	6c	0.64/0.36(1)	¼	½	0	1.0(1)
Si1	6d	1	¼	0	½	0.6(1)
O1	24i	1	0.1497(1)	0.1373(1)	0.4289(1)	0.9(1)
O2	8e	1	0.3784(2)	0.3784	0.3784	1.1(2)

continued

Atom	Site	Occupancy	x	y	z	B[$\text{pm}^2 \cdot 10^4$]
Na ₆ [Al _{0.75(1)} Ga _{0.25(1)} SiO ₄] ₆ (H ₂ O) ₈ ; a = 884.03(3) pm; R _{wp} = 0.035; R _p = 0.027; R _i = 0.022; R _F = 0.012						
Na1	8e	0.75	0.1602(6)	0.1602	0.1602	4.6(2)
Al1/Ga1	6c	0.75/0.25(1)	1/4	1/2	0	1.8(1)
Si1	6d	1	1/4	0	1/2	2.0(2)
O1	24i	1	0.1501(4)	0.1401(4)	0.4310(4)	2.3(2)
O2	8e	1	0.3819(4)	0.3819	0.3819	2.9(4)
Na ₆ [Al _{0.80(1)} Ga _{0.20(1)} SiO ₄] ₆ (H ₂ O) ₈ ; a = 884.03(8) pm; R _{wp} = 0.046; R _p = 0.035; R _i = 0.019; R _F = 0.010						
Na1	8e	0.75	0.1642(1)	0.1642	0.1642	4.6(2)
Al1/Ga1	6c	0.80/0.20(1)	1/4	1/2	0	1.6(1)
Si1	6d	1	1/4	0	1/2	0.6(2)
O1	24i	1	0.1495(1)	0.1381(1)	0.4330(1)	1.2(4)
O2	8e	1	0.3823(3)	0.3823	0.3823	2.5(1)
Na ₆ [AlSiO ₄] ₆ (H ₂ O) ₈ ; a = 884.72(2) pm; R _{wp} = 0.096; R _p = 0.071; R _i = 0.021; R _F = 0.011						
Na1	8e	0.75	0.1663(3)	0.1663(3)	0.1663(3)	4.8(1)
Al1	6c	1	1/4	1/2	0	1.8(1)
Si1	6d	1	1/4	0	1/2	1.0(1)
O1	24i	1	0.1485(1)	0.1390(1)	0.4343(1)	1.44(9)
O2	8e	1	0.3825(3)	0.3825	0.3825	2.9(3)

^{a, b}linear constraints were used within the same composition.